Aus dem Munich Cluster for Systems Neurology (Synergy) am Institut für Schlaganfall- und Demenzforschung (ISD) am Klinikum der Universität München

Vorstand: Prof. Dr. med. Martin Dichgans

GABARAPL2-ACSL3 interaction links ufmylation and lipid droplet formation

Dissertation

zum Erwerb des Doktorgrades der Naturwissenschaften

an der Medizinischen Fakultät der

Ludwig-Maximilians-Universität München

vorgelegt von

Franziska Mirjam Renate Eck

aus München

2021

Gedruckt mit Genehmigung der Medizinischen Fakultät der Ludwig-Maximilians-Universität München

Betreuer:	Prof. Dr. rer. nat. Christian Behrends
Zweitgutachter:	Prof. Dr. rer. nat. Jürgen Bernhagen
Dekan:	Prof. Dr. med. Thomas Gudermann

Tag der mündlichen Prüfung: 31.03.2022

Table of Content

1. Summary

Protein homeostasis, an important part of cellular integrity, is achieved through balanced protein synthesis and degradation. One of the main protein degradation pathways in mammals is macroautophagy (hereafter referred to as autophagy) which regulates the recycling of protein aggregates, defective organelles or pathogens. Induction of autophagy leads to membrane expansions from organelles, such as the ER (endoplasmic reticulum), capturing cargo inside double membrane vesicles termed autophagosomes. Fusion of autophagosomes with lysosomes induces cargo degradation and the release of building blocks. Autophagosomal degradation is mediated by a group of genes termed Autophagy-related (ATG) genes. Mechanistically a distinction is made between bulk autophagy, the global turnover of cytoplasmic content upon nutrient deprivation, and selective autophagy, the specific recognition and degradation of substrates. In selective autophagy cargo dedicated for degradation is recognized by autophagy receptors which are recruited to expanding autophagosomal membranes through ATG8 proteins. Beside their functions in cargo recognition, ATG8s are involved in all steps of the autophagic pathway and moreover, fulfill autophagy unrelated functions. A special characteristic of the six human ATG8 (hATG8) proteins which are subdivided in GABARAPs (γ-aminobutyric acid receptor-associated proteins) and LC3s (microtubule-associated proteins 1A/1B light chain 3) is their high structural similarity which complicates studying distinct functions of the proteins.

As isoform specific antibodies are difficult to produce and studies of hATG8 proteins are mostly performed in overexpressing cell systems potentially masking distinct functions of hATG8s, we used CRISPR (clustered regularly interspaced short palindromic repeats)/Cas9 technology in the first part of this study to generate a set of HeLa cell lines each expressing one endogenous HA (hemagglutinin)-tagged hATG8. An exception was LC3A, as we were not able to integrate the HA-tag at the N-terminus of LC3A. Correctly engineered knock-in of the epitope tag and posttranslational conjugation of hATG8 proteins to phosphatidyl-ethanolamine was validated through sequencing and biochemical assays, respectively.

In the second part of the study, we employed interactome proteomics to identify ACSL3 (long-chain-fatty-acid CoA ligase 3), an ER associated, single-pass type III membrane protein, as novel GABARAPL2 interactor. The association of both proteins was further validated through immunoprecipitations and immunofluorescence-based microscope assays. Pulldown and subcellular fractionation assays showed that recruitment of GABARAPL2 to the ER and binding between ACSL3 and GABARAPL2 is mediated by conserved structural elements in both proteins, namely a LC3 interacting region (LIR) in ACSL3 and the LIR docking site (LDS) in GABARAPL2. In addition, there is a second LDS-LIR independent binding site that contributes to the interaction between the two proteins. Recent findings that UFM1 (ubiquitin-like protein ubiquitin fold modifier 1) -activating enzyme UBA5 (ubiquitin-like modifier-activating enzyme 5), the E1 enzyme of the ubiquitin-like UFM1 conjugation machinery, is transported to the ER membrane by GABARAPL2, raised the question whether ACSL3 serve as docking site for the GABARAPL2-UBA5 complex at the ER. Consistent with this notion, interaction between ACSL3 and UBA5 was confirmed through image-based techniques and immunoprecipitations. Further, ACSL3 knockdown experiments revealed that GABARAPL2 UBA5 as well as DDRGK1 (DDRGK domain-containing protein 1) and UFL1 (E3 UFM1-protein ligase 1) which are part of the UFM1 E3 ligase complex are all stabilized by ACSL3 supporting the view that ACSL3 is part of UFM1 conjugation machinery. The accumulation of neutral lipids in single membrane vesicles called lipid droplets is, besides other proteins, dependent on the enzymatic activity of ACSL3. Interestingly, induction of lipid droplet formation through oleic acid treatment and thus, activation of enzymatic activity of ACSL3 and partial relocalization to lipid droplets reduced the protein abundance of UBA5, DDRGK1 and UFL1. In accordance to the recently reported regulation of starvation induced ER-phagy by DDRGK1 and UFL1, we detected inhibition of ER-phagy upon lipid droplet formation and thus, reduced UFL1 and DDRGK1 protein levels. Taken together we identified ACSL3 and lipid droplet biogenesis as novel regulators of the ufmylation pathway.

2. Zusammenfassung

Proteinhomöostase, ein wichtiger Teil der zellulären Integrität, wird erreicht durch die Balance zwischen Proteinsynthese und Proteinabbau. Einer der Hauptabbauwege von Proteinen in Säugetieren ist Makroautophagie (im Folgenden als Autophagie bezeichnet), welche das Recyceln von Proteinaggregaten, schadhaften Organellen und Pathogenen steuert. Wenn Autophagie eingeleitet wird, werden Membranen von Organellen wie dem ER (Endoplasmatisches Retikulum) expandiert, um Substrate durch eine Doppelmembran in einem Vesikel, dem sogenannten Autophagosom, einzuschließen. Die Fusion von Autophagosomen mit Lysosomen leitet den Abbau der Substrate und die Rückführung der gewonnenen Abbauprodukte in das Zytosol zur Neusynthese ein. Dieser Prozess wird durch eine Gruppe Autophagie Gene (ATG) gesteuert. Mechanistisch unterscheidet man zwischen Bulk-Autophagie, dem unspezifischen Abbau von zytoplasmatischem Material, ausgelöst durch Nährstoffmangel, und selektiver Autophagie, dem spezifischen Erkennen von Substraten und deren gezieltem Abbau. In der selektiven Autophagie werden die Substrate von autophagie-spezifischen Rezeptoren erkannt und von ATG8 Proteinen zu den sich ausstülpenden Membranen, die später das Autophagosom bilden, transportiert. Neben der Funktion in der Substraterkennung sind ATG8 Proteine in vielen anderen Schritten des Autophagie-Prozesses involviert und haben zusätzlich noch autophagie-unabhängige Funktionen. Ein besonderes Merkmal aller sechs humanen ATG8 Proteine (hATG8), die in GABARAPs (γ-aminobutyric acid receptor-associated proteins) und LC3s (microtubule-associated proteins 1A/1B light chain 3) unterteilt werden, ist deren strukturelle Ähnlichkeit, die das Erforschen von individuellen Funktionen dieser Proteine erschwert.

Antikörper, die nur eine der Isoformen detektieren, sind sehr schwer herzustellen, und Studien über hATG8 Proteine werden meistens in Überexpressions-Zell-Systemen gemacht, die die individuellen Funktionen verbergen könnten. Deshalb haben wir mit CRISPR (clustered regularly interspaced short palindromic repeats)/Cas9 HeLa Zelllinien hergestellt, von denen jede ein hATG8 Protein mit einem HA (hemagglutinin)-Tag endogen exprimiert. Als Ausnahme ist LC3A zu nennen, da wir den HA-Tag nicht in den N-Terminus von LC3A integrieren

konnten. Die korrekte Integrierung des Epitop-Tags mit CRISPR/Cas9 und die posttranslationale Modifikation von ATG8 mit dem Lipid Phosphatidylethanolamin wurde durch Sequenzierung, beziehungsweise biochemische Experimente überprüft.

Im zweiten Teil der Arbeit haben wir durch interaktionsbasierte Proteomik das ER assoziierte Membranprotein ACSL3 (long-chain-fatty-acid CoA ligase 3) als ein mit GABARAPL2 interagierendes Protein identifiziert. Die Bindung zwischen den beiden Proteinen wurde durch Immunpräzipitation und verschiedene Immunfluoreszenzmikroskopietechniken bestätigt. Anhand von Bindestudien und Zell-fraktionierung konnten wir zeigen, dass der Transport von GABARAPL2 zum ER und die Interaktion zwischen ACSL3 und GABARAPL2 durch ein konserviertes strukturelles Element in beiden Proteinen bedingt wird. Die Bindestelle in ACSL3 wird als LC3 Interaktionsstelle (LIR) bezeichnet die mit der LIR Andockstelle (LDS) in GABARAPL2 interagiert. Außerdem gibt es eine weitere LDS-LIR unabhängige Bindung zwischen den beiden Proteinen. UBA5 (ubiquitin-like modifier-activating enzyme 5) ist ein Enzym im Konjugationsprozess von UFM1 (ubiquitin-like protein ubiquitin fold modifier 1) an andere Proteine und übernimmt in diesem die Aktivierung von UFM1. Die Tatsache, dass UBA5 durch GABARAPL2 an die ER Membran rekrutiert wird, führt zu der Annahme, dass ACSL3 eine Rolle als ER Andockstelle für den GABARAPL2-UBA5 einnehmen könnte. Damit übereinstimmend hat die Depletion von ACSL3 gezeigt, dass sowohl GABARAPL2, UBA5 sowie die UFM1 E3 Ligase Komponenten DDRGK1 (DDRGK domain-containing protein 1) und UFL1 (E3 UFM1-protein ligase 1) von ACSL3 stabilisiert werden. Außerdem konnten wir durch verschiedene Mikroskopietechniken und Immunpräzipitation bestätigen, dass ACSL3 auch mit UBA5 assoziiert und damit zusammengenommen als ein Teil des UFM1 Konjugationsystems anzusehen ist. Die Anreicherungen von neutralen Fetten in Vesikeln mit einer singulären Membran werden als Lipidtröpfchen bezeichnet, deren Bildung unter anderem von der enzymatischen Aktivität von ACSL3 abhängig ist. Die Bildung von Lipidtröpfchen kann durch die Behandlung von Zellen mit Ölsäure eingeleitet werden, was folglich die enzymatische Aktivität von ACSL3 anregt und ACSL3 teilweise auf Lipidtröpfchen lokalisiert. Interessanterweise führt die Behandlung von Zellen mit Ölsäure auch zur Verringerung der

Proteinmenge von UBA5, DDRGK1 und UFL1, was zusätzlich eine regulative Verbindung zwischen ACSL3 und UFM1 Konjugationskomponenten nahelegt. Erst kürzlich wurde gezeigt, dass im Fall von Nährstoffmangel der selektive Abbau von ER Membranen durch Autophagie (ER-phagie) von DDRGK1 und UFL1 reguliert wird. In Übereinstimmung damit konnten wir demonstrieren, dass die Bildung von Lipidtröpfchen, die mit einer Verringerung der Proteinmengen von DDRGK1 und UFL1 einhergeht, auch ER-phagie hemmt.

Zusammengefasst konnten wir mit unseren Experimenten zeigen, dass ACSL3 und die Bildung von Lipidtröpfchen als neue Regulatoren des UFM1 Konjugationprozesses fungieren.

3. Introduction

3.1. Protein degradation systems in eukaryotic organisms

Proteostasis in eukaryotic organisms, essential for cellular viability, functionality and health, is achieved by balanced protein synthesis and protein degradation. Internal and external stimuli induce synthesis of proteins through transcription of DNA and translation of mRNA followed by folding of the newly synthesized protein. Hereby a highly evolved protein quality control system, comprising of molecular chaperones and degradation systems, ensures protein integrity. De novo protein folding and refolding of misfolded proteins is mediated by chaperones while mainly the ubiquitin-proteasome system (UPS) and the autophagy-lysosome pathway take responsibility for degradation and recycling of damaged, misfolded, aggregated and short-lived proteins (1-3) (**Fig. 1**). Due to size restrictions, the proteasome degrades mostly redundant, unfolded, misfolded or damaged single proteins whereas protein aggregates, unwanted organelles and pathogens are recognized and cleared by autophagy (4,5).

Both pathways recognize posttranslational protein modifications with Ubiquitin (Ub) as signal for substrate degradation (5,6). Ubiquitination is a reversible process that covalently conjugates Ub to substrate proteins individually or in polyubiquitin chains via an enzymatic cascade. First, deubiquitinating enzymes (DUBs) cleave the C-terminal end of the precursor form of Ub (proUb) to expose a C-terminal glycine. Next, Ub is activated in an ATP-dependent reaction through adenylation of its exposed C-terminal glycine by an E1 Ub activating enzyme, subsequent by the hand over to the active-site of an E2 Ub conjugating enzyme. Finally, Ub is linked to a lysine residue of the substrate through an E3 protein ligase (**Fig. 1 I**) (7). In the UPS Ub receptors, located at the 19S regulatory particle (RP) which is attached to one or both ends of the 20S core particle (CP) of the 26S proteasome, recognize ubiquitinated substrates. Identified substrates are then deubiquitinated by DUBs followed by protein unfolding and degradation in the barrel-shaped 20S CP (**Fig. 1 II**) (2,8).

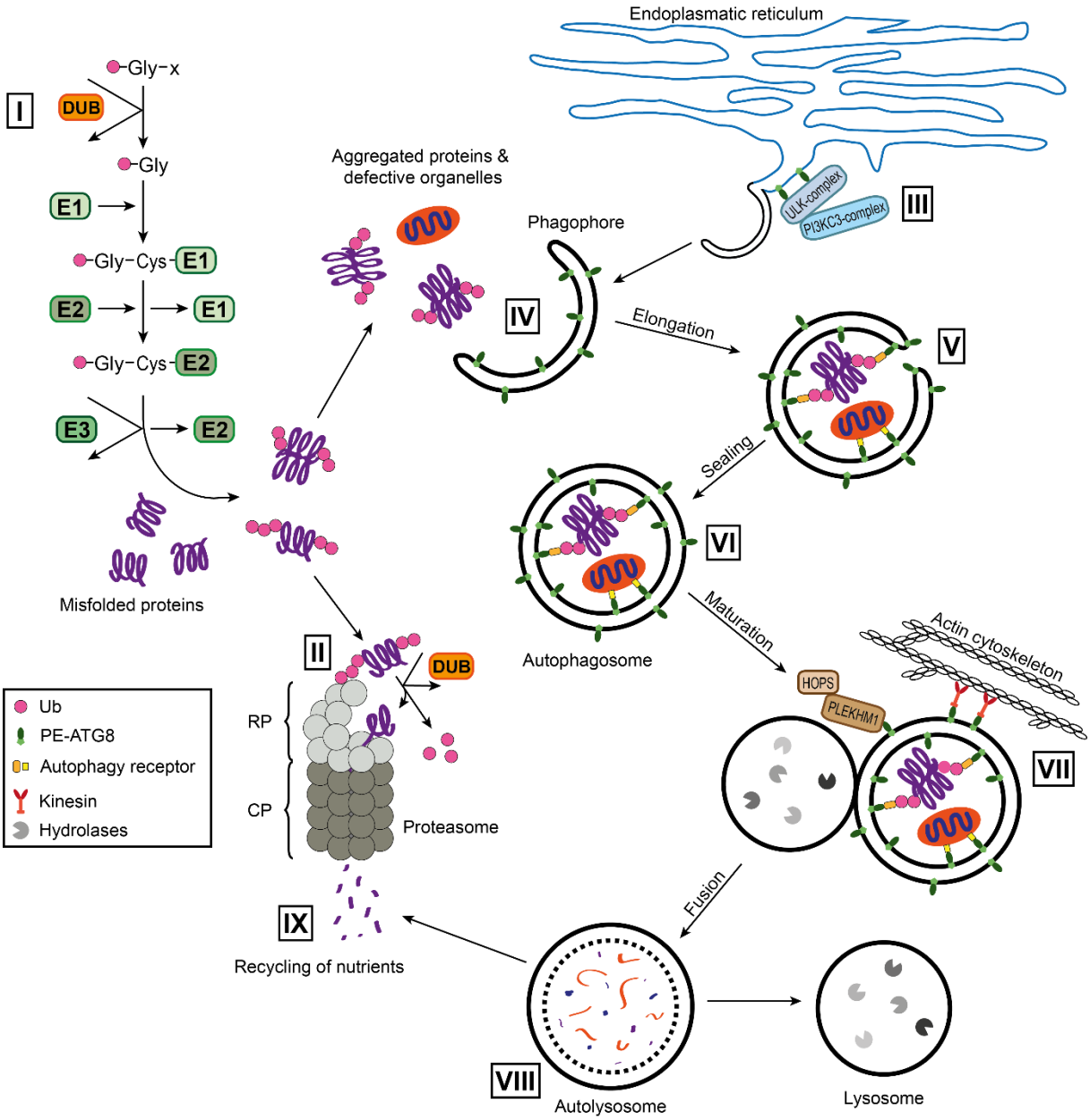

Figure 1: Degradation pathways: Ub-conjugation (I): The precursor form of Ub is processed by DUBs exposing a C-terminal glycine. Ub is subsequently activated by an E1 enzyme, handed over to an E2 enzyme and finally conjugated to misfolded or aggregated proteins by E3. **UPS (II)**: Misfolded proteins are recognized by Ub receptors located at the RP of the 26S proteasome. After deubiquitylation through DUBs, misfolded proteins are unfolded and degraded by the proteasomal CP. **Autophagy (III-IX)**: Upon autophagy induction, GABARAP proteins recruit the ULK-complex to the endoplasmic reticulum (ER) and together with the PI3KC3-complex phagophore formation is triggered (**III**). PE-ATG8s located at the outer and inner phagophore membrane (**IV**) capture ubiquitinated cargo via autophagy receptors (**V**). Upon sealing of the phagophore, cargo is enclosed inside the autophagosome (**VI**). During maturation autophagosomes are transported via the cytoskeleton and tethered to lysosomes through the HOPS complex and PLEKHM1 (**VII**). Upon autophagosomal-lysosomal fusion, the autolysosome is formed and cargo is degraded by lysosomal hydrolases (**VIII**). Nutrients are released into the cytosol (**IX**).

There are three autophagy branches, macroautophagy, microautophagy and chaperone-mediated autophagy, which deliver cytosolic content to the lysosome for degradation. The best

characterized pathway of these processes is macroautophagy (hereafter referred to as autophagy). In response to environmental stimuli, such as starvation, membrane expansions called phagophores or isolation membranes are formed from preexisting membranes, such as the endoplasmic reticulum (ER), and are elongated. Closure of phagophores capture cytosolic cargo inside autophagosomes which are capable of fusing with lysosomes and subsequently forming autolysosomes. Lysosomal hydrolases (proteases, nucleases and lipidases) disassemble the captured autophagosomal content and nutrients, such as amino acids, are released (**Fig. 1 III-IX**) (9,10). But other than proteasomal degradation, autophagy is also able to degrade cargo independently of Ub (5,6).

A subset of genes termed autophagy-related (ATG) genes mediate autophagy and are mostly conserved from yeast to human. ATG genes were first discovered in yeast and to date more than 37 have been identified (11-15).

3.2. ATG8 protein family

The ATG8 proteins, belonging to a highly conserved protein family from yeast to humans, are involved in all steps of the autophagosomal biogenesis (15). While in yeast there was found only one ATG8, the ATG8 protein family in humans (hATG8) comprises at least six orthologs with high structural similarities. These are subclassified into γ-aminobutyric acid receptor-associated proteins (GABARAPs) including GABARAP, GABARAPL1 and GABARAPL2 and the microtubule-associated proteins 1A/1B light chain 3 (MAP1LC3s) including LC3A, LC3B and LC3C. The hATG8 protein family belongs to the group of small ubiquitin-like modifiers (Ubls) and therefore exhibit an Ub-like fold even though there is no similarity between the sequences of hATG8s and Ub (16-18). Usually binding of hATG8s to interacting proteins is mediated by a LIR-docking site (LDS) in hATG8 proteins and the corresponding LC3-interacting region (LIR; also known as hATG8 family-interacting motif (AIM)) in binding partners (19-22). It was recently discovered that proteins with an ubiquitin-interacting motif (UIM) can also interact with the UIM-docking site (UDS) within hATG8 proteins (23,24).

3.2.1. Lipidation of hATG8 proteins

A major feature of hATG8 proteins is the reversible association of hATG8s to membranes directed through covalent attachment of phosphatidylethanolamine (PE) to the C-terminal protein end (**Fig. 2 I**) (25,26). During PE-hATG8 conjugation the C-terminal part of pro-hATG8s is cleaved by the cysteine protease ATG4A-D, exposing a glycine residue (**Fig. 2 II**), followed by activation of hATG8s through E1-like activating enzyme ATG7 (**Fig. 2 III**) (27). The E2-like conjugating enzyme ATG3 and the E3-like enzyme complex ATG12-ATG5-ATG16L are finally conjugating the hATG8 proteins to PE (**Fig. 2 IV&V**) (28,29). This conjugate formation is reversible by cleavage via ATG4A-D (**Fig. 2 VI**) (27).

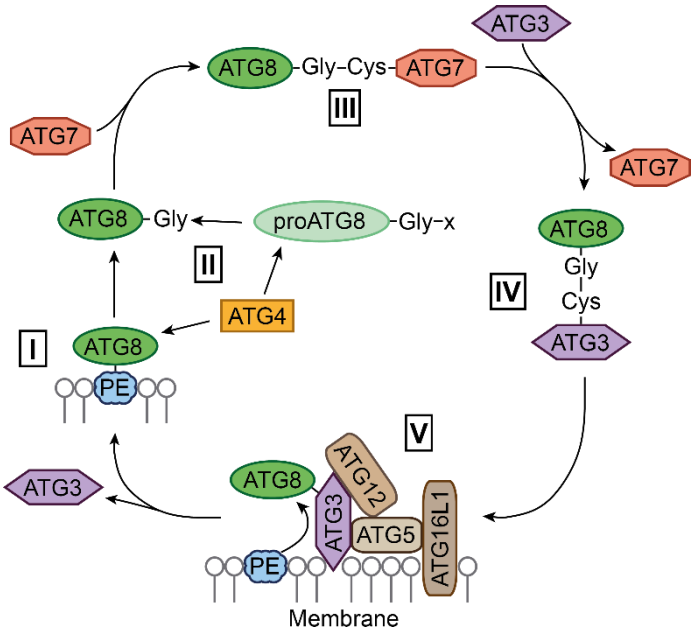

Figure 2: PE-ATG8 conjugation: ATG8 is covalently conjugated to PE and integrated into membranes (**I**). Cleavage at the C-terminal part of pro-ATG8 by ATG4 results in an exposed glycine and matured ATG8 (**II**). Activation of ATG8 by ATG7 (**III**) is followed by the binding to ATG3 (**IV**) and its final conjugation to PE through the E3-like enzyme complex ATG12-ATG5-ATG16L (**V/I**). PE-ATG8 conjugation is reversed by cleavage via ATG4 (**II**).

3.2.2. Cellular Functions of ATG8 proteins

3.2.2.1. ATG8 proteins in autophagosome biogenesis

As mentioned above, ATG8 proteins are tightly linked to the autophagic pathway and are reported to be essential in biogenesis of autophagosomes. In recent years, it was suggested that GABARAP recruits ULK complex to the phagophore assembly site (PAS) and furthermore, this interaction sustains ULK1 kinase activity (30,31). Unc-51-like kinase 1 (ULK1) is a key component of the autophagy initiation complex that is responsible for initiation of phagophore

formation. In its inactive state ULK1 is bound and phosphorylated by the negative autophagy regulator serine/threonine kinase mTOR. Upon autophagy inducing stimuli, ULK1 is dephosphorylated and released from mTOR complex (32,33). Subsequent to autophosphorylation of dissociated ULK1, it forms the initiation complex together with ATG13, FIP200 (RB1-inducible coiled-coil protein 1), both phosphorylated by active ULK1, and ATG101 (34-36). Together with the PI3KC3 complex I (class III PI3K) nucleation of the phagophore is triggered (**Fig. 1 III**) (9,30,31). Next, membrane expansions through membrane fusions lead to elongation of the phagophore membrane and are induced by PE-ATG8 (preferentially LC3) conjugation and their attachment to the outer and inner phagophore membrane leaflets (**Fig. 1 IV**) (37-40). The enlarged phagophore encloses cytosolic content dedicated for degradation. The ability of the autophagic machinery to recognize and degrade specific cargo was reported in recent years and is termed selective autophagy. Hereby, substrate recognition is achieved by specific autophagy receptors that recognize and bind ubiquitinated cargo such as defective mitochondria (mitophagy) or pathogens (xenophagy) or aggregated proteins (aggrephagy) (41-48). Importantly, these receptors are recruited by GABARAPs and LC3s located at the phagophore membrane (**Fig. 1 V**) (10,49,50). Fusion of the inner and outer phagophore membrane leaflets generates the autophagosome and even though it is reported that GABARAP proteins are involved in this process, the exact function of GABARAPs during autophagosomal sealing remains unknown (38,40). Prior to autophagosomal-lysosomal fusion and recycling of nutrients (**Fig. 1 VIII**&**IX**), nascent autophagosomes undergo maturation (9). This process involves cytosolic transport of autophagosomes to lysosomes via kinesin motor proteins along the cytoskeleton, recruitment of autophagosomal-lysosomal fusion machinery and cleavage of ATG8 proteins from the outer membrane of the autophagosome (**Fig. 1 VII**) (51-54). GABARAPs and LC3s play a crucial role during maturation and fusion as they link kinesins to the autophagosome and tether the homotypic fusion and protein sorting (HOPS) complex via PLEKHM1 (pleckstrin homology domain containing family M member 1) to the autophagosomal membrane (**Fig. 1 VII**) (55,56).

3.2.2.1. ATG8 functions beyond autophagy

Over the past years it was shown that ATG8 proteins also fulfill functions in many other pathways besides autophagy.

GABARAPs and LC3s promote diverse regulatory functions in trafficking processes

With yeast-two hybrid experiments GABARAP was first identified as interactor of $GABA_A$ receptor, an anion-permeable channel located in the brain (57,58). $GABA_A$ receptors are built from five out of 18 different subunits, dedicating location and function of the receptor. After assembly of $GABA_A$ subunits in the ER, the receptor is transported via the Golgi to the plasma membrane and inserted. GABARAP has been found to interact with γ2 subunits of $GABA_A$ receptors and is involved in enhanced intracellular trafficking and clustering of $GABA_A$ receptors at the plasma membrane (57,59-61).

GABARAPL2 was first named as Golgi-associated ATPase enhancer of 16 kDa (GATE-16) involved in intra-Golgi trafficking and reassemble of post-mitotic Golgi fragments (62,63). Vesicle transport includes vesicular budding, trafficking, membrane docking and fusion with target membranes. In intra-Golgi transport docking of a vesicle with a membrane is mediated by integral membrane proteins (SNAREs) in the vesicle (v-SNARE) (**Fig. 3 I**) forming a complex (trans-SNARE complex) with t-SNAREs located in the target membrane (**Fig. 3 II**) (64). Next, the vesicle membrane fuses with the acceptor organelle (65). In fused membranes

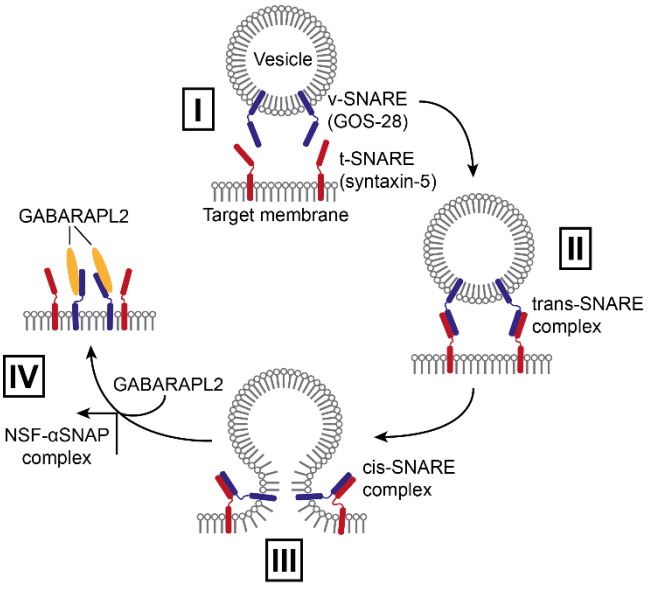

Figure 3: SNARE assembly and disassembly: Docking of vesicles with target membranes involve v-SNAREs and t-SNAREs located at the vesicle or target membrane, respectively (**I**). v-SNAREs, reaching their target membrane, form a stable trans-SNARE complex with t-SNAREs and promote vesicle-membrane fusion (**II**). v- and t-SNAREs located within the same membrane form a highly stable, unproductive cis-SNARE complex (**III**). Disassembly of the cis-SNARE complex is mediated through ATP hydrolyses by NSF/αSNAP. Further, NSF recruits GABARAPL2 to v-SNARE GOS-28 to prevent reassembly with t-SNARE syntaxin-5 (**IV**).

v- and t-SNAREs form the highly stable cis complex (**Fig. 3 III**). The vesicle fusing ATPase NSF (N-ethylmaleimide-sensitive fusion protein), interacting via αSNAP (α-soluble NSF attachment protein) with the cis-SNARE complex, mediates complex disassembly through ATP hydrolyses (66-68). This process is enhanced through GABARAPL2 binding to NSF. Additionally, GABARAPL2 is recruited through NSF/αSNAP to now unpaired Golgi v-SNARE protein GOS-28 and prevents its reassembly with syntaxin-5 (Golgi t-SNARE) to unproductive cis-SNARE complexes (**Fig. 3 IV**) (63,69-71).

Recently, it was shown that LC3B and LC3C fulfill essential scaffold functions in COPII-dependent trafficking between ER and Golgi (72). Transport from ER to Golgi starts at ER exit sites with the formation of COPII coated vesicles. SEC24D, forming a subunit with SEC23A which is part of the inner layer of COPII coated vesicles, is tethered to the membrane and stabilized through the interaction with Tectonin beta-propeller repeat-containing protein 2 (TECPR2) (73). TECPR2 in turn is anchored to the membrane through binding to lipidated LC3B or LC3C. Compromised LC3-TECPR2-SEC24D interaction leads to impaired ER export of cargo in COPII-dependent manner and a decreased number of functional ER exit sites. Taken together LC3B and LC3C are involved in the regulation of ER exit sites and ER to Golgi transport of COPII coated vesicles (72,73).

GABARAPs and LC3s regulate reorganization of the cytoskeleton

In the past years it was shown that GABARAPs and LC3s are involved in Rho GTPase dependent regulation of cytoskeleton remodeling (74,75). GTPases act as molecular switches in signaling pathways, constantly alternating between an active (GTP-bound) and inactive (GDP-bound) conformation. Replacement of GDP by GTP, induced through guanine nucleotide exchange factors (GEFs), activates GTPases while GTP hydrolysis to GDP, promoted by GTPase activating proteins (GAPs), inactivates them (76). GABARAP proteins affect the activity of the Rho GTPase RAC1 (Ras-related C3 botulinum toxin substrate 1) as it is required for degradation of the RAC1 activating protein TIAM1 (T-lymphoma invasion and metastasis-inducing protein 1) (75,77). The E3 ubiquitin ligase CUL3-KBTBD6/KBTBD7 is

anchored to vesicle membranes via KBTBD6/KBTBD7 binding to lipidated GABARAPs. This interaction is essential for ubiquitination of TIAM1 and its proteasomal degradation and therefore the negative regulation of RAC1 activity (75).

Furthermore, yeast-two hybrid screenings revealed LC3 interaction with AKAP13 (A-kinase anchor protein 13). AKAP13 acts as GEF for the Rho GTPase RhoA. Interaction of AKAP13 with LC3 prevents activation of RhoA by AKAP13 and thus, negatively regulates actin stress fiber formation (74,78).

GABARAPs and LC3s influence immune response

Studies revealed that ATG8 proteins are also involved in clearance of pathogens independent of xenophagy (79-84). One part of the cellular immune response, called phagocytosis, is the uptake of extracellular particles such as pathogens or immune complexes into the cell in single membrane vesicles (85). In LC3-associated phagocytosis (LAP) specific surface receptors induce inclusion of cargo in phagosomes. Lipidated ATG8 proteins are associated to the phagosomal membrane through parts of the autophagic machinery, forming the LAPosome. The ATG8 proteins on the vesicle surface mediate and notably enhance fusion between lysosomes and phagosomes and therefore cargo degradation (86-88).

3.3. UFM1 conjugation system

A valid method to study the functions of proteins, is the screening for interactors and characterization of interactions with other proteins. In a yeast-two hybrid screen Ubiquitin-like modifier activating enzyme 5 (UBA5), a member of the E1-like enzyme family, was identified as interactor of GABARAP proteins. UBA5 is part of an ubiquitin-like modification system called ufmylation, that covalently conjugates the Ub-like protein Ub fold modifier 1 (UFM1) to substrate proteins (**Fig. 4-I**) (89,90).

3.3.1. Pathway components

As many other Ubls, UFM1 shows a high similarity with ubiquitin in its tertiary structure but not in its amino acid sequence and is synthesized in an inactive precursor form (proUFM1).

Premature UFM1 consists of 85 amino acids with a molecular weight of 9.1 kDa (91). Removal of the last two C-terminal amino acids of proUFM1 by UFM1-specific protease 2 (UFSP2) results in mature UFM1 with an exposed glycine residue (**Fig. 4 II**) (92). This amino acid is adenylated by the adenylation domain of UBA5. In a next step UBA5 forms a thioester bond with UFM1 and AMP is released (**Fig. 4 III**) (93). Recently it was shown that UFM1 activation not only depends on this two-step mechanism but also on homodimerization of UBA5 and the UBA5-UFM1 interaction. Interestingly, UBA5 interaction with GABARAP proteins also occurs via the UFM1 interaction sequence (UIS) which is an atypical LIR motif (94-98). After activation, UFM1 is transferred to the E2 enzyme UFM1-conjugating enzyme 1 (UFC1) in a trans mechanism forming a thioester bond (**Fig. 4 IV**) (89,97).

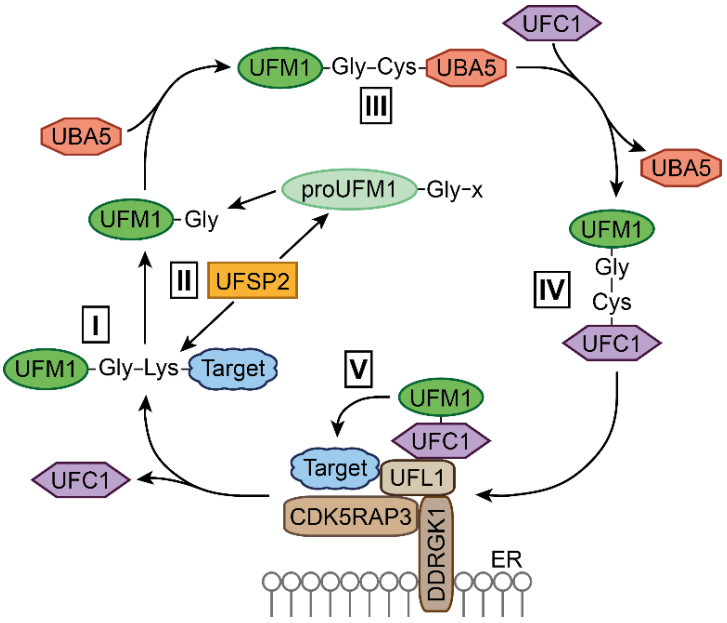

Figure 4: UFM1 conjugation: UFM1 is covalently attached to lysines of target proteins (**I**). Through cleavage at the C-terminal part of proUFM1 by UFSP2 a glycine residue is exposed and mature UFM1 is generated (**II**). UBA5 binds and activates UFM1 (**III**) which is then transferred to UFC1 (**IV**). UFC1-UFM1 interacts with UFL1-CDK5RAP3-DDRGK1 complex (**V**) followed by UFM1 conjugation to target proteins via UFL1 (**I**).

Finally, UFC1 binds the E3 UFM1-protein ligase 1 (UFL1) and UFM1 is conjugated to target proteins (**Fig. 4 V&I**) (99). As UFL1 does not have a typical E3 ligase domain, such as a RING finger, HECT or RBR domain, and is not directly binding to UFM1, it is still unknown how UFM1 is transferred to target proteins (99-101). Possibly UFL1 serves as a scaffold type E3-like ligase that recruits the E2 enzyme as well as the targets (**Fig. 4 V**) (99). Together with DDRGK domain-containing protein 1 (DDRGK1) and CDK5 regulatory subunit-associated protein 3 (CDK5RAP3), UFL1 forms a complex of approximately 440 kDa located at the cytosolic ER membrane (102-104). DDRGK1 (also known as C20orf116 and UFM1-binding protein 1 containing PIC domain (UFBP1)) was first discovered as UFM1 target (99) and is reported to

be involved in the regulation of ER homeostasis (105). Besides, DDRGK1 acts as scaffold protein for an Ub-E3-ligase system and promotes protein degradation via the ubiquitin-proteasome pathway independent of ufmylation events (106). CDK5RAP3 (alternative names: LZAP or C53) first identified as CDK5R1 (Cyclin-dependent kinase 5 activator 1) interacting protein (107), is involved in tumor suppression, cell survival and DNA damage response (108-110). Recently, CDK5RAP3 was also described as ER-phagy receptor binding to GABARAP or GABARAPL1 upon ribosome stalling and linking autophagy with the ufmylation pathway (102). Formation of UFL1-DDRGK1-CDK5RAP3 ternary complex is essential for some types of ufmylation events (102-104,111,112) but not for all (113), suggesting that DDRGK1 and CDK5RAP3 act as ufmylation adaptor. However, interaction of DDRGK1 via its C-terminal PIC domain with UFL1 is crucial for proper UFM1 conjugation (103), as it anchors UFL1 with its N-terminal transmembrane domain to the ER (103,113).

3.3.2. Cellular roles

Since the discovery of the UFM1 conjugation pathway in 2004 (89), it has been associated with many cellular pathways and several diseases, partially connected to the ER and its tasks. Nevertheless, the molecular function of ufmylation remains poorly understood (90,114-120). In the following paragraphs some of the known UFM1 targets and their cellular functions are introduced.

Ufmylation affecting the unfolded protein response

In many studies ufmylation has been connected to ER homeostasis and unfolded protein response (UPR). Upon ER stress, like the impairment of ER protein-folding and accumulation of misfolded proteins in the ER lumen, the UPR is activated to restore ER homeostasis. Reduction of protein synthesis, enlarged ER-folding capacity, ER associated degradation (ERAD), remodeling of ER sheets through ER-phagy and induction of apoptosis, as last resort, are part of the UPR. These pathways are coordinated and regulated by the three UPR sensors inositol-requiring enzyme 1 (IRE1), PKR-like ER protein kinase (PERK) and activating transcription factor 6 (ATF6) (121). Studies in different cell-types and animal models showed

that ER stress upregulates UFM1 expression, while deficiency of UFM1, UBA5, CDK5RAP3, DDRGK1 induces ER stress and activates the UPR (101,104,105,112-114,116,117). Further Liu and colleagues showed that in breast and liver cancer cell lines (MCF7, HepG2) as well as in murine hematopoietic stem cells DDRGK1 binds and stabilizes IRE1α in dependency of DDRGK1 K267 ufmylation. Deficiency of DDRGK1 promotes IRE1α degradation and PERK activation (105). This outcome has been challenged by another study performed in murine B cells also reporting PERK activation upon DDRGK1 deficiency but upregulated expression of IRE1α (122). These results were confirmed in MCF7 and HEPG2 cells as well as in the colon cancer cell line HECT116 by Liang and colleagues (113).

Ufmylation is required for ER-phagy

Recent studies showed a connection between ER-phagy and ufmylation. ER-phagy, a type of selective autophagy, involves the selective recognition and engulfment of parts of the ER in autophagosomes and their degradation in the lysosome. Activated upon ER stress, recovery from ER stress or starvation ER-phagy controls the ER volume but also the degradation of misfolded proteins inside the ER lumen which are unamenable to the ERAD system (123). In a genome-wide CRISPR screen it was shown that the ufmylation pathway is essential for starvation induced ER-phagy. Loss of DDRGK1 inhibited the degradation of ER-sheets but not of ER-tubules through ER-phagy and activation of the UPR (113).

Ufmylation is linked to the clearance of ribosome stalling

Current reports link ufmylation with the clearance of ribosomes stalled during co-translational translocation (111,124). Membrane and secreted proteins are synthesized by ribosomes directly into the ER lumen through the translocon, a protein conduction channel. Polyadenine stretches or mRNAs without stop codon can result in arrested translation and stalled ribosomes at the ER membrane (125). 60S ribosomal protein L26 (RPL26) is a ribosomal protein located on the large ribosomal subunit close to the translocon binding site. In dependency of two ufmylated lysines, RPL26 participates in dissolving the arrested ribosomes at the ER and facilitates the degradation of the incomplete proteins (111,124).

Ufmylation has been linked to promotion and inhibition of tumor formation

UFM1 conjugation has been assigned to promoting but also inhibiting functions in tumor growth (119,120). Ufmylation of ASC1 (activating signal cointegrator 1) was linked to activation and nuclear translocation of ER-α (estrogen receptor α) and breast cancer development (120). ER-α, a nuclear hormone receptor that regulates gene expression and thereby influences cell proliferation and differentiation, is expressed in more than 75% of breast cancer. Binding of 17β-estradiol to ER-α induces ER-α-dimer formation, its nuclear translocation and transcription of ER-α target genes (126). Yoo and colleagues showed in cells that under fed conditions transcriptional coactivator ASC1 is bound by UFSP2 but in the presence of 17β-estradiol ER-α replaces UFSP2 at the ASC1 binding site and allows polyufmylation of ASC1. UFM1 conjugation of ASC1 in turn promotes binding of other transcriptional coactivators and expression of ER-α target genes and thus, leads to tumor growth (120). In contrast, a recent study showed that multi-mono-ufmylation at four lysine residues prevents p53 from degradation upon DNA damage and promotes p53's tumor suppressor functions (119). p53 is a DNA binding protein and regulates the expression of genes controlling cell cycle progression and apoptosis. Under normal conditions p53 is ubiquitinated by the E3 ligase MDM2 (mouse double minute 2 homologue) and degraded through the proteasome (127). Upon DNA damage, UFL1 replaces MDM2 and p53 is stabilized through UFM1 conjugation (119).

DNA damage response

Recently, it was shown that ufmylation plays an important role in the repair of DNA double-strand breaks (DSBs) (115,128,129). Endogenous and exogenous genotoxic stress such as oxidative stress, UV light radiation or genotoxic agents can induce DNA damage such as DSBs or nucleotide modifications. To protect the cell against genomic instability which is linked to tumorigenesis and other diseases, DNA repair mechanisms are activated by DNA damage sensing (130). MRE11-RAD50-NBS1 (MRN) complex formation upon DSBs activates a major player of DSB repair mechanism, namely the ATM (ataxia-telangiectasia mutated) kinase that controls recruitment of DNA repair proteins and cell cycle checkpoints (131,132). MRN

complex assembly and activation of ATM is dependent on ufmylation of lysine K228 in MRE11 (double-strand break repair protein MRE11) (115). Additionally, ATM activity is further enhanced through activation of Tip60 which involves ufmylation of histone H4 (128,129).

UFM1 pathway components are crucial for erythrocyte differentiation and embryogenesis

The development of mature erythrocytes from hematopoietic stem cells is termed erythropoiesis (133). Knockout of either UBA5, UFL1, DDRGK1 or CDK5RAP3 in mice affected liver development, impaired erythropoiesis and led to prenatal lethality, while heterozygous mice were viable and appeared normal (112,116,134,135). Additionally, adult mice with conditional inducible UFL1 or DDRGK1 knockout exhibited defective hematopoiesis (116,135). Collectively, these data suggest that ufmylation plays an important role in regulation of murine hematopoiesis and development. However, the exact role of ufmylation in this context remains elusive.

3.4. Lipid droplets

Lipid droplets (LDs), found in single- and multi-celled organisms, are organelles for storage of fatty acids (136). Besides their function as lipid supplier for energy metabolism (137,138) and membrane synthesis (139,140), LDs are involved in lipid trafficking (141,142), viral replication (143), protein degradation (144,145), protection against lipotoxicity (146,147) and ER homeostasis (148-151). Further, LDs have been linked to lipid related (for instance obesity and neutral lipid storage disease) (152) and lipid unrelated diseases (for instance neuropathies and viral hepatitis) (153,154). Emerging from the ER, LDs consist of a phospholipid monolayer associated with integral and peripheral proteins, that encircles a core of neutral lipids mostly sterol esters and triacylglycerols (TAG) (**Fig. 5-V**) (155,156). After budding, LDs can move bidirectional along microtubules and built-up membrane contact sites with the ER and other organelles such as mitochondria and peroxisomes (141,142,157-160). Positioning in close proximity and formation of membrane contact sites between these organelles enable communication and metabolite transfer independent of vesicular trafficking (161).

3.4.1. Lipid droplet formation

LDs are either formed through splitting from existing LDs or de novo at the ER membrane. Biogenesis of newly formed LDs starts with the activation of fatty acids through esterification with coenzyme A (CoA) followed by synthesis of neutral lipids, mostly TAGs and sterol esters (**Fig. 5 I**) (155). Reaching a concentration of 5-10 mol%, neutral lipids coalesce between the leaflets of the cytosolic and luminal ER bilayer and form lipid lenses (**Fig. 5 II**) (162-164). Lipid lenses grow through further neutral lipid synthesis as well as fusion of two lipid lenses (**Fig. 5 III**) and finally bud from the ER into the cytosol (**Fig. 5 IV**) (165). Thereby, the LD surrounding phospholipid monolayer originates from the cytosolic leaflet of the ER membrane (**Fig. 5 V**) (166). LD budding is promoted by the phospholipid monolayer composition. Phospholipids influence membrane surface tension and its decrease induces LD budding. Furthermore, the geometry of some phospholipids favors the rounded shape of lipid droplets (167,168). Through lipid bridges LDs can also stay connected with the ER to exchange lipids (169-172). Separated from the ER LDs cycle between growth and consumption depending on the nutrient status of the cell (173). Growth is promoted through synthesis of TAGs on the LD surface (172), fusion of two LDs (**Fig. 5 VI**) (174,175) and transfer of lipids between LDs and the ER (171), while LDs are degraded through lipolysis and lipophagy (**Fig. 5 VII**&**VIII**) (176-180). In lipolysis lipases associate with LDs and hydrolyze ester bonds between the fatty acid chains and the glycerol backbone of TAGs. Adipose triglyceride lipase (ATGL), hormone sensitive lipase (HSL) and monoglyceride lipase (MGL) generate stepwise diacylglycerols, monoglycerides, glycerol and fatty acids from TAGs (180-183). Free fatty acids are directed to LD-connected mitochondria and degraded by β-oxidation, producing energy in form of ATP (**Fig. 5 VII**) (141). In recent years, it has become evident that also autophagy participates in LD breakdown. Upon induction of lipophagy, LDs are selectively targeted and engulfed by autophagosomes and numbers of LDs are reduced. However, the autophagy receptor targeting LDs is still unknown (**Fig. 5 VIII**) (178,184-186). Lipophagy is regulated through deacetylation of important autophagy proteins, including ATG5, ATG7 and ATG8, through SIRT1 (NAD-dependent protein deacetylase sirtuin-1). SIRT1 activation in turn is promoted by

ATGL1 (187-189). Recently, Schott and colleagues suggested a model in which LD uptake by autophagosomes is restricted through LD diameter to <1 µm. Further, they mostly found ATGL1 on large LD, promoting formation of smaller LDs that can be engulfed by autophagosomes (190). Interestingly, bulk autophagy activated during nutrient deprivation leads to unselective degradation of cellular organelles. The free fatty acids and lipids from the membrane organelles are then stored as TAGs in LDs (137,147,191).

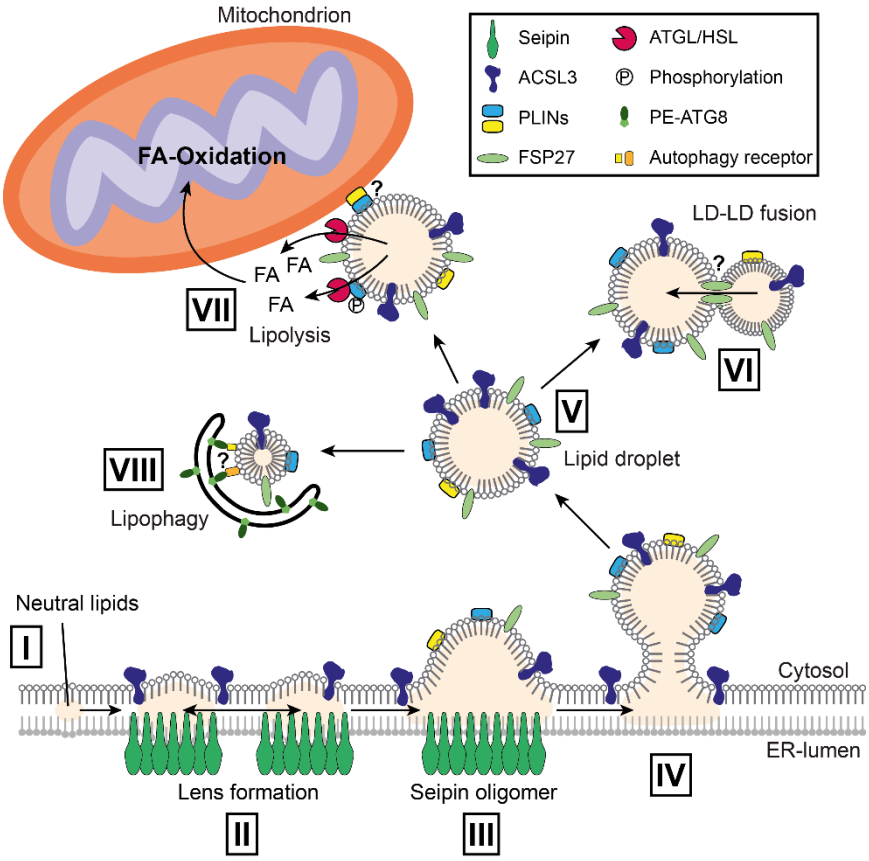

Figure 5: LD formation and degradation: LD biogenesis is started through the synthesis of TGA and sterol esters and their accumulation between the leaflets of the ER bilayer (**I**). ACSL3 and Seipin enrich early at LD-formation sites at the ER, facilitating LD biogenesis (**II**). Neutral lipids coalesce to lipid lenses (**II**) which grow through fusion of two lipid lenses and ongoing neutral lipid synthesis (**III**&**VI**). LDs, emerging from the ER into the cytosol, consist of a neutral lipid core surrounded by a phospholipid monolayer. The phospholipid monolayer is associated with peripheral and integral proteins promoting LD biogenesis and function (**V**). LD growth is promoted by LD-LD fusion. It is suggested that FSP27 is enriched at LD-LD contact sites forming a channel like structure and promoting lipid transfer (**VI**). LDs are degraded through lipolysis and lipophagy (**VII**&**VIII**). During lipolysis ester bonds in neutral lipids are hydrolyzed by lipases generating fatty acids (FA) which are directed to mitochondria for β-oxidation. Degradation is facilitated by phosphorylation of PLINs. It is suggested that PLINs enriched at LD-mitochondrion contact sites might mediate tethering upon lipolysis (**VII**). Small LDs are also degraded via lipophagy. The autophagy receptors for selective targeting of LDs are still unknown (**VIII**).

3.4.2. Lipid droplet surface proteins and their functions

The phospholipid monolayer of LDs is loaded with peripheral and integral proteins that contribute to biogenesis, maturation and stability of LDs in dependency of nutrient availability and cell type. Mass spectrometry analysis of LD enriched cell fractions unraveled the LD proteomes of different cell types that consist of approximately 100-150 proteins. Detected proteins are mainly involved in metabolism such as lipid and sterol biosynthesis and lipolysis as well as in vesicular trafficking, protein degradation (ERAD) and membrane organization (192-197). LD associated proteins are categorized in proteins stably inserted into the ER membrane that diffuse via membrane bridges to LDs (class I) and proteins that are recruited from the cytosol to LDs (class II) (136,198). Class I proteins are integrated halfway into the LD monolayer via hydrophobic hairpins facing the cytosol while class II proteins are typically associated with LD through amphipathic helices or lipid-anchors (172,199,200). It still remains elusive what mechanism targets proteins to LDs.

Perilipin protein family regulates lipolysis

Some of the most abundant structural proteins on LD surface are members of the perilipin protein family. Perilipins (PLINs) act as scaffold proteins and are involved in lipid metabolism and storage. PLIN2 and PLIN3 are produced broadly in most tissues while PLIN1 is only expressed in adipocytes, PLIN4 is mainly found in white adipose tissue and PLIN5 is expressed in brown adipose tissue, the liver, cardiac and skeletal muscle (201,202). Lipolysis is predominantly prevented by PLIN1 and PLIN5 through sequestering lipases (ATGL) or their cofactors. Phosphorylation of PLIN1 and PLIN5 results in release of bound proteins and provides a docking site for lipases and thus, inducing lipolysis (203-206). PLIN1 and PLIN5 were both found at mitochondria-LD contact sites and might mediate tethering during lipolysis (**Fig. 5-VI**) (160,206,207). PLIN2 inhibits lipolysis in a moderate way by preventing access of lipases to LDs and knockdown of PLIN2 changes lipid composition of LDs in mice (196). PLIN3 was suggested to influence LD biogenesis in absence of PLIN1 and PLIN5 (208) while PLIN4 interacts with neutral lipids and might be able to replace the LD monolayer (209).

Seipins promote LD growth

The multi-pass membrane protein Seipin, located at the ER membrane and on lipid droplets, is a key protein for normal LD biogenesis. Depletion of Seipin leads to defects in de novo LD formation and is suggested to define sites for LD biogenesis at the ER (**Fig. 5-II**). Additionally, Seipin is present at ER-LD contact sites and facilitates neutral lipid transfer from the ER to LDs and thus, is involved in LD size regulation (170,171,210-212).

CIDE protein family mediates LD-LD fusion

The Cell death-inducing DNA fragmentation factor alpha (DFFA)-like effector (CIDE) protein family comprises three members CIDEA, CIDEB and FSP27 (alternative name: CIDEC) which all have been found associated with LDs. While CIDEB is mainly expressed in liver tissue, CIDEA and FSP27 (Cell death activator CIDE-3) are found in adipose tissue (213-216). It is suggested that CIDE proteins enrich at LD-LD contact sites and form a pore like structure. This promotes lipid transfer from smaller to larger LDs leading to LD fusion and growth (**Fig. 5-VI**) (174,215,217). FSP27 mediated LD fusion and growth is further enhanced by interaction with PLIN1 (218). Additionally, FSP27 was found to inhibit lipolysis by suppressing promotor activity of ATGL and direct binding to ATGL inhibiting lipase activity (219,220).

Fat inducing transcript (FIT) proteins influence LD budding

FIT1 and FIT2 belong to the FIT protein family and are integral ER membrane proteins. While FIT2 is ubiquitously expressed in most tissues, FIT1 is only found in skeletal muscle and heart cells (221,222). Collectively, it was shown that FIT proteins participate in LD biogenesis since depletion of FIT proteins decreases LD size and numbers and prevent LD from budding, and thereby keeping them embedded in the ER membrane (162,222). Recently, it was shown that FIT2 is an acyl-CoA diphosphatase facing the ER lumen and required for glycerolipid synthesis (221,223,224). However, to date it is not clear how FIT2 enzyme function contributes to normal LD biogenesis and budding.

Long-chain-fatty-acid CoA ligase 3 (ACSL3) is essential for LD biogenesis

ACSL3 belongs to the acyl-CoA synthetase (ACS) family and is an important player in LD biogenesis and regulation (155,225). In a two-step process ACSL3 activates long-chain fatty acids and generates acyl-CoA which is necessary for both neutral lipid synthesis and β-oxidation (225-228). ACSL3 is a single-pass type III membrane protein located at the outer leaflet of the ER membrane with both N- and C-terminal parts reaching into the cytosol, and was found associated with LDs (**Fig. 5**) (229,230). Time laps experiments paired with confocal microscopy showed that ACSL3 accumulates very early at ER microdomains where LDs are formed (169,231). Loss of ACSL3 reduced nucleation and size of LDs while increased expression of ACSL3 elevated the numbers of pre- and mature LDs. ACSL1 and ACSL4 also found on LDs did not alter LD biogenesis upon their depletion or overexpression underlining the importance of ACSL3 in LD nucleation and biogenesis (169,194,231). Interestingly, expression of enzymatic deficient ACSL3 in cells impaired LD growth and expansion but not LD nucleation. This supports the notion that even though enzymatic activity of ACSL3 is crucial for LD biogenesis other features of ACSL3 are involved in LD nucleation (169). Taken together, ACSL3 influences LD nucleation, participates in neutral lipid synthesis for LD growth and promotes fatty acid β-oxidation and thus, plays an important role in lipid homeostasis.

3.5. CRISPR-Cas

Short repetitive DNA sequences separated by non-repeating sequences (spacers) are named ‘clustered regularly interspaced short palindromic repeats’ (CRISPR) and are found in the genome of approximately 80% of archaea and 45% of bacteria (232,233). Spacers are in the prokaryotic genome integrated external DNA fragments originating from bacteriophages and other extrachromosomal elements such as plasmids and transposons (234-236). An AT-rich leader sequence that acts as promotor, flanks the CRISPR array (**Fig. 6 II**) (233). CRISPR-associated proteins (Cas) and CRISPR arrays are responsible for memorizing initial infections as well as for recognizing and repelling reoccurring infections. It is the only known adaptive immune response in prokaryotes (237). In recent years, the unique mode of action of targeting

and cutting specific DNA sequences was adapted as versatile tool for genome editing in various studies of cellular pathways and diseases (238-242).

3.5.1. Mechanism of action of CRISPR-Cas systems in prokaryotes

The first CRISPR sequence has been identified in the intergenic region upstream of the Iap gene of *Escherichia coli* in 1987 (243). Since then, many studies revealed the mechanisms of CRISPR-Cas which is divided into adaptation, expression, maturation and interference (**Fig. 6**) (244,245). There are two major classes in CRISPR-Cas systems which are classified in six types and several sub-types. The division of the classes is based on the effector Cas proteins which carry out expression, maturation and interference states. While in class I multisubunit protein complexes carry out these processes, a single large polypeptide is sufficient in class II (246-248). For all CRISPR-Cas systems a multisubunit complex including Cas1 and Cas2 proteins is essential for each step of spacer acquisition (249,250). Foreign DNA pieces are recognized in dependency of a proto-spacer adjacent motifs (PAM) and processed by the Cas1-Cas2 protein complex to approximately 33 base pairs (bp) long protospacers (**Fig. 6 I**&**II**) (249,251,252). The protospacer is integrated as new spacer at the first CRISPR repeat along with the duplication of the repeat (250,253). Transcription of CRISPR arrays promotes the production of long precursor CRISPR RNAs (pre-crRNAs) (**Fig. 6 III**) which are cleaved within the repeat sequences to obtain mature crRNAs (**Fig. 6 IV-VII**) (254-257). Next, Cas-crRNA complexes are formed that identify target nucleic acids through classical base pairing. After spacer recognition, Cas proteins induce DNA or RNA strand breaks promoting the clearance of the extracellular elements (**Fig. 6 VIII-XI**) (239,256,258-262).

In class I systems mainly Cas6 cleaves pre-crRNAs (**Fig. 6 IV**&**V**), while the Cas-crRNA complex is formed of several Cas proteins depending on the CRISPR-Cas type (**Fig. 6 VIII**&**IX**) (257,263-265). In contrary, a single Cas protein (Cas12 or Cas13) is responsible for pre-crRNA maturation and DNA interference of the class II CRISPR-Cas systems (**Fig. 6 VII**&**XI**) with the exception of the CRISPR-Cas9 system (254-256). Here, a non-coding RNA called transactivating crRNA (tracrRNA) partially complementary with pre-crRNA repeats associates

with pre-crRNA. Base pairing triggers Cas9 binding and cleavage of pre-crRNA to mature crRNAs through RNAase III (**Fig. 6 VI**). Cas9 is then guided to target DNA by the tracrRNA:crRNA duplex to induce double strand breaks (**Fig. 6 X**) (239,254).

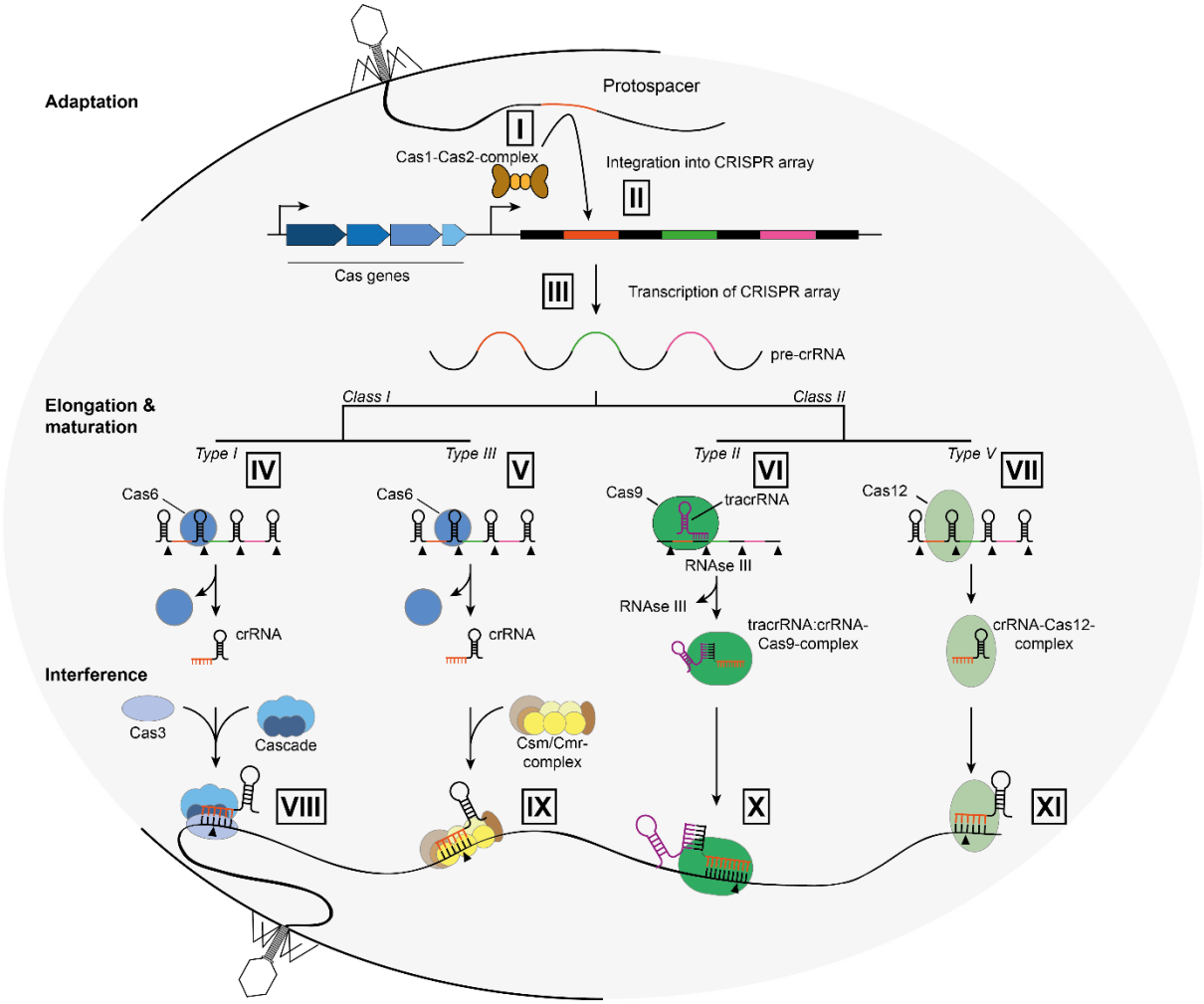

Figure 6: Mechanism of CRISPR-Cas systems: Adaptation (**I&II**): Viral DNA pieces are recognized (**I**) and integrated into the first CRISPR repeat of a CRISPR array by Cas1-Cas2 complex (**II**). **Elongation and maturation** (**III-VII**): Long pre-crRNAs are produced upon transcription of a CRISPR-array (**III**). In class I CRISPR systems mostly Cas6 cleaves pre-crRNA resulting in crRNA (**IV&V**), while in class II crRNA maturation runs differently. In the type II system Cas9 is recruited by tracrRNA to pre-crRNA which is processed to crRNA through RNAse III, whereas in type V a single Cas12 protein is sufficient to cut pre-crRNA. **Interference** (**VIII-XI**): Invasive nucleic acids are recognized and bound by crRNA. Strand breaks are induced by Cas proteins. In class I systems multiprotein complexes such as Cascade (type I; **VIII**) or Csm/Cmr-complex (type III; **IX**), formed by several Cas proteins, are responsible for the induction of strand breaks. Complexes of tracrRNA:crRNA-Cas9 (type II; **X**), crRNA-Cas12 (type V; **XI**) or crRNA-Cas13 (type VI, not shown) are promoting recognition and cleavage of DNA or RNA in class II systems.

3.5.2. CRISPR-Cas adapted for gene editing

Shortly after the discovery of the CRISPR-Cas9 system, single guide RNAs (sgRNAs) have been constructed by hybridization of tracrRNA and crRNA. These hybrid RNAs mediate cleavage of the complementary DNA sequence through Cas9 (239,254). Since then, the class II CRISPR-Cas systems (Cas9, Cas12, Cas13) are used for manipulation of DNA or RNA in many kinds of organisms (266-273). For genome editing with the Cas9-system Cas9 and sgRNA are delivered into cells through viral vectors, transfection or electroporation (238,241,274). The target DNA sequence is identified by the sgRNA in dependency of a PAM site (275). Cas9 introduces a DSB at the identified site which is repaired through endogenous DNA repair pathways either non-homologous end joining (NHEJ) or homology directed repair (HDR) (276). During NHEJ the two DNA termini are processed by polymerases and/or nucleases which results in random nucleotide insertions or deletions followed by ligation of the DNA strands (277). These insertions or deletions can lead to changes in the promotor or coding region of a gene leading to production of nonfunctional proteins or complete prevention of transcription and therefore, gene knockout. In HDR a homologous DNA sequence is used as template for DNA repair and thus, specific insertion, point mutations or deletions can be generated to create knockouts or knockins (276).

Due to its simplicity of application and usability in a wide range of cells and organisms, the CRISPR-Cas technology is used in many research areas (278,279). Generation of sgRNA libraries enables genomic screenings to identify genetic functions or perform drug target validations (280-283). Molecular diagnostic platforms take advantage of the sgRNAs ability to identify specific DNAs and RNAs to detect for example viral infections (262,284-286). Further, studies in mice, human cells and embryos demonstrated the potential to cure genetic diseases through modification or elimination of associated genes or chromosomes with CRISPR-Cas (287-292).

3.6. Aim of the study

Other than in yeast there are at least six genes in the human genome that code for ATG8 proteins which might have evolved through duplications (17). GABARAPs or LC3s have been studied mostly using cell lines overexpressing one of the hATG8 proteins (293,294). The discoveries from these experiments showed that the hATG8 protein family exhibit functions within as well as beyond autophagy. However, overexpression of proteins decreases their binding specificity due to their high abundance. This is especially problematic for GABARAPs and LC3s as they have a high structural similarity and overexpressed hATG8 protein might take over functions of the other family members. Besides, transient overexpression of LC3 by transfection tend to form aggregates independent of autophagy (295). It was also reported, that immunolabeling of LC3 can lead to variable nuclear staining in dependency of the reagents used for permeabilization and antibody used for immunodetection (296). Also, generating isoform specific antibodies for GABARAPs and LC3s is difficult since they exhibit a high similarity in structure and sequence within the subfamilies (17). To unravel protein or subfamily specific functions of GABARAPs and LC3s, it is important to overcome the hurdle of unspecific protein binding or aggregation due to overexpression or the lack of isoform-specific antibodies. Thus, tools such as AIM/LIR based fluorescence sensors detecting subfamily specific hATG8 members (297,298) or HeLa cell lines with triple or hexa knockouts of GABARAPs and LC3s (56) facilitate functional studies of GABARAPs and LC3s. Here, we sought to employ CRISPR/Cas9 to engineer cell lines with the epitope tag hemagglutinin (HA) fused to the N-terminus of endogenous GABARAPs and LC3s. These cell lines were then used to study protein specific functions of hATG8s on endogenous level using different biochemical cell biological and proteomics techniques.

4. Materials and Methods

4.1. Materials

4.1.1. Chemicals and Reagents

Acetic acid/Merck/100063

Acetic acid/Sigma-Aldrich/49199

Acetone/Merck/100014

Acetonitrile (ACN)/Roth/AE70

Acrylamide 4K Solution (30%)/PanReac AppliChem/A0951

Ammonium bicarbonate (ABC)/Sigma-Aldrich/09830

Ammonium peroxydisulphate (APS)/ Roth/9592

Ampicillin sodium salt/Roth/K029

ATG7 Inhibitor/Takeda - ML00792183

Bacto Agar/BD Diagnostic Systems/214030

Bacto Tryptone/BD Diagnostic Systems/ 21699

Bacto Yeast Extract/BD Diagnostic Systems/212720

Bafilomycin A1 (BafA1)/Biomol/Cay11038

BbsI/New England Biolabs/R0539

BC Assay Reagent A/Interchim/UP95424A

BC Assay Reagent B/Interchim/UP95425A

Benzonase Nuclease HC/Millipore/71205

Betaine/Sigma-Aldrich/61962

Blasticidine/Invivo Gen/ant-bl-1

Bovine Serum Albumin (BSA)/Sigma-Aldrich/A8022

Bromophenol blue/Thermo Fisher/32712

Bortezomib (Btz)/LC laboratories/B-1408

BsmBI/New England BioLabs/R0739

Carbenicillin disodium salt/PanReac AppliChem/A1491

Chloramphenicol/Sigma-Aldrich/C0378

cOmplete EDTA-free Protease Inhibitor Cocktail/Roche/04693132001

Coomassie Brilliant blue R/PanReac AppliChem/A1092

Dimethyl sulfoxide (DMSO) Cell culture grade/PanReac AppliChem/A3672

Dithiothreitol (DTT)/Biomol/04010

DL-Dithiothreitol/Sigma-Aldrich/43815

Doxycycline/Sigma-Aldrich/D9891

Dulbecco`s modified Eagles`s Medium (DMEM) (1x) + GlutaMAX-I/Gibco/ 61965026

DMEM for SILAC/Thermo Fisher/88364

DNA Gel Loading Dye (6x)/Thermo Scientific/R0611

Dulbecco's Phosphate buffered Saline (PBS)/Gibco/14190144

Earle's balanced salt solution (EBSS)/Life technologies/24010-043

Ethanol (EtOH)/Roth/9065

Fetal Bovine Serum (FBS)/Gibco/ 10270106

Fetal Bovine Serum, dialyzed/Gibco/ 26400044

Fluorescence mounting medium/Dako/ S3023

Formic acid (FA)/Merck/100264

FuGENE^{R} HD Transfection Reagent/ Promega E2311

Gateway^{TM} BP Clonase^{TM} II Enzyme mix/Thermo Fisher/11789100

Gateway^{TM} LR Clonase^{TM} II Enzyme mix/Thermo Fisher/11791020

GeneRuler 100bp DNA Ladder/Thermo Scientific/SM0241

Glycerol/Roth/3783

Glycine/PanReac AppliChem/131340

Hydrochloric acid 32%/Merck/100319

IGEPAL CA-630 (NP-40)/Sigma-Aldrich/ I8896

Influenza Hemagglutinin (HA) Peptide/ Sigma-Aldrich/I2149

Iodoacetamide (IAA)/Sigma-Aldrich/I1149

Isopropyl β-D-1-thiogalactopyranoside/ Sigma-Aldrich/I5502

Kanamycin sulphate/Roth/T832

1 kb DNA Ladder/NEB/N3232

KOD Hot Start DNA Polymerase/Sigma-Aldrich/71086

Lysozyme/Merck/105281

L-Arginine/Sigma-Aldrich/A8094

L-Arginine:HCL (13C6, 99%; 15N4, 99%)/ Cambridge Isotope Laboratories/ CNLM-539-H-PK

L-Glutamine 200mM/Gibco/25030024

L-Glutathione reduced/Sigma-Aldrich/ G4251

L-Lysine monohydrochloride/Sigma-Aldrich/L8662

L-Lysine:2HCL (13C6, 99%; 15N2, 99%)/ Cambridge Isotope Laboratories/CNLM-291-H-PK

Lipofectamine 2000/Invitrogen/11668019

Lipofectamine RNAiMAX/ Invitrogen/ 13778100

Lumigen ECL Ultra/Lumigen/TMA-6

Methanol/Merck/106009

Methanol/Roth/AE71

MIDORI Green Advance/Genetics/MG04

Molecular Probes ProLong Gold Antifade Mountant/Invitrogen/P36931

Oleic acid/ Millipore/4954

One-Taq DNA Polymerase/New England BioLabs/M0480

Optimal modified Eagle`s Medium (Opti-MEM) I + GlutMAX-I/Gibco/51985026

Paraformaldehyde (PFA) solution 4% in PBS/Chemcruz/sc-281692

Phenol non stabilized:Chloroform:Isoamyl Alcohol 25:24:1/PanReac AppliChem/ A0944

Phenylmethanesulfonyl fluoride (PMFS)/Sigma-Aldrich/P7626

PhosSTOP/Roche/04906837001

PIPES/Sigma-Aldrich/P6757

Polybrene Transfection Reagent/ Millipore/TR-1003-G

Ponceau S/Sigma-Aldrich/P3504

Powdered milk/Roth/T145

2-Propanol/Merck/109634

Puromycin dihydrochloride/Sigma-Aldrich/P8833

Q5 Hot Start High-Fidelity DNA Polymerase/New England BioLabs/M0493

SeaKem LE Agarose/Lonza/50004

Sequencing Grade Modified Trypsin/Promega/V5113

Sodium acetate trihydrate/Roth/6779

Sodium chloride/Roth/3957

Sodium deoxycholate/Sigma-Aldrich/D6750

Sodium dodecyl sulfate (SDS)/Serva/ 20765

Sodium pyruvate 100mM/Gibco/11360039

Spectinomycin dihydrochloride pentahydrate/Sigma-Aldrich/S4014

T4 DNA Ligase/New England BioLabs/ M020

TEMED/Roth/2367

Thiourea/Sigma-Aldrich/T7875

Torin1/Tocris/4247

Trichloroacetic acid solution (TCA)/Sigma-Aldrich/T0699

Trifluoroacetic acid (TFA)/Sigma-Aldrich/ 302031

0.25% Trypsin-ETDA (1x)/Gibco/25200056

Tris-EDTA buffer solution/Sigma-Aldrich/ 93302

Tris ultrapure/PanReac AppliChem/A1086

Triton X-100/Millipore/108603

Titriplex III (ethylenedinitrilotetraacetic acid/EDTA)/Merck/108418

Tropix I-BLOCK/Invitrogen/T2015

Tween-20/Sigma-Aldrich/822184

Urea/Serva/24524

Water LC-MS Grade/Roth/AE72

Western Lightning Plus-ECL/Perkin Elmer/ NEL105001EA

4.1.2. Materials

Amersham Protran 0.45 µm NC/GE Healthcare Life science/10600002

Blotting Paper/Macherey-Nagel/MN742112

Capillary micro tips/Biozym/729005

Caps/Agilent/5181-1211

Countess cell counting chamber slides/ Invitrogen/C10228

CryoTubes/VWR/479-1261

Cuvettes/Sarstedt/537-046290

Dounce homogenizer/VWR/432-1270

Empore SPE Disks C18/Sigma/66883-U

Gel Loading Tips/Sorenson/28480

Glass vials/Agilent/5183-4494

Glutathione Sepharose 4B (GST)/GE Healthcare/ 17-0756-01

Microfuge Tube/Beckman coulter/357448

Microscope cover glasses/Marienfeld/ 0111550

Microscope slides/Fisher Scientific/ 10150491

Mini-PROTEAN short plates/Bio-Rad/ 1653308

Mini-PROTEAN spacer plates/Bio-Rad/ 1653311

4-10% Mini-PROTEAN TGX gels/Bio-Rad/ 456-1094

Monoclonal Anti-HA-Agarose/Millipore/ A2095

Mr Frosty cryo box/Thermo Scientific/ 5100-0001

Nunc Cell-Culture treated multidishes 6/ Thermo Scientific/140675

Nunc Cell-Culture treated multidishes 12/ Thermo Scientific/150628

Nunc Cell-Culture treated multidishes 24/ Thermo Scientific/142475

Nunc Cell Culture Petri Dishes 100x17/ Thermo Scientific/150350

Nunc Cell Culture Petri Dishes 150x21/ Thermo Scientific/168381

96 Nunc-Immuno Plate/Thermo Scientific/ 442404

Nunc MicroWell 96-well/Thermo Scientific/ 167008

pH test stripe/Macherey-Nagel/92110

Pierce anti-c-myc-agarose/Thermo Scientific/20168

ReproSil-Pur 120 C18-AQ 1.9µm/Dr. Maisch/r119.aq.

SilicaTip Emitters/New Objective/FS-360-75-8-N-20

Slide-A-Lyzer Dialysis Cassette-20000 MWCO/Thermo Scientific/66003

Sterile syringe filter 0.45µm/VWR/514-0075

Super RX-N/Fujifilm/47410 19289

Thermo Scientific Abgene 96 well polypropylene deep well storage plate/Thermo Scientific/AB-1127

Ultra-clear centrifuge tubes/Beckman coulter/344058

Ultrafree-CL HV Filter – 0.45µm/Millipore/ UFC40HV00

Ultrafree-CL HV Filter – 0.45µm/Millipore/ UFC30HV00

Vial inserts/Agilent/5181-8872

4.1.3. Buffer and Solutions

Lysogeny broth (LB)-medium [pH 7.0]: 10 g/L bacto trypton, 5 g/L bacto yeast extract, 5 g/L NaCl

LB-Plates: 12 g/L bacto agar in LB-medium

Transformation buffer [pH 6.6]: 50 mM $CaCl_2$, 10 mM PIPES, 15% Glycerol

PBS [pH 7.4]: 0.6 mM Na_2HPO_4 x $2H_2O$, 0.018 mM KH_2PO_4, 0.27 mM KCl, 1.36 M NaCl

PEI transfection reagent: 100 mM PEI dissolved in water at 70 °C, set [pH 7.0] with HCl

TNE: 100 mM NaCl, 10 mM Tris-HCl [pH 8.0]. 1 mM EDTA, 1.5% SDS

TAE [pH 8.3]: 40 mM Tris-HCl, 1 mM EDTA, 0.1% Acetic acid

TBS [pH 7.6]: 20 mM Tris-HCl, 150 mM NaCl

TBS-T: TBS, 1% Tween-20

SDS-PHAGE-running-buffer: 25 mM Tris-HCl, 190 mM Glycine, 0.1% SDS

Western blot-transfer-buffer: 25 mM Tris-HCl, 190 mM Glycine

Ponceau: 0.2% Ponceau S (m/v), 3% acetic acid

3x Lämmli SDS-PAGE loading dye: 200 mM Tris-HCl [pH 6.8], 6% SDS, 20% Glycerol, 10% DTT (m/v), Bromophenol Blue

Protein purification and pulldown assay:

Wash buffer (Protein purification): 50 mM Tris-HCl [pH 8.0], 150 mM NaCl

Coomassie: 0.1% Brilliant Blue R, 40% EtOH, 10% Acetic acid

Destainer (Coomassie): 40% EtOH, 10% Acetic acid

Storage buffer (Protein purification): 50 mM Tris-HCl [pH 8.0], 150 mM NaCl, 5% Glycerol

Elution buffer (Protein purification): 10 mM Reduced glutathione, 50 mM Tris-HCl [pH 8.0]

Lysis-buffer:

RIPA lysis buffer: 50 mM Tris-HCl [pH 7.4], 150 mM NaCl, 0.5% SDS, 1% NP-40, 0.5% Natrium Deoxycholate, 1x protease inhibitor, 1x phosphatase inhibitor

Glycerol lysis buffer: 20 mM Tris-HCl [pH 7.4], 150 mM NaCl, 5 mM EDTA, 0.5% Triton X-100, 10% Glycerol, 1x protease inhibitor, 1x phosphatase inhibitor

MCLB buffer: 50 mM Tris-HCl [pH 7.4], 150 mM NaCl, 0.5% NP-40, 1x protease inhibitor, 1x phosphatase inhibitor

Incorporation check:

Denaturation buffer: 6 M Urea, 2 M Thiourea, 10 mM Tris-HCl [pH 8.0]

In-gel digestion buffers:

Wash buffer: 50 mM ABC, 50% EtOH

Reduction buffer: 10 mM DTT, 50 mM ABC

Alkylation buffer: 55 mM IAA, 50 mM ABC

Trypsin solution: 12 ng/µl Trypsin, 50 mM ABC

Elution buffer 1: 30% ACN, 3% TFA in LC-MS grade water

Elution buffer 2: 70% ACN in LC-MS grade water

Elution buffer 3: 100% ACN in LC-MS grade water

Binding buffer: 5% ACN, 1% TFA in LC-MS grade water

In-solution buffers:

HA-peptide: 250 µg/ml HA-peptide in PBS

Trypsin solution: 10% ACN, 50 mM ABC, 8 ng/ul Trypsin

Stop solution: 5% ACN, 5% FA

Dissolving/binding buffer: 5% ACN, 1% TFA in LC-MS grade water

Stage tip buffers:

Buffer A: 0.1% FA in LC-MS grade water

Buffer B: 80% ACN, 0.1% FA in LC-MS grade water

4.1.4. Kits

GenElute HP plasmid miniprep kit/Sigma-Aldrich/NA0160-1KT

GenElute HP plasmid maxiprep kit/Sigma-Aldrich/NA0310-1KT

QIAquick gel extraction kit/Qiagen/28706

QIAquick PCR purification kit/Qiagen/28106

Genomic DNA mini kit/Thermo Scientific/K182002

Endoplasmic reticulum isolation kit/Sigma-Aldrich/ER0100

4.1.5. Mammalian cells and Bacteria

Table 1: Cell lines used in this study.

Mammalian cells			
Cell line	**Description**	**Company**	**Catalogue number**
HeLa	Human epithelial cells from the cervix	ATCC	CCL-2
HEK 293T	Human epithelial cells from the embryonic kidney	ATCC	CRL-3216

Table 2: Bacterial strains used in this study.

***E. coli* bacteria**	
Strain	**Description**
DB3.1	For transformation and amplification of empty Gateway entry and destination vectors
Rosetta	For transformation and protein expression of ORF-containing pDEST60 vector
TOP10	For transformation and amplification of ORF-containing Gateway entry and destination vectors
XL 10 Gold	For transformation and amplification of gRNA-containing px330 and pLentiCRISPR-HF1 vectors

4.1.6. Oligonucleotides

All oligonucleotides use in this study were purchased from Sigma Aldrich. For sequencing mutagenesis, gateway cloning and sgRNAs desalted oligonucleotides were used while for CRISPR DNA-templates HPLC purified oligonucleotides were ordered.

Table 3: Oligonucleotides used for sequencing.

Name	**Sequence**
For stable cell lines	
M13 forward	TGTAAAACGACGGCCAG
M13 reverse	CAGGAAACAGCTATGAC
CMV forward	CGCAAATGGGCGGTAGGCGTG
C-TAP-HA reverse	GGAATTCTAGGCGTAGTCG
U6 forward	GAGGGCCTATTTCCCATGATTCC
pET60 DEST forward	ATGCTTGAAGGAGCGGTTTT
pET60 DEST reverse	CTAGTTATTGCTCAGCGG
T7	TAATACGACTCACTATAG GG
ATG7-1	CAGAAGGAGTCACAGCTCTTCC
ATG7-2	CAAATGTCTGCTGCTTGGAG
ATG7-3	GACTTGTGTCCAAACCACCC
p62	AATCAGCTTCTGGTCCATCG
UBA5	GGAATCTGGGGTCAGTGAAA
ACSL3-1	AGGGCATCATTGTGCATACC
ACSL3-2	CACTGTGCGACAGCTTTGTT
TOLLIP	GACTTGTGTCCAAACCACCC
For endogenous cell lines	
Blasticidine forward	GCCATAGTGAAGGACAGTGATGGACAGCCG
Blasticidine reverse	GCCCTCCCACACATAACCAGAGGGCAGCAATTCACGAATC
GABARAP forward	ATCTTAGCGGGGGGGGCAGTCCCCGATAGT
GABARAP reverse	TTTCATCCTGGGTCCCAAGGACAGCAGTTT
GABARAPL1 forward	TCTGAGCACACCTTGACGTC
GABARAPL1 reverse	CGGGGTTTTAAAAGCTCTACAGTCTGGACG

Name	Sequence
GABARAPL2 forward	CATAACCAACTTCTTCGCCACCGCAGCCCA
GABARAPL2 reverse	GCATCTGTGTTCTGTGGGAGAAACAAACGGGGCTGAC
LC3B forward	TTTCGCCCATCGCGCACGCGCACACACCTG
LC3B reverse	AAAACCAGCCCTGAAGGTGACGCGCTGGGT
LC3C forward	CAGGTGGCGATTCCATTTCCATCAGAACTG
LC3C reverse	CCAGCAACTTCCTCTTGTCTGATTGCTGTG
ACSL3 forward	GTTGGTTGTGCATTTTGATGGATACGCA
Neon Green reverse	CTGTTAACTACCGCTACACCTACGAGG

Table 4: Oligonucleotides used for gateway cloning.

Name	Sequence forward	Sequence reverse
GABARAL2	GGGGACAACTTTGTACAAAAAAGTTGGC ATGAAGTGGATGTTCAAGGAGG	GGGGACAACTTTGTACAAGAAAGTTGGG CATCAGAAGCCAAAAGTGTTCTCTC
ACSL3	GGGGACAACTTTGTACAAAAAAGTTGGC ATGAATAACCACGTGTCTTCAAAA	GGGGACAACTTTGTACAAGAAAGTTGGG TATTATTTTCTTCCATACATTCGCTC
ACSL3 1-85	GGGGACAACTTTGTACAAAAAAGTTGGC ATGAATAACCACGTGTCTTCAAAA	GGGGACAACTTTGTACAAGAAAGTTGGA CATCCAGGGTATAATACTGAAGCC
ACSL3 86-718	GGGGACAACTTTGTACAAAAAAGTTGGC GATACTTTAGATAAAGTTTTTACATATGCA A	GGGGACAACTTTGTACAAGAAAGTTGGT CCATACATTCGCTCAATGTC

Table 5: Oligonucleotides used for mutagenesis.

Name	Sequence forward	Sequence reverse
GABARAPL2 ΔLBS	GAACTGAGCCACAGTGATATCAGATGGA ACTGCTGCCTTCCGTTTGTCAATGTCAAC AATCTGAGA	TCTCAGATTGTTGACATTGACAAACGGAA GGCAGCAGTTCCATCTGATATCACTGTG GCTCAGTTC
GABARAPL2 ΔUBS	AAGGATCCAGCTTCCTTCTGAAAAGGCG GCCGCCGCGGCTGTGGATAAGACAGTC CCACAGTCCAGC	GCTGGACTGTGGGACTGTCTTATCCACA GCCGCGGCGGCCGCCTTTTCAGAAGGAA GCTGGATCCTT
GABARAPL2 F77A	CTGTCTTATCCACAAACAGGGCGATCGC CTTTTCAGAAGGAA	TTCCTTCTGAAAAGGCGATCGCCCTGTTT GTGGATAAGACAG

Table 6: Oligonucleotides used for preparation of CRISPR DNA-templates.

Name	Sequence forward	Sequence reverse
GABARAP	GCGTCGCCGCCGTCGTCGCCGCCCCCC GTCCCGGCCCCCCTGGGTTCCCTCAGCC CAGCCCTGTCCAGCCCGGTTCCGGGGA GGATGAAGCCGGCCAAGCCTTTGTCTCA AGAAGAATCC	CTCACCGGCACCCGGTCCGGGTATTTCT TTCGGATCTTCTCGCCCTCAGAGCGGCG CTTCTCGAACGGATGCTCTTCTTTGTACA CGAACTTGCCAGCGTAATCTGGAACATC GTATGGG
GABARAPL1	TGACGTCGGCTGAGGGAGCGGGACAGG GTCAGCGGCGAAGGAGGCAGGCCCCGC GCGGGGATCTCGGAAGCGCTGCGGTGC ATCATGAAGCCGGCCAAGCCTTTGTCTC AAGAAGAATCC	CTCACGGGGACCCTGTCCGGATATTTCT TCCGGATCTTTTCTCCTTCCTTTTTCCGA TACTCAAAGGGATGGTCCTCCTTGTACTG GAACTTGCCAGCGTAATCTGGAACATCG TATGGG
GABARAPL2	CGCTGCCGCCGTCGTTGTTGTTGTGCTC GGTGCGCTGAGCTCCGCGGCTCCGCGA GCCGGTTCCGTCCCCTTCCCGCCGCGG CCATGAAGCCGGCCAAGCCTTTGTCTCA AGAAGAATCC	GGGGAGGGGGCCCACCCGCCGCCCCAG CCCCCAGCAGCCGGGCCGACGACCAAG TGCTTACCCAGCGAGTGGTCCTCCTTGA ACATCCACTTGCCAGCGTAATCTGGAAC ATCGTATGGG
LC3A	GGCGCGGAGCCCCCGGAGCCCCCAAAC CGCAGACACATCCCCGCGCCCCAGAGC CCCGGCCTGCGCGCCCAGCCGGGCCGG CGCGATGCCCGCCAAGCCTTTGTCTCAA GAAGAATCCAC	CGGGGTCGGCCGGCACCCCTGCCCCAG AGCTCGCAGCTCGCCTGCCGGGCCTCA CCGAAGCTCCGCCGCTGCTTGAAAGGCC GGTCTGAGGGGCCAGCGTAATCTGGAAC ATCGTATGGG
LC3B	GATTCGCCGCCGCAGCAGCCGCCGCCC CCGGGAGCCGCCGGGACCCTCGCGTCG TCGCCGCCGCCGCCGCCCAGATCCCTG CACCATGCCGGCCAAGCCTTTGTCTCAA GAAGAATCCAC	TCCACAGCTCGGACCCCGGCCCCGCCG CACCCGCCGCCCTCGCGGCGACACTCA CCGAAGGTGCGGCGCTGCTTGAAGGTCT TCTCCGACGGGCCAGCGTAATCTGGAAC ATCGTATGGG

Name	Sequence forward	Sequence reverse
LC3C	GGAAGCAGCTGGAGGAATGAGTTAGGTT CCCGGTTGCGGGACAGTTTTTTTTTCTTT TTTAAAACAGACACAGCTACTGAGTGCAA TGCCGGCCAAGCCTTTGTCTCAAGAAGA ATCCAC	CTTTAGATAACCCAGAAAGCTACCCCAAG AAATTTACCCAAGCTTTTTCGCTGCTTGA AGGGTCTGACGCTTGGGATTTTCTGTGG AGGCGGGCCAGCGTAATCTGGAACATCG TATGGG
ACSL3	GATGCCTTCAAGCTGAAACGCAAAGAGC TTAAAACACATTACCAGGCGGACATTGAG CGAATGTATGGAAGAAAAGCTGGCGGCA TGGTGAGCAAGGGCGAGGAGGATAACAT GGCCTCT	TTGCAGCTTGAGACATGCATTTCAAGTAT TTTGCGATTTGATCTGAGCTCACTGTAGC AAACTGATGCCAGAAGAGAATAACGGTT AGCCCTCCCACACATAACCAGAGGGCAG CAATTC

Table 7: Oligonucleotides used for preparation of sgRNAs.

Name	Sequence
GABARAP	GGAGGATGAAGTTCGTGTAC
GABARAPL1	TGCGGTGCATCATGAAGTTC
GABARAPL2	CCATGAAGTGGATGTTCAAG
LC3A	CGCGATGCCCTCAGACCGGC
LC3B	AGATCCCTGCACCATGCCGT
LC3C	GCGTCAGACCCTTCAAGCAG
ACSL3	AGAAAATAATTATTCTCTTC

4.1.7. Small interfering (si)RNAs

siRNAs were obtained from Thermo Fisher Scientific (LC3B) or Horizon (all others).

Table 8: siRNAs used in this study.

Name	Sequence
GABARAP	GGUCAGUUCUACUUCUUGA
GABARAPL1	GAAGAAAUAUCCGGACAGG
GABARAPL2	GCUCAGUUCAUGUGGAUCA
LC3B	GUAGAAGAUGUCCGACUUA
LC3C	GCUUGGCAAUCAGACAAGAGGAAGU
ACSL3 #1	UAACUGAACUAGCUCGAAA
ACSL3 #2	GCAGUAAUCAUGUACACAA
UBA5	GUAUUGAGCUGGUAUCUGA
sictrl	UGGUUUACAUGUUUUCCUA

4.1.8. Vectors and open reading frames (ORFs)

Table 9: Vectors used in this study.

Name	Description	Resistance
CrisprR/Cas9		
px330	For mammalian expression	Carbenicillin/Puromycin
Gateway vectors		
pDONR223	Gateway entry vector	Spectinomycin
pHAGE-N-FLAG-HA	For mammalian expression	Carbenicillin/Puromycin
pHAGE-C-FLAG-HA	For mammalian expression	Carbenicillin/Puromycin
pET-60-DEST	For bacterial expression	Carbenicillin/Puromycin
pDEST-MYC-GAW-IP	For mammalian expression	Carbenicillin/Puromycin
pNCS-mNEONGreen	For mammalian expression	Carbenicillin/Puromycin
pCSF107mT-GATEWAY-3'Mcy tag	For mammalian expression	Carbenicillin/Puromycin
ER-phagy assay		
TETOn-mCherry-GFP-RAMP4	For mammalian expression	Carbencillin/Neomycin
Packaging vectors		
psPAX2	Packaging plasmid for viral transduction	Carbenicillin
pMD.2	Packaging plasmid for viral transduction	Carbenicillin

The ORF for ACSL3 was purchased from Horizon. Other ORFs were from the laboratory stocks.

Table 10: ORFs used in this study.

ORF	Accession number
ACSL3	BC041692.1
ATG7	NM_001349232.2
GABARAPL2	NM_007285.7
p62	NM_003900.5
UBA5	NM_024818.6

4.1.9. Antibodies

Table 11: Primary antibodies used in this study for immunoblotting and immunolabeling.

Gene	Company	Order number
Immunoblotting		
Anti-ACSL3	Santa Cruz Biotechnologie	sc-166374
Anti-ACTIN	Sigma-Aldrich	A1978
Anti-ATG7	Cell Signaling	8558
Anti-Calnexin	Cell Signaling	2433
Anti-CoxIV	Cell Signaling	4850
Anti-DDRGK1	Sigma-Aldrich	HPA013373
Anti-GM130	Abcam	ab52649
Anti-HA	Covance	MMS-101P
Anti-HA	Cell Signaling	3724S
Anti-Lamin A/C	Abcam	ab108595
Anti-c-Myc	Bethyl	A190-104A
Anti-c-Myc 9E1	Monoclonal Antibody Core Facility, Helmholtz Zentrum Munich	
Anti-c-Myc 9E10		
Anti-NeonGreen	Chromotek	32F6
Anti-p62	MBL	PM045
Anti-p62	BD	610832
Anti-PCNA	Santa Cruz	sc-7907
Anti-TECPR2	Immunoglobe	selfmade
Anti-α-Tubulin	Abcam	ab64503
Anti-UBA5	Proteintech	12093-1-AP
Anti-UBA5	Sigma-Aldrich	HPA017235
Anti-UFC1	Proteintech	15783-1-AP
Anti-UFL1	Abcam	ab226216
Anti-UFM1	Abcam	ab109305
Immunolabeling		
Anti-HA	Roche	11867423001
Anti-HA	Sigma-Aldrich	H9658
Anti-LC3B	MBL International	PM036
Anti-LAMP1	DSHB	H4A3
Anti-p62	BD Transduction Laboratories	610832
Anti-Calnexin	Stressgene	SPA-860
Anti-Calnexin	Abcam	ab22595
Anti-SEC13	Novus	AF9055-100
Anit-UBA5	Proteintech	12093-1-AP

Table 12: Secondary antibodies and lipid stains used in this study for immunoblotting and immunolabeling.

Gene	Company	Order number
Immunoblotting		
Goat anti-mouse IgG, HRP	Promega	W402B
Goat anti-rabbit IgG, HRP	Promega	W401B
Donkey anti-goat IgG, HRP	Dianova	705-035-003

Gene	Company	Order number
Anti-rat-IgG1, HRP	Monoclonal Antibody Core Facility, Helmholtz Zentrum Munich	
Immunolabeling		
Goat anti-mouse IgG Alexa Fluor 488	Thermo Fisher	A-11001
Goat anti-rabbit IgG Alexa Fluor 488	Thermo Fisher	A-11008
Goat anti-rat IgG Alexa Fluor 647	Thermo Fisher	A-21247
Lipid stains		
HCS LipidTOX™ Red Phospholipidosis Detection Reagent	Thermo Fisher	H34351
HCS LipidTOX™ Red Phospholipidosis Detection Reagent	Thermo Fisher	H34477

4.2. Methods

4.2.1. Molecular biological methods

4.2.1.1. Preparation of chemical competent bacteria cells

Competent cells were prepared for all bacteria strains (**Table 2**). Bacteria were grown overnight (o/n) at 37 °C, rotating at 200 rpm (rotations per minute) in LB medium. On the next day, 1:20 of the o/n culture was diluted in 200 ml fresh LB medium and grown (200 rpm/37 °C) until an OD_{600} (optical density) of 0.2 was reached. The bacterial culture was placed on ice for 10 min followed by centrifugation (10 min/5000 rpm/4 °C). The cell pellet was resuspended in 100 ml transformation buffer and left on ice for 20 min. Next, cells were spun down (10 min/5000 rpm/4 °C) and resuspended in 10 ml transformation buffer. Cells were aliquoted in sterile microfuge tubes and stored at -80 °C until usage.

4.2.1.2. Transformation of bacteria and plasmid purification

Competent cells were thawed on ice and incubated with approximately 100 ng/µl plasmid DNA for 20 min. Cells were placed in a heat block for 1 min at 37 °C followed by a 10 min recovery period on ice. Next, bacteria were grown with fresh LB for 45 min at 37 °C and then streaked on LB plates containing respective antibiotics for selection. LB plates were incubated for 16 h at 37 °C or for three days at room temperature (RT ≈ 22 °C). For plasmid purification, one bacterial colony from an LB plate was inoculated in 5 ml LB medium, supplemented with the appropriate antibiotics, for 16 h at 37 °C and shaking at 200 rpm. The o/n culture was spun down (10 min/4000 rpm/RT) and plasmid DNA was purified from the pellet with GenElute HP

plasmid miniprep or maxiprep kit (start culture: 250 ml) according to the manufacture's guidance. Plasmid DNA concentration was measured with a Nanodrop 2000 (Thermo Fisher) at 260 nm.

4.2.1.3. Polymerase chain reaction (PCR)

To obtain DNA templates for Gateway cloning and endogenous tagging, PCR was performed in a T100™ thermal cycler (Bio-Rad). For Gateway cloning, cDNA was amplified from purchased ORFs (**Table 10**) using KOD-Hot Start DNA polymerase following the manufactures instruction and corresponding primers (**Table 4**).

To generate the DNA templates for CRISPR/Cas9 tagging, Q5 High-Fidelity polymerase was used according to the instruction of the manufacturer. A vector containing the blasticidine-P2A-HA or the NeonGreen-T2A-blasticidine construct served as template. For validation of the endogenous tagged cell lines, we performed PCRs with genomic DNA from single cell clones with One-Taq DNA polymerase according to the manufacturer and the related sequencing primers (**Table 3**). To improve amplification of genomic DNA, 1 M betaine was added to the PCR master mix. The ATG8 DNA templates were designed as follows: 87 bp of the corresponding hATG8 5'UTRs including the start codon, the blasticidine resistant gene, P2A, HA and 92 bp downstream of the start codon of the corresponding hATG8 (**Fig. 7**). For the ACSL3-NeonGreen cell line, we prepared a homology PCR template containing the last 75 bp of the last ACSL3 exon, NeonGreen (Allele Biotech), T2A, the blasticidine resistant gene and 84 bp downstream of the last ACSL3 exon (**Fig. 17**).

For all PCRs, the annealing phase temperature was adjusted to the used primers with Tm calculator from NEB. The duration of the elongation phase was adapted according to the size of the PCR product.

4.2.1.4. Gel electrophoresis

To separate the DNA according to the size, gel electrophoresis was performed with 0.8-1% agarose gels (melted m/v agarose in 1x TAE) containing the DNA dye Midori Green. Agarose

gels were run for 25 min at 100 V. DNA ladders for 1 kb and 100 bp were also loaded onto the gels as reverence to estimate the DNA size of the PCR products. For visualization and excision of gel bands, the GelDoc^{TM} XR+Imager (BioRad) was used.

4.2.1.5. DNA purification

Genomic DNA was extracted from cells using Genomic DNA mini kit according to the manufacturer or phenol-chloroform precipitation. For DNA isolation with phenol-chloroform, cells were harvested, washed with PBS and mixed with TNE buffer by vortexing. Next, Phenol non stabilized:Chloroform:Isoamyl alcohol was added to TNE in a 1:1 ratio. Samples were inverted 30 times and centrifuged (2 min/3000 rpm/RT). The aqueous phase was transferred into a fresh tube and DNA was precipitated by adding 3 M NaAc and 100% cold ethanol (EtOH), shaking the tube and centrifugation (10 min/20000x g (gravity)/4 °C). The DNA pellet was washed with 75% EtOH and finally the DNA was resuspended in TE buffer. DNA was stored at 4 °C

DNA cut from agarose gels was purified with QIAquick gel extraction kit according to the manufacture's guidance.

4.2.1.6. Gateway cloning

In Gateway cloning, attB-flanked cDNA fragments are cloned into attP-entry vectors with a BP clonase enzyme mix. Next, cDNA can be transferred from the donor vector in any attR-containing destination vector with an LR clonase enzyme mix. We designed primers for Gateway cloning with the online tool Primer3Plus (**Table 4**). In brief, cDNA fragments were obtained through PCR with corresponding primers. Then BP clonase, pDONR223 and cDNA (2.5 µl PCR insert/0.5 µl pDONR223/1 µl H_2O/1 µl BP Clonase II) were mixed and incubated for 16 h at RT to prepare the entry vector. After transformation and amplification, the cDNA containing entry vector, the destination vector (**Table 9**) and LR clonase (1.5 µl pDONR233 with cDNA/0.5 µl destination vector/2 µl H_2O/1 µl LR Clonase II) were incubated for 4 h at RT to obtain the cDNA containing destination vector.

4.2.1.7. sgRNA cloning

The online tool from Broad Institute (https://portals.broadinstitute.org/gpp/public/analysis-tools/sgrna-design) was used to design the sgRNAs for endogenous tagging of the HeLa cell lines. The sgRNA sequences were purchased as primers (**Table 7**) and first diluted to a stock solution of 100 µM with TE:H_2O (1:4). Forward and reverse primers were mixed 1:1 and diluted (1:10) with H_2O. The primer dilution was incubated for 5 min at 95 °C for primer annealing. Next, the sgRNAs were cloned into Cas9 containing vector px330 (digested with BSbI as instructed by the manufacturer). Ligation was performed with T4 DNA ligase for 40 min at RT (final reaction mix: 50 nM annealed primer/100 ng digested px330/1x T4 ligase buffer/2.5U T4 ligase). For transformation and amplification of sgRNA containing px330 vectors, XL 10 Gold *E. coli* bacteria cells were used.

4.2.1.8. Site-directed mutagenesis

With QuickChange primer design tool from Agilent we designed primers for site-directed mutagenesis. For each primer, a first PCR reaction with 8 cycles (denaturation/annealing/ elongation) (**Table 5**) was performed using KOD-Hot Start DNA polymerase and a vector containing the target cDNA. The two corresponding PCRs were mixed and a second PCR was performed with fresh KOD-Hot Start DNA polymerase. Next, the DNA template was digested with DpnI for 2 h at 37 °C followed by DNA cleanup with QIAquick PCR purification kit. Finally, DNA was transformed into bacterial cells.

4.2.1.9. Protein expression and purification in bacteria

For protein expression and purification, the cDNA was cloned into Gateway destination vector pET-60-DEST followed by transformation into Rosetta *E. coli*. One bacterial colony was inoculated in LB medium for 16 h (200 rpm/37 °C). On the next day, the culture was added to 500 ml LB medium to a starting OD_{600} of 0.05 and incubated at 37 °C, 200 rpm shaking till OD_{600} 0.5 was reached. To induce protein expression, 1 mM IPTG was added and again incubated (37 °C/200 rpm) for 4 h. Cells were harvested, resuspended in wash buffer and 100 µg/ml Lysozyme was added for lysis. After 30 min incubation on ice, 1 mM PMSF and

1 mM DTT was added and the sample was sonicated for 10 min (30 sec sonification/30 sec break on ice) at an amplitude of 50%. To clear lysates from cell debris, samples were centrifuged (30 min/30000x g/4 °C) followed by incubation o/n with pre-equilibrated glutathione-Sepharose 4B (GST-beads) at 4 °C with end-over-end rotation. On the next day, coupled glutathione beads were washed several times with wash buffer (5 min/800x g/4 °C). To elute GST-tagged proteins from beads, coupled glutathione-Sepharose was incubated thrice (30 min/1 h/30 min) with elution buffer and eluates were merged in a fresh tube. Finally, the buffer wash changed through dialysis with a Slide-A-Lyzer cassette for 16 h in TBS at 4 °C. Purified GST-tagged proteins were kept at -80 °C in aliquots. To monitor the efficiency of protein expression and purification, samples were taken throughout the whole experiment. The samples were boiled with 3x Lämmli SDS-PAGE loading dye at 95 °C and SDS-PHAGE was performed. The gel was run for 1 h at 120 V and then stained with Coomassie. After 30 min, the gel was incubated with destainer for 10 min followed by several wash steps with H_2O.

4.2.1.10. Sequencing

To examine the DNA sequences, purified plasmid and genomic DNA was sent to Eurofins genomics (former GATC services) with the according sequencing primers. The obtained sequences were controlled using the free version of Codon code aligner (V. 8.0.2.) and the reference sequences from NCBI.

4.2.2. Cell biological methods

4.2.2.1. Maintenance of Cell lines

HeLa and 293T cells were cultured in Dulbecco`s modified Eagle`s medium (DMEM) plus GlutaMAX-I supplemented with 10% fetal bovine serum (FBS), 1 mM sodium pyruvate and antibiotics (**Table 1**). To endogen HA- or NeonGreen-tagged cells blasticidine (4 µg/ml) was added to the medium, while for cells stable expressing a pHAGE vector the culture medium was supplemented with puromycin (2 µg/ml). All cell lines were grown at 37 °C and 5% CO_2. For maintenance, cells were grown in 10 cm dishes. Upon 80-90% confluency, cells were

washed with PBS, detached with 0.25% typsin/EDTA and resuspended in culture medium. An appropriate cell fraction was then placed in a new 10 cm dish. For long term storage at -80 °C, detached cells were washed twice with PBS, resuspended in FBS plus 10% DMSO and transferred in cryo tubes. For a slow freezing process, cryo tubes were placed in a Mr. Frosty cryo box. Frozen cells were thawed at RT and transferred in 10 cm dishes with fresh medium. The medium was changed on the next day to remove the DMSO.

4.2.2.2. Stable-isotope labelling by amino acids in cell culture (SILAC)

DMEM for SILAC supplemented with 10% dialyzed FBS, 2 mM glutamine, 1 mM sodium pyruvate, 73 µg/ml L-lysine solution in PBS and 42 µg/ml L-arginine solution in PBS was used to label cells with heavy amino acids. For labeling with heavy amino acids, we used heavy L-lysine (R8) and heavy L-arginine (R10) from Cambridge Isotope Laboratories, while for labeling with light amino acids we supplemented the SILAC medium with light L-lysine (R0) and light L-arginine (R0). Cells were grown in a 6 well plate and transferred into the next well upon confluency. Every second day the medium was changed to reach a label efficiency of 95% of the cells. Incorporation of amino acids was tested with incorporation check (4.2.3.10).

4.2.2.3. Treatments

Treatments were performed with 80-100% confluent cells depending on the treatment time. All inhibitors except oleic acid were solved in DMSO. Oleic acid was solved in EtOH. Torin1 was used with a final concentration of 250 nM for 2 h. Cell were incubated for 2 h with 200 nM Bafilomycin A1 (BafA1). ATG7 Inhibitor was added for 24 h to the medium with a final concentration of 1 µM. Bortezomib (Btz) was used at a working concentration of 1 µM and cells were treated for 8 h. Oleic acid was added to cell in a final concentration of 0.6 mM. Cells were kept for 30 min, 4 h, 8 h or 24 h in medium containing oleic acid or EtOH. For each experiment on dish was cells was incubated with the inhibitor-solvent (DMSO or EtOH) and analysed to control the experimental settings.

4.2.2.4. Transfection with siRNA or plasmid DNA

Experiments with siRNAs were performed through reverse transfection using Lipofectamine RNAi Max according to the manufacture's guidance (**Table 8**). In brief, OptiMEM, siRNA (30 nM end concentration) and RNAiMax were mixed and placed in plates. After 20 min, cells were added on the transfection mix. Cells were harvested 72 h after transfection.

For transient transfection of HeLa and HEK cells, we used Lipofectamin 2000 according to the instructions. Lipofectamine and DNA were mix with OptiMEM in separate tubes and incubated. After 5 min, mixtures were combined and incubated for 25min. Finally, transfection mix was added dropwise on cells seeded on the day before transfection. After 48 h, cells were harvested for downstream experiments.

4.2.2.5. Generation of stable cell lines

For N-terminal HA-tagging of hATG8s and C-terminal NeonGreen-tagging of ACSL3, DNA templates and px330 containing sgRNAs were prepared as described (4.2.1.3 and 4.2.1.7). HeLa cells were seeded in 6 well plates one day prior to transient transfection with px330 and the corresponding DNA template using Lipofectamine 2000. After 24 h, the medium was replaced with fresh growth medium and 48 h post transfection cells were placed in medium containing blasticidine to select for cells with insert. Additionally, cells were subjected to single cell selection in 96 well plates. ACSL3-NeonGreen cells were FACS sorted according to the fluorescence signal. With PCR and sequencing cell clones were examined for correct insertion.

Stable cell lines overexpressing pHAGE plasmids were prepared with lentiviral transduction. For viral production, HEK cells were seeded in a 6 well plate, one well per cell line. Confluent cells were transfected with Lipofectamine 2000 with plasmids encoding for viral packaging and envelope proteins and the pHAGE vector encoding for the gene of interest (**Table 9**). One day after transfection, virus containing medium was collected and stored in tubes and fresh growth medium was added to virus producing cells. Recipient cells were seeded in a 6 well plate ($3x10^5$ cells per well/cell line) with one extra well as control. 48 h post transfection virus containing medium was again collected and combined with the stored virus supernatant. Next,

the virus was filtered through a sterile syringe filter (0.45 µM) and mixed with 8 µg/ml polybrene. The medium of the recipient cells was replaced with the virus containing, filtered medium. One day after transduction, the medium was replaced by fresh growth medium. Two days after transduction, the medium was replaced with medium substituted with appropriate antibiotics to select for cells with integrated pPHAGE plasmid. When control cells, not transfected with virus, died expression levels of integrated vectors were monitored with immunoblot analysis.

4.2.3. Biochemical methods

4.2.3.1. Harvesting and lysis of cell culture cells

For harvesting, the cell culture medium was removed and cells were washed twice with cold PBS. To detach cells from the plate surface, trypsin/EDTA was added dropwise on the cells. Next, trypsin/EDTA was diluted with PBS and the cell suspension was transferred into fresh tubes. Cells were spun down (5 min/1000x g/4 °C) and washed twice with PBS. Cell pellets, snap frozen with liquid nitrogen, were stored at -80 °C until usage or lysis. To lyse cells, we used RIPA (for immunoblot analysis) MCLB (HA-LC3B IPs) or Glycerol buffer (IP-MS and HA-GABARAPL2 IP-WB). Cell pellets were thawed on ice and mixed with lysis buffer. Next, cells were incubated for 30-45 min on ice followed by centrifugation (10 min/20000x g/4 °C). Supernatant was transferred into fresh tubes and protein concentration was measured with BCA-Assay according to the manufacturer instruction. Protein concentration of samples were adjusted with lysis buffer. For immunoblot analysis, samples were mixed with 3x Lämmli SDS-PAGE loading dye and boiled at 95 °C.

4.2.3.2. Immunoblotting

With SDS-PHAGE proteins were size separated on self-casted SDS containing gels with different acrylamide concentration (**Table 13**). SDS-PHAGE was typically performed for 1 h at 120 V with SDS-PHAGE-running-buffer using the electrophoreses chamber system from Bio-Rad. With Mini Trans Blot® cell system from Bio-Rad proteins were transferred from gels on

nitrocellulose membranes for 2 h at 0.3 mA (milli Ampere) with western blot-transfer-buffer. After protein transfer, membranes were boiled for 5 min in PBS to improve visibility of the HA-hATG8 proteins. Equal sample loading of GST-pulldown immunoblots was controlled by 5 min Ponceau staining. Ponceau was removed from membranes by washing with TBS-T. To prevent unspecific antibody binding, blots were incubated with blocking solution for 1 h (TBS-T supplemented with 5% low-fat milk or 5% BSA or 0.2% I-Block protein-based blocking reagent) prior to incubation with primary antibodies. Primary antibodies were typically diluted 1:1000 in the blocking solution and blots were kept o/n at 4 °C. As an exception, c-Myc antibodies were diluted 1:100. Next, blots were washed with TBS-T for several times followed by secondary antibody incubation for 1 h at RT. Secondary antibodies were diluted 1:10000 in TBS-T supplemented with 1% milk or BSA or 0.2% I-Block protein-based blocking reagent. After several washing steps with TBS-T, Western Lightning Plus-ECL was used to induce enzymatic reaction of HRP (Horsh radish peroxidase), coupled to the secondary antibodies, which was captured on films. An AGFA Curix developing machine was used to develop the films.

Table 13: Self-casted gels

Reagents	Stacking gel	Running gel
Acrylamid	8%, 10%, 12%, 15%	6%
Tris-HCl	375 mM [pH 8.8]	125 mM [pH6.8]
SDS	0.1%	0.1%
APS	0.1%	0.1%
TEMED	0.01%	0.01%

4.2.3.3. Quantification of immunoblots

Quantification of protein bands from western blot films was performed with ImageJ (version 1.52) and Excel. Statistical analysis was undertaken with Python (version 3.7) by calculations of the statistical significance with Student's t-test. Data are represented with mean±sem (standard error of the mean).

4.2.3.4. Subcellular fractionation

For subcellular fractionation of HeLa cells, we harvested 4x10 cm cell culture dishes for each sample. The experiment was performed with the Endoplasmic reticulum isolation kit according

to the manufacture's guidance. In brief, harvested cells were incubated on ice for 20 min with hypotonic extraction buffer, provided in the kit. Next, cells were centrifuged (5 min/600x g/4 °C), resuspended in isotonic extraction buffer, included in the kit, and homogenized with a dounce homogenizer (mild lysis sample). The sample was centrifuged (10 min/1000x g/4 °C) and the post nuclear supernatant (PNS) was transferred into a fresh tube. The PNS was subjected to faster centrifugation (15 min/12000x g/4 °C) to obtain the post mitochondrial fraction (PMF) in the supernatant. Through ultracentrifugation (1 h/100000x g/4 °C) of the PMF the crude microsomal fraction (CMF) was isolated in the pellet. Resuspension of the pellet was performed through homogenization with isotonic extraction buffer. All samples were boiled with 3x Lämmli SDS-PAGE loading dye at 95 °C and analyzed with immunoblots.

4.2.3.5. Pulldown Assay

For pulldown assays, the purified protein was always freshly coupled to pre-equilibrated glutathione-Sepharose 4B. An appropriate amount of purified GST-protein was thawed on ice and incubated with the required bead slurry (40 µl per reaction) for 2 h at RT or 16 h at 4 °C with end-over-end rotation. After coupling, beads were washed several times with wash buffer. To ensure equal addition of the different GST-tagged proteins to the samples, we performed serial-dilutions of the coupled beads and monitored protein-bead binding with SDS-PHAGE followed by Coomassie staining (4.2.1.9). According to the protein concentration, coupled beads were diluted with pre-equilibrated unbound glutathione beads and later added to the lysates. To prepare lysates, we harvested 2x10 cm confluent cell culture plates and lysed the cells with glycerol buffer (1 h/ 4 °C). Next, lysates were cleared of cell debris through centrifugation (10 min/20000x g/4 °C) followed by preclearing with uncoupled glutathione beads for 1 h at 4 °C with end-over-end rotation. The protein concentrations were adjusted with BCA assay and lysates were incubated with coupled glutathione beads for 16 h at 4 °C with end-over-end rotation. On the next day, beads were washed with glycerol buffer, boiled for 5 min at 95 °C with 3x Lämmli SDS-PAGE loading dye and samples were analyzed by immunoblotting.

4.2.3.6. Immunoprecipitation (IP)

For IPs subjected to immunoblotting, we used 2x10 cm cell culture plates, while for IP-MS experiments we harvested 4x15 cm dishes. Cells were thawed on ice and lysed for 30 min at 4 °C with glycerol buffer or MCLB buffer (HA-LC3B samples). After centrifugation (10 min/20000x g/4 °C), protein concentrations were adjusted with BCA assay and lysates were incubated with pre-equilibrated anti-HA-agarose or anti-c-Myc-agarose (16 h/4 °C) with end-over-end rotation. Next, beads were washed for several times with lysis buffer. Samples, analyzed with immunoblots or subjected to in-gel tryptic digest were mixed with 3x Lämmli SDS-PAGE loading dye and cooked for 5 min at 95 °C. For in-solution tryptic digest, proteins were eluted from beads for 30 min with HA-peptide solved in PBS. Elution was performed thrice at RT and next, subjected to TCA precipitation.

4.2.3.7. Laser scanning microscopy (LSM)

For LSM, cells were seeded on 15 mm coverslips. The medium was aspirated and cells were washed several times with PBS prior to fixation with 4% PFA for 10 min at RT. Next, cells were washed with PBS, permeabilized with 0.1% Triton X-100 in PBS or 0.1% saponin in PBS (15 min, RT) and washed again with PBS. To prevent unspecific binding of antibodies, cells were incubated with 1% BSA-PBS (1 h, RT). Staining with primary and secondary antibody was performed sequentially in 0.1% BSA-PBS (1 h, RT). Between each antibody incubation, cells were washed with PBS. Finally, coverslips were washed with deionized water and mounted with PorlongGold Antifade with Dapi. Imaging was performed with a LSM 800 Carl Zeiss microscope using a 63x oil-immersion objective. ZEN blue edition software and ImageJ was used for image analysis.

4.2.3.8. Super-resolution radial fluctuation imaging (SRRF)

Compared to LSM microscopy, contrast and resolution of images is increased with the SRRF technique (299). GABARAPL2^{endoHA}/ACSL3^{endoNeonGreen} cells were seeded on coverslips and fixed for 15 min with 4% PFA at RT (2×10^5 cells per 35 mm dish). Next, cells were washed thrice with PBS, one time with 50 mM NH_4Cl (5 min) and permeabilized with 0.5% Triton X-100

(5 min). Cells were then incubated for 40 min with 1% BSA and stained with anti-Calnexin (Abcam), anti-HA (Sigma) and anti-UBA5 diluted in 1% BSA for 1 h. Lastly, cells were incubated with secondary fluorescence antibody followed by confocal microscopy on Andor Dragonfly spinning disk using a Nikon Ti2 inverted optical microscope [60× TIRF objective (Plan-APOCHROMAT 60×/1.49 oil)]. The SRRF imaging was performed by Santosh Phuyal and Hesso Farhan (University of Oslo).

4.2.3.9. ER-phagy assay

One day prior to transfection, cells were seeded on coverslips in 12 well plates. Transfection with TETOn-mCherry-GFP-RAMP4 (Addgene #109014) was performed with FuGENE® HD transfection reagent according to the manufacture's instruction. After transfection, cells were directly treated with 4 µg/ml doxycycline. The medium was changed 24 h after doxycycline treatment and changed again 40 h after transfection to EBSS in order to starve cells. In parallel cells were treated with oleic acid or EtOH. After 8 h, cells were fixed for 10 min with 4% PFA at RT, washed for several times with PBS and stained in the penultimate washing step with DAPI. Finally, coverslips were mounted with fluorescence mounting medium from Dako. The confocal microscope Nikon A1R TiE was used to capture images as z-projections merged from at least three z-steps. For quantification, three biological replications were made and at least 90 cells across the replicates were scored blindly for red-only puncta. For each data set the mean±sem was calculated. The ER-phagy assay was performed by Matthew D. Smith and Simon Wilkinson (University of Edinburgh).

4.2.3.10. Incorporation Check

To control integration of heavy amino acids in proteins of cells treated with SILAC medium, cells from one 6 well were harvested and the pellet was resuspended in denaturation buffer. Lysates were incubated with 0.5 µl Benzonase (15 min, 25 °C) followed by centrifugation (10 min/16000x g). 20 µl of the supernatant was transferred into a new tube and diluted with 80 µl 20 mM ABC. Tryptic digest was performed with 0.4 µl trypsin at RT and stopped with 10 µl 10% TFA on the next day. Peptides were loaded on stage tips followed by desalting,

elution and analysis with an Q Exactive HF mass spectrometer. Raw data were analyzed with MaxQuant and labeling of the cells with L-lysine and L-arginine was calculated with Excel.

4.2.3.11. In-gel tryptic digest

After HA IP, proteins were size separated by SDS-PAGE with (BioRad 4-20% gels). The acrylamide gel was cut alongside the sample lines and further cut in 12 equal sized bands. Each band was chopped in smaller gel pieces and per band placed in one well of a 96 well plate. With wash buffer gel pieces were washed thrice followed by denaturation with 100% EtOH (twice for 5 min). By vacuum centrifugation remaining EtOH was evaporated. Proteins were reduced with reduction buffer (45 min/56 °C) and free sulfhydryl groups were blocked with alkylation buffer (30 min/RT/in the dark). Remaining solutions were removed by washing with 50 mM ABC (15 min), dehydration with 100% EtOH (15 min) and again washing with 50 mM ABC (15 min). Prior to tryptic digest gel pieces were dehydrated with 100% EtOH (twice for 15 min) and remaining EtOH was removed by vacuum centrifugation. To each well 40 µl trypsin solution was added and incubated at 4 °C. After 15 min, 50 mM ABC was added to fully cover the gel pieces and tryptic digest was performed for 16 h at 37 °C. Elution of peptides from the gel pieces was performed trice with elution buffers (20 min/RT). With each elution the acetonitrile concentration was increased. For each well, eluates were combined in one tube after each elution step. Eluates were evaporated to a volume of 80 µl-100 µl and mixed in a 1:1 ratio with binding buffer. Samples were desalted with stage tips.

4.2.3.12. TCA-precipitation

TCA was added to the samples in a final concentration of 20%. The samples were vortexed and incubated on ice for 20 min to precipitate proteins from the solution. Next, samples were centrifuged (30 min/14000 rpm/4 °C) and except for 20 µl, supernatant was discarded. Cold 10% TCA (500 µl) was added to the supernatant and spun down (30 min/14000 rpm/4 °C). The supernatant was discarded and the precipitated proteins were washed thrice with 1 ml cold acetone to fully remove TCA (10 min/14000 rpm/4 °C). The remaining acetone was evaporated with vacuum centrifugation.

4.2.3.13. In-solution-tryptic digest

Precipitated proteins were solved in 30 µl 50 mM ABC 10% ACN [pH 8.0] and 0.5 µl trypsin was added for tryptic digest (4 h/37 °C). The digest was stopped with 30 µl 5% ACN 5% FA (stop solution) for 10 min at RT and finally peptides were dried by vacuum condensation (1 h). Peptides were resuspended in binding buffer followed by desalting with stage tips.

4.2.3.14. Stage tipping

Stage tips were self-made with two C18 resin disks embedded in a 200 µl pipette tip. Prior to sample loading, stage tips were activated with methanol, equilibrated with buffer B and washed with buffer A. Importantly, C18 resin was always kept wet with buffer. After sample loading, stage tips were desalted with buffer A and peptides were eluted with buffer B into a fresh tube. With vacuum condensation buffer B was evaporated and peptides were resuspended in 10 µl buffer A. Mass spectrometry samples were stored at -80 °C until measuring on the Mass spectrometer.

4.2.3.15. Mass spectrometry (MS) analysis

Samples were placed in a 96 well plate and peptides were loaded with an Easy-nLC1200 liquid chromatography (Thermo Scientific) on 75 µm×15 cm fused silica capillaries (New Objective) filled with C18AQ resin. Peptide detection was performed with an Q Executive HF mass spectrometer (Thermo Scientific). For 30 sec dynamic exclusions was enabled and species singly charged or with a charged not assigned were rejected. With MaxQuant (version 1.6.0.1) raw data from the mass spectrometer was processed and further analyzed with Excel. First, common contaminants, identification based on site-specific modifications and reveres identifications were excluded. Next, Log_2 heavy-light ratios were calculated and the threshold was set on a log_2 fold change of greater than 1.0-fold or less than -1.0-fold. Additional requirements were at least two MS counts, unique peptides and razor peptides. Proteins with at least two MS counts for unique and razor peptides and no counts in HeLa control IPs were selected. True hits were obtained through more stringent filtering of the ratio heavy:light

isocounts (≥1) and the average log_2 ratios of the replicates (≥1 or ≤-1). The platform DAVID was used for functional annotation analysis (https://david.ncifcrf.gov/).

5. Results

5.1. Generation and validation of endogenous HA-tagged ATG8 cell lines

5.1.1. Design and development of ATG8^{endoHA} cell lines with CRISPR-Cas9

The strategy to prepare knock-in cell lines with CRISPR-Cas9 is based on HDR which uses homolog DNA sequences to repair DSBs (276). Upon a DSB, resections of the DNA ends create 3'-ended, single-stranded DNA which anneals with a homolog DNA template and accordingly the DNA is repaired by polymerases. Providing cells with a DNA template homolog to a double strand breakage site enables a CRISPR-Cas9-mediated inclusion of base pairs or a DNA sequence into a specific locus (300). Hence, we prepared double stranded DNA pieces homolog to the 5'UTR and the first exon of the corresponding hATG8 gene additionally to specific sgRNAs to generate HA-tagged hATG8 cell lines (**Fig. 7**).

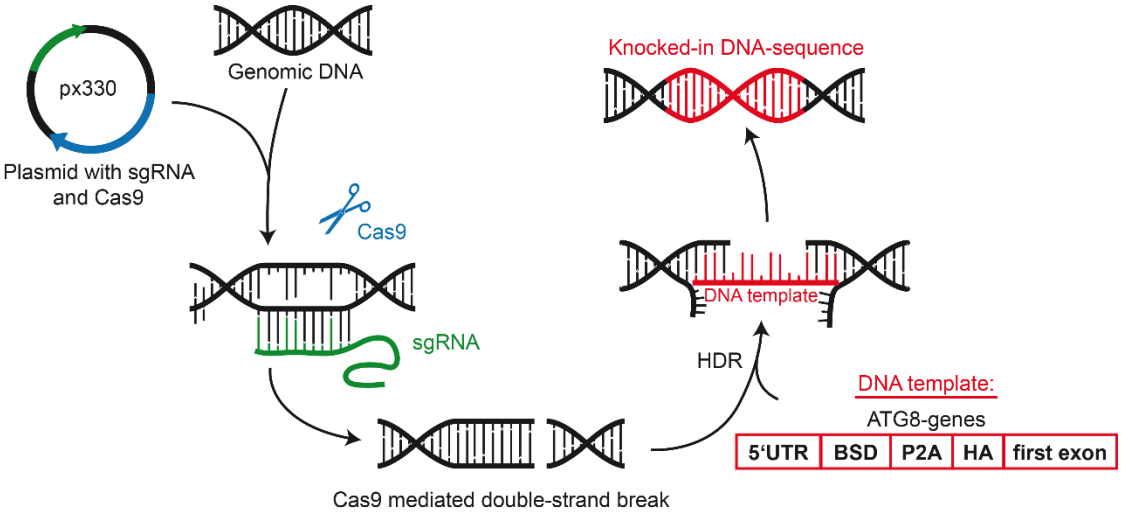

Figure 7: Workflow of endogenous HA-tagging of hATG8s in HeLa cells with CRISPR-Cas9: Cells are transfected with specific sgRNA and Cas9 containing plasmid and the corresponding DNA template. Cas9 is guided by the sgRNA to its homolog genomic DNA sequence and induces a DSB. Through HDR the DSB is repaired and the blasticidine resistance gene and the HA tag are integrated into the genomic DNA.

For selection we integrated a blasticidine-resistant gene directly after the start codon. A P2A sequence was included between the resistant gene and the HA tag to guarantee the expression of blasticidine and hATG8s as single proteins. sgRNAs of the GABARAPs and LC3s were designed with an online tool provided by the Broad institute. The obtained sgRNAs (**Table 7**) were cloned into the px330 vector which includes the SpCas9 gene. Hela cells were

transfected with sgRNA in px330 and the corresponding DNA template followed by selection with blasticidine (**Fig. 7**). Two weeks after transfection, single cell clones were tested by PCR and SANGER sequencing for correct knockins (**Table 14**).

Table 14: Sequences of the hATG8^{endoHA} cell lines obtained by Sanger sequencing of the 5'UTR and start codon regions. Bold letters indicate the introduced sequences.

Cell lines	Sequences
GABARAP^{endoHA}	TTCGTGGATCGCTCCGCTGAATCCGCCCGCGCGTCGCCGCCGTCGTCGCCGCCCC CCGTCCCGGCCCCCCTGGGTTCCCTCAGCCCAGCCCTGTCCAGCCCGGTTCCGGG GAGGATG**AAGCCGGCCAAGCCTTTGTCTCAAGAAGAATCCACCCTCATTGAAAGA** **GCAACGGCTACAATCAACAGCATCCCCATCTCTGAAGACTACAGCGTCGCCAGCG** **CAGCTCTCTCTAGCGACGGCCGCATCTTCACTGGTGTCAATGTATATCATTTTACT** **GGGGGACCTTGTGCAGAACTCGTGGTGCTGGGCACTGCTGCTGCTGCGGCAGCT** **GGCAACCTGACTTGTATCGTCGCGATCGGAAATGAGAACAGGGGCATCTTGAGCC** **CCTGCGGACGGTGCCGACAGGTGCTTCTCGATCTGCATCCTGGGATCAAAGCCAT** **AGTGAAGGACAGTGATGGACAGCCGACGGCAGTTGGGATTCGTGAATTGCTGCC** **CTCTGGTTATGT**
GABARAPL1^{endoHA}	TGCACACTCGGCCCAGCGCTGTTGCCCCCGGAGCGGACGTTTCTGCAGCTATTCTG AGCACACCTTGACGTCGGCTGAGGGAGCGGGACAGGGTCAGCGGCGAAGGAGGC AGGCCCCGCGCGGGGATCTCGGAAGCGCTGCGGTGCATCATG**AAGCCGGCCAAG** **CCTTTGTCTCAAGAAGAATCCACCCTCATTGAAAGAGCAACGGCTACAATCAACA** **GCATCCCCATCTCTGAAGACTACAGCGTCGCCAGCGCAGCTCTCTCTAGCGACGG** **CCGCATCTTCACTGGTGTCAATGTATATCATTTTACTGGGGGACCTTGTGCAGAAC** **TCGTGGTGCTGGGCACTGCTGCTGCTGCGGCAGCTGGCAACCTGACTTGTATCGT** **CGCGATCGGAAATGAGAACAGGGGCATCTTGAGCCCCTGCGGACGGTGCCGACA** **GGTGCTTCTCGATCTGCATCCTGGGATCAAAGCCATAGTGAAGGACAGTGATGGA** **CAGCCGACGGCAGTTGGGATTCGTGAATTGCTGCCC**
GABARAPL2^{endoHA}	GCCCCTTTACGTGCGGCCCCGCCCCTTGGCGTGGCGCCCTGACAAATGGCGCCGG AAGCCCCGCCCCCGGCCGGTTGCTAGGCTCCGACAGCCGGAAGTCCCGCCTGCC GTGTAGTCGCCGCCGTCGCTGCCGCTGCCGCTGCCGCCGTCGTTGTTGTTGTGCT CGGTGCGCTGAGCTCCGCGGCTCCGCGAGCCGGTTCCGTCCCCTTCCCGCCGCG GCCATG**AAGCCGGCCAAGCCTTTGTCTCAAGAAGAATCCACCCTCATTGAAAGAG** **CAACGGCTACAATCAACAGCATCCCCATCTCTGAAGACTACAGCGTCGCCAGCGC** **AGCTCTCTCTAGCGACGGCCGCATCTTCACTGGTGTCAATGTATATCATTTTACTG** **GGGGACCTTGTGCAGAACTCGTGGTGCTGGGCACTGCTGCTGCTGCGGCAGCTG** **GCAACCTGACTTGTATCGTCGCGATCGGAAATGAGAACAGGGGCATCTTGAGCCC** **CTGCGGACGGTGCCGACAGGTGCTTCTCGATCTGCATCCTGGGATCAAAGCCATA** **GTGAAGGACAGTGATGGACAGCCGACGGCAGTTGGGATTCGTGAATTGCTGCCCT** **CTGGTTATGTGTGGGAGGGC**
LC3B^{endoHA}	CTGCGTGCCGCTGCTGGGTTCCGCCACGCCCGTCATGGCGGCGGCCCCGGCCGG CTCTGGCCCCGCCCCTCGGTGACGCGTCGCGAGTCACCTGACCAGGCTGCGGGCT GAGGAGATACAAGGGAAGTGGCTATCGCCAGAGTCGGATTCGCCGCCGCAGCAGC CGCCGCCCCCGGGAGCCGCCGGGACCCTCGCGTCGTCGCCGCCGCCGCCGCCCA GATCCCTGCACCATG**CCGGCCAAGCCTTTGTCTCAAGAAGAATCCACCCTCATTGA** **AAGAGCAACGGCTACAATCAACAGCATCCCCATCTCTGAAGACTACAGCGTCGCC** **AGCGCAGCTCTCTCTAGCGACGGCCGCATCTTCACTGGTGTCAATGTATATCATTT** **TACTGGGGGACCTTGTGCAGAACTCGTGGTGCTGGGCACTGCTGCTGCTGCGGCA** **GCTGGCAACCTGACTTGTATCGTCGCGATCGGAAATGAGAACAGGGGCATCTTGA** **GCCCCTGCGGACGGTGCCGACAGGTGCTTCTCGATCTGCATCCTGGGATCAAAGC** **CATAGTGAAGGACAGTGATGGACAGCCGACGGCAGTTGGGATTCGTGAATTGCTG** **CCCTCTGGTTATGTGTGGGAGGGC**
LC3C^{endoHA}	AGGGGAGGGAGAGGAGAGGCCTGATGTCACTCAGCCCTACATAAGGGCCTCCTTC AGGCTCCTGCAGGCAGTTTGGAAGCAGCTGGAGGAATGAGTTAGGTTCCCGGTTG CGGGACAGTTTTTTTTTCTTTTTTAAAACAGACACAGCTACTGAGTGCAATG**CCGGC** **CAAGCCTTTGTCTCAAGAAGAATCCACCCTCATTGAAAGAGCAACGGCTACAATC** **AACAGCATCCACATCTCTGAAGACTACAGCGTCGCCAGCGCAGCTCTCTCTAGCG** **ACGGCCGCATCTTCACTGGTGTCAATGTATATCATTTTACTGGGGGACCTTGTGCA** **GAACTCGTGGTGCTGGGCACTGCTGCTGCTGCGGCAGCTGGCAACCTGACTTGTA** **TCGTCGCGATCGGAAATGAGAACAGGGGCATCTTGAGCCCCTGCGGACGGTGCC** **GACAGGTGCTTCTCGATCTGCATCCTGGGATCAAAGCCATAGTGAAGGACAGTGA** **TGGACAGCAGACGGCAGTTGGGATTCGTGAATTGCTGCCCTCTGGTTATGTGTGG** **GAGGGC**

For each hATG8 gene except LC3A we identified clones with the correct sequence. HeLa cells transfected with LC3A specific sgRNA and DNA template did not survive selection with blasticidine. Presumably this is due to suppressed expression of LC3A in tumor cell lines (301). To distinguish between endogenous tagged cell lines from those stably overexpressing the tagged gene, the endogenous cell lines are named hATG8^{endoHA} and accordingly in the following.

5.1.2. Validation of ATG8^{endoHA} cell lines

To validate the clones with correct DNA sequence, we tested whether the knockin sequences were expressed correctly and integrated gene specifically. Immunoblot analysis showed the presence of HA tags at the corresponding hATG8 protein size in the engineered cell lines but not in parental HeLa cells (**Fig. 8 A-E**). Further, we performed knockdown experiments in the engineered cell lines with gene specific siRNAs followed by immunoblotting with an anti-HA antibody. hATG8 protein levels in siRNA treated cells were remarkably decreased compared to cells treated with control siRNA (**Fig. 8 F-J**). Consistently, laser scanning microscopy (LSM) of GABARAPL2^{endoHA} cells immunostained with a HA antibody showed a decrease in GABARAPL2 protein levels upon GABARAPL2 knockdown (**Fig. 8 K**). As described in the introduction, lipidation and membrane integration of GABARAPs and LC3s are linked to their functions. Therefore, we tested whether the HA-tagged hATG8s were still lipidated using several small molecule inhibitors (**Fig. 8 L-P**). Upon treatment with autophagy inducing stimuli, such as the mTOR inhibitor Torin1, lipidation of hATG8 proteins is activated (302). However, lipidated hATG8 proteins are located at autophagosomal membranes and thus, are degraded by autophagy. Therefore, PE-hATG8 protein levels also decrease upon autophagy induction. The small molecule inhibitor Bafilomycin A1 (BafA1) blocks autophagosomal-lysosomal fusion. Thus, lipidated hATG8s accumulate inside of autophagosomes and PE-hATG8 protein levels increase. Additionally, we blocked PE conjugation with a small molecule inhibitor against ATG7 (ATG7 Inhibitor) which prevents hATG8 activation during the lipidation process. In immunoblot analysis of the hATG8^{endoHA} cell lines treated with these small molecule inhibitors we observed

altered lipidation levels as expected and changes in the expression patterns of GABARAPs and LC3s (**Fig. 8 L-P, 14 D**).

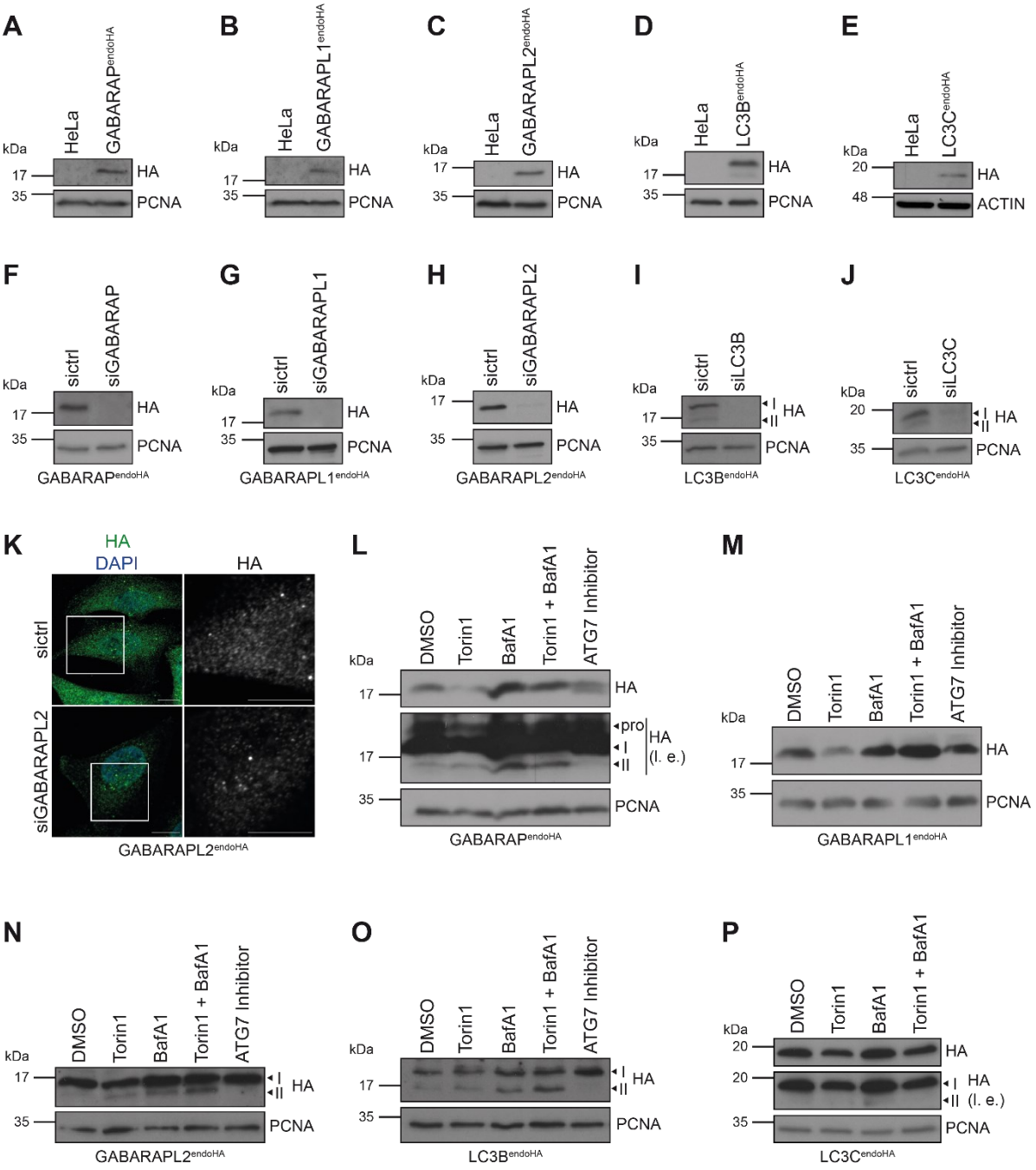

Figure 8: Validation of hATG8^{endoHA} cell lines: (**A-E**) Immunoblot analysis of GABARAP^{endoHA} (**A**), GABARAPL1^{endoHA} (**B**), GABARAPL2^{endoHA} (**C**), LC3B^{endoHA} (**D**), LC3C^{endoHA} (**E**) and parental HeLa cell lysates (**A-E**) with anti-HA, anti-PCNA and anti-ACTIN antibodies. PCNA and ACTIN detecting antibodies were used as loading control. (**F-K**) Revers transfection for 72 h of GABARAP^{endoHA} (**F**), GABARAPL1^{endoHA} (**G**), GABARAPL2^{endoHA} (**H&K**), LC3B^{endoHA} (**I**), LC3C^{endoHA} (**J**) with non-targeting (sictrl) or gene specific siRNA was followed by lysis and immunoblot analysis (**F-J**) or fixation and immunolabeling with anti-HA antibody (**K**). Scale bars: 10 µm. (**L-P**) GABARAP^{endoHA} (**L**), GABARAPL1^{endoHA} (**M**), GABARAPL2^{endoHA} (**N**), LC3B^{endoHA} (**O**), LC3C^{endoHA} (**P**) cell lines were treated as indicated prior to cell lysis and immunoblot analysis. Arrows mark precursor (pro), lipidated (II) and non-lipidated (I) GABARAPs and LC3s. l.e means long exposure.

LC3B is the best characterized hATG8 protein and mainly used as marker for autophagy. Therefore, we also validated LC3B binding to the known interactors ATG7, p62 and TECPR2. With LC3B^{endoHA} and parental cells we performed HA IPs followed by immunoblotting with antibodies against p62, ATG7 and TECPR2, and confirmed their binding to endogenously HA-tagged LC3B (**Fig. 9**).

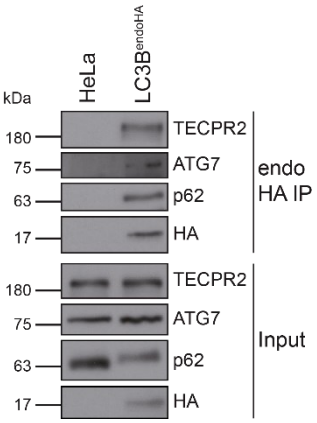

Figure 9: Validation of LC3B interactors: HA IP of LC3B^{endoHA} and parental cells was analyzed using immunoblotting with indicated antibodies.

In the following we focused on the GABARAPL2^{endoHA} cell line for a more precise validation and characterization. To examined the subcellular localization and distribution of GABARAPL2, GABARAPL2^{endoHA} cells were immunolabeled with lysosomal (anti-LAMP1

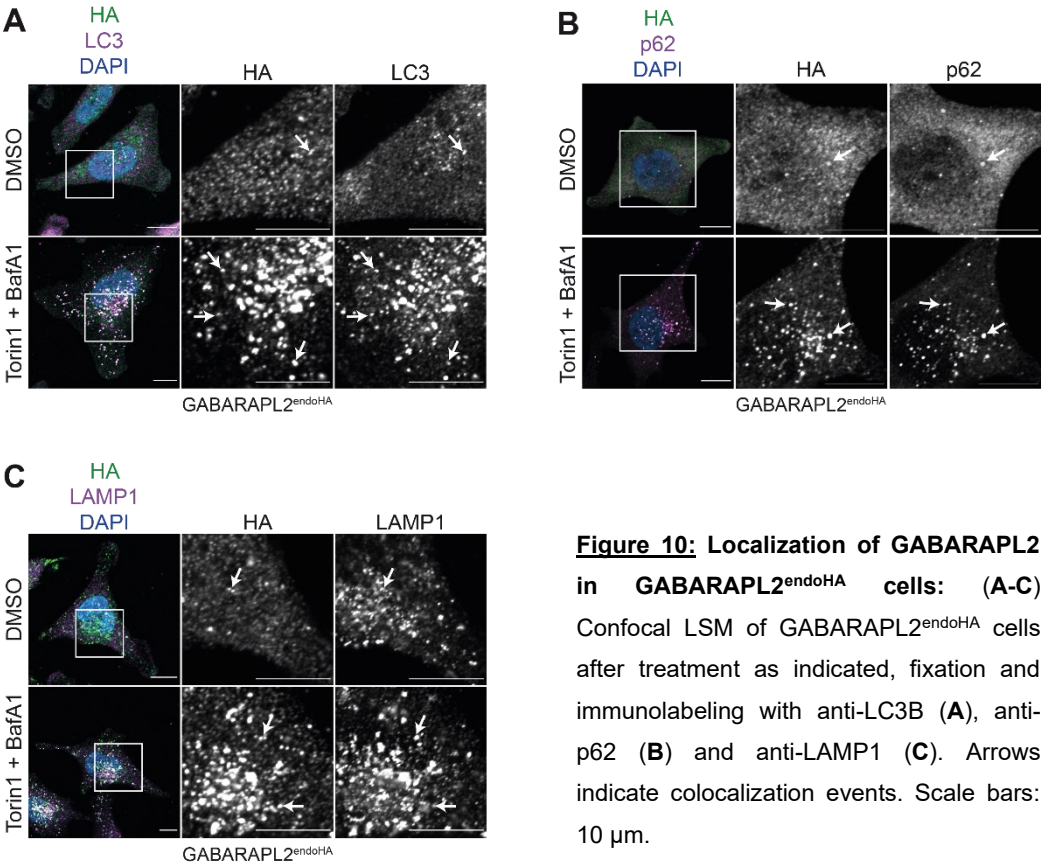

Figure 10: Localization of GABARAPL2 in GABARAPL2^{endoHA} cells: (**A-C**) Confocal LSM of GABARAPL2^{endoHA} cells after treatment as indicated, fixation and immunolabeling with anti-LC3B (**A**), anti-p62 (**B**) and anti-LAMP1 (**C**). Arrows indicate colocalization events. Scale bars: 10 µm.

antibody) and autophagosomal markers (anti-p62 and anti-LC3B antibodies), under basal and autophagy inducing conditions. Confocal LSM revealed colocalization of GABARAPL2 with LAMP1, LC3B and p62 under basal conditions which became even more prominent upon treatment with Torin1 and BafA1 (**Fig. 10 A-C**).

Together, these results demonstrate site-specific integration of the HA tag in the hATG8 gene loci. Further, epitope tagging with CRISPR-Cas9 did not interfere with hATG8 lipidation and functionality.

5.2. Interactome analysis of the GABARAPL2^{endoHA} cell line

5.2.1. Experimental workflow of the interactome analysis

So far, interactome studies of hATG8 family members were mostly performed with cell lines overexpressing a tagged hATG8 protein (293,294). To examine which mass spectrometry (MS) approach is most suitable for endogenous expressed proteins with regards to efficiency, we performed two commonly used methods for MS analysis with the GABARAPL2^{endoHA} cell line (**Fig. 11**) (303,304). First, cells were lysed, followed by immunoprecipitation (IP) with anti-HA-agarose. The enriched protein samples were then either subjected to in-gel tryptic digest

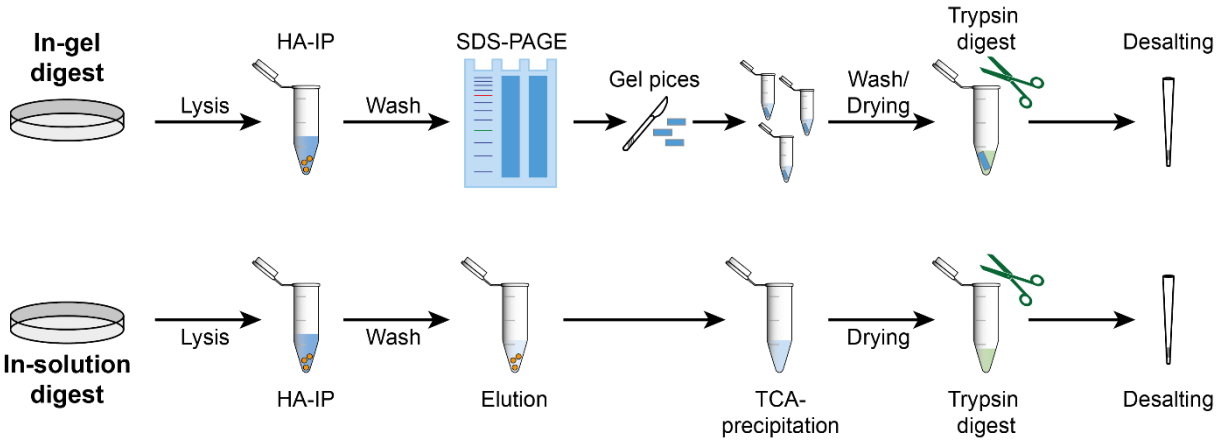

Figure 11: Workflow of MS-approaches: For In-gel and In-solution digest, cells were harvested and lysed prior to immunoprecipitation with anti-HA-agarose (HA IP). For the In-gel method, enriched proteins coupled to anti-HA-agarose were removed through boiling with Lämmli SDS-PAGE loading dye and loaded on SDS-page for size separation. Next, lanes were cut in pieces keeping size separation, transferred to multiple tubes and prepared for tryptic digest of proteins. After digestion of proteins with trypsin, peptides were eluted from gel pieces and desalted with stage tips. For the In-solution method, proteins were eluted from anti-HA-agarose with HA peptide followed by TCA-precipitation. Next, proteins were digested with trypsin and desalted with stage tips.

or in-solution tryptic digest. In the former method immunoprecipitated proteins are subjected to tryptic digestion in an SDS-PAGE gel following size separation. Peptides are then eluted from the gel pieces and desalted through stage tips. By contrast for the In-solution method enriched proteins are eluted from anti-HA-agarose. Proteins are precipitated before the digest with trypsin and desalting on stage tips (**Fig. 11**). As negative controls, HeLa cells were treated and prepared in the same way for both experimental settings.

In our experiments we also wanted to distinguish between GABARAPL2 anchored to membranes through PE-modification and unconjugated GABARAPL2, as lipidation might influence the GABARAPL2 interactome. Therefore, we performed stable isotope labeling with amino acids in cell culture (SILAC) and treated labeled cells with ATG7 inhibitor (heavy) or a combination of Torin1 and BafA1 (light). Heavy and light labeled cells were mixed in a 1:1 ratio prior to lysis and HA IP.

5.2.2. MS-analysis of endogenous GABARAPL2 interactome

Desalted samples were analyzed with liquid chromatography tandem MS and evaluated with MaxQuant and Excel. The In-gel approach was performed in duplicates while for the In-solution approach three experiments were performed. With both methods we found similar amounts of proteins. Identified proteins that were changed in their abundance (log_2 SILAC ratio ≥1.0 or ≤-1.0) are regulated in response to the treatments and are candidates GABARAPL2 interacting proteins (**Table 15**). One half of the identified proteins in the in-gel approach was regulated, while only a sixth of the identified proteins showed changes in their abundance in the in-solution approach. After stringent filtering, 233 high confident hits were found in the in-gel

Table 15: Numbers of proteins interacting with GABARAPL2, identified through in-gel or in-solution liquid chromatography tandem MS.

			All regulated proteins			High confident hits		
	Identified in		Total	Lipidated	Delipidated	Total	Lipidated	Delipidated
In-gel:	total	783	374	340	34	233	219	14
	1 replicate	553	341	308	33	114	101	13
	2 replicates	230	33	32	1	19	18	1
In-solution:	total	784	125	87	38	14	8	6
	1 replicate	227	115	79	36	8	4	4
	2 replicates	120	4	4	0	1	1	0
	3 replicates	438	6	4	2	5	3	2

approach while 14 were identified in the in-solution approach.

With both experimental settings we identified well characterized GABARAPL2 interactors such as p62, ATG7, ATG3, CCPG1, HADHA, HADHB, IPO5, RB1CC1, TRIM21 and UBA5. Possible GABARAPL2 interactors identified in large scale screenings such as the nucleoprotein AHNAK2, the small GTPase IRGQ, the ribosomal protein RPS2, the ribophorin membrane protein RPN1 and the mitochondria outer membrane protein VDAC1 were also found in these data sets (**Fig. 12 A&B**) (305-307). Next, regulated proteins were subjected to a functional annotation enrichment analysis with the DAVID tool which unveiled an unexpected connection between GABARAPL2 and lipid metabolism. For the proteins found in the in-gel

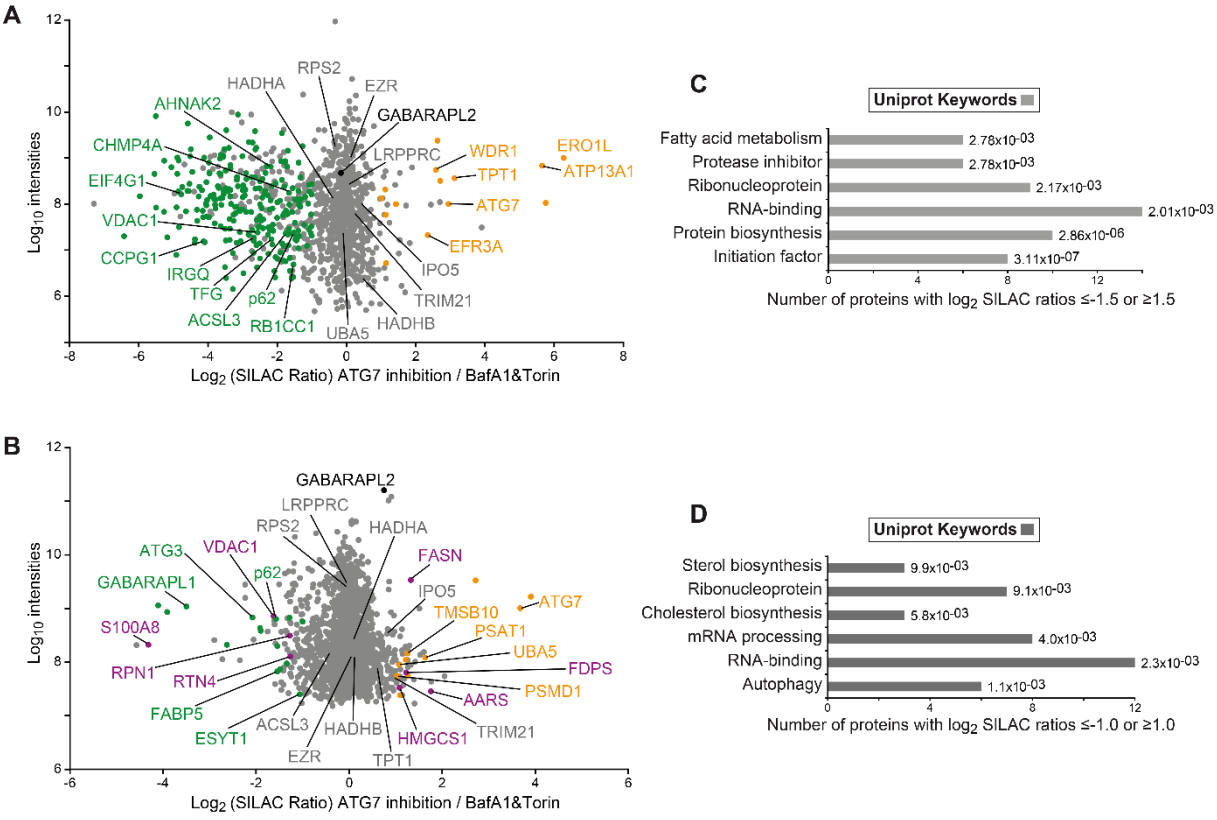

Figure 12: Interactome datasets of endogenous GABARAPL2: (**A&B**) Scatterplots illustrating interactome data of SILAC labeled GABARAPL2^{endoHA} cells prepared with either In-gel (**A**) or In-solution (**B**) MS approaches. Cells were treated with either a combination treatment of Torin1 and Baf1 (light) or ATG7 inhibitor (heavy). Proteins that changed upon treatment more than two-fold (log_2 SILAC ratio ≥1.0 or ≤-1.0) are highlighted in green, orange (high confident hits) and purple (selected, regulated hits). Unchanged proteins are colored in gray. (**C&D**) Proteins from the GABARAPL2^{endoHA} interactome datasets were subjected to an annotation enrichment analysis with DAVID. From the In-gel approach all proteins with SILAC ratios ≥1.5 or ≤-1.5 (**C**) were used for the DAVID analysis while from the In-solution approach all regulated proteins with a SILAC ratio ≥1.0 or ≤-1.0 (**D**) were analyzed. Significantly overrepresented Uniprot keywords are depicted in bar graphs.

experiments, DAVID analysis revealed the gene ontology (GO) term ‘fatty acid metabolism’, while proteins identified with the in-solution method were connected to the terms ‘sterol biosynthesis’ and cholesterol biosynthesis’ (**Fig. 12 C**&**D**). In the following, we focused on the connection between GABARAPL2 and fatty acid metabolism and characterized the interaction between GABARAPL2 and ACSL3 as it was also one of the proteins found in both approaches.

5.2.3. Validation of ACSL3-GABARAPL2 interaction

To characterize ACSL3, we first validated the GABARAPL2 and ACSL3 interaction with HA IPs. Lysates from parental and GABARAPL2^{endoHA} cell transiently transfected with Myc-tagged ATG7, p62 or ACSL3 and untreated cells were subjected to HA IPs followed by immunoblot analysis with tag- and gene specific antibodies. IPs with ATG7 and p62 were performed as positive controls. Endogenous GABARAPL2 associated with overexpressed (**Fig 13 A-C**) as

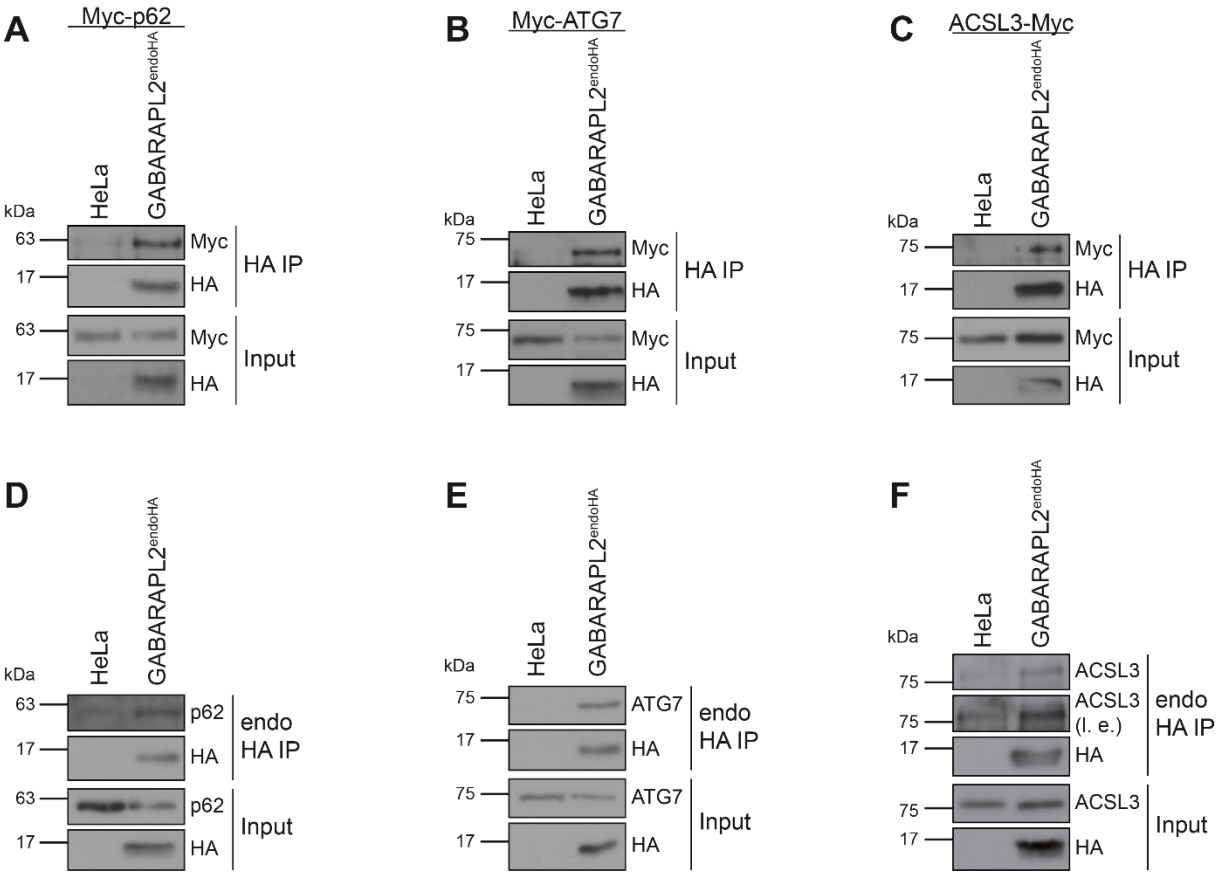

Figure 13: Validation of GABARAPL2 interactors: (**A-C**) Parental and GABARAPL2^{endoHA} cells were transiently transfected with Myc-ATG7 (**A**), Myc-p62 (**B**) or ACSL3-Myc (**C**) prior to HA IPs and immunoblot analysis. (**D-F**) HA IPs of parental and GABARAPL2^{endoHA} cells were analyzed using immunoblotting with anti-p62 (**D**), anti-ATG7 (**E**) and anti-ACSL3 (**F**) antibodies. l.e. means long exposure.

well as endogenous ATG7, p62 and ACSL3 (**Fig. 13 D-F**). Taken together, the results show that the generated hATG8^{endoHA} cell lines are useful tools to study and characterize the interactome from hATG8 proteins. Further GABARAPL2 indeed binds ACSL3 in a direct or indirect manner.

5.3. ACSL3, a novel interactor of GABARAPL2

5.3.1. ACSL3 is neither an autophagy receptor nor an autophagy substrate

Given the role of GABARAPL2 in selective autophagy (308), we first investigated whether ACSL3 is a novel autophagy receptor or a substrate of autophagy. GABARAPL2^{endoHA} cells treated with Torin1, BafA1 or ATG7 inhibitor (**Fig. 14 A**) or reversely transfected with GAPARAPL2 specific and non-targeting control siRNAs (**Fig. 14 B**) were analyzed by immunoblotting with an ACSL3 antibody. Both experiments showed no changes in ACSL3 protein abundance which indicates that ACSL3 is not degraded via autophagy under the tested conditions.

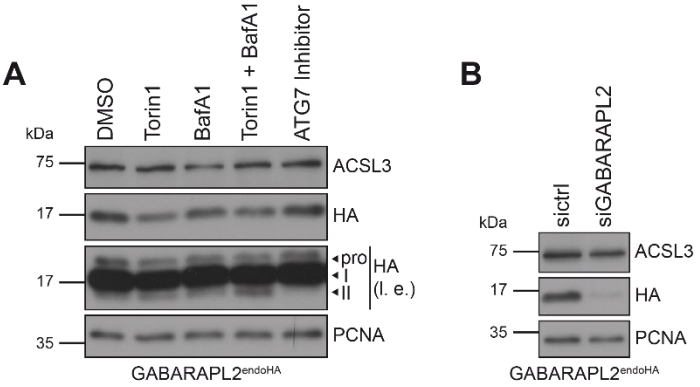

Figure 14: ACSL3 is not associated with autophagy: (**A**&**B**) GABARAPL2^{endoHA} cells treated with Torin1, Baf1A, ATG7 inhibitor (**A**) or siRNA (**B**) as indicated were analyzed with immunoblotting and anti-ACSL3 antibody. Arrows mark precursor (pro), lipidated (II) and non-lipidated (I) GABARAPL2. l.e. means long exposure.

5.3.2. GABARAPL2 is stabilized by the interaction with ACSL3

Next, we examined the abundance of GABARAPL2 protein upon ACSL3 depletion. GABARAPL2^{endoHA} cells were reversely transfected with two different ACSL3 siRNAs followed by immunoblot analysis. In four independent experiments we could show that GABARAPL2 is significantly decreased upon ACSL3 knockdown and thus, is stabilized by ACSL3 (**Fig. 15 A**). To investigate whether the absence of ACSL3 induced degradation of GABARAPL2 through

autophagy or the proteasome, we treated GABARAPL2^{endoHA} cells with the autophagosomal inhibitor BafA1 or the proteasome inhibitor Bortezomib (Btz) upon ACSL3 knockdown. Cell lysates from three independent experiments were analyzed by immunoblot analysis. GABARAPL2 protein levels were partially restored through blockage of autophagy but not

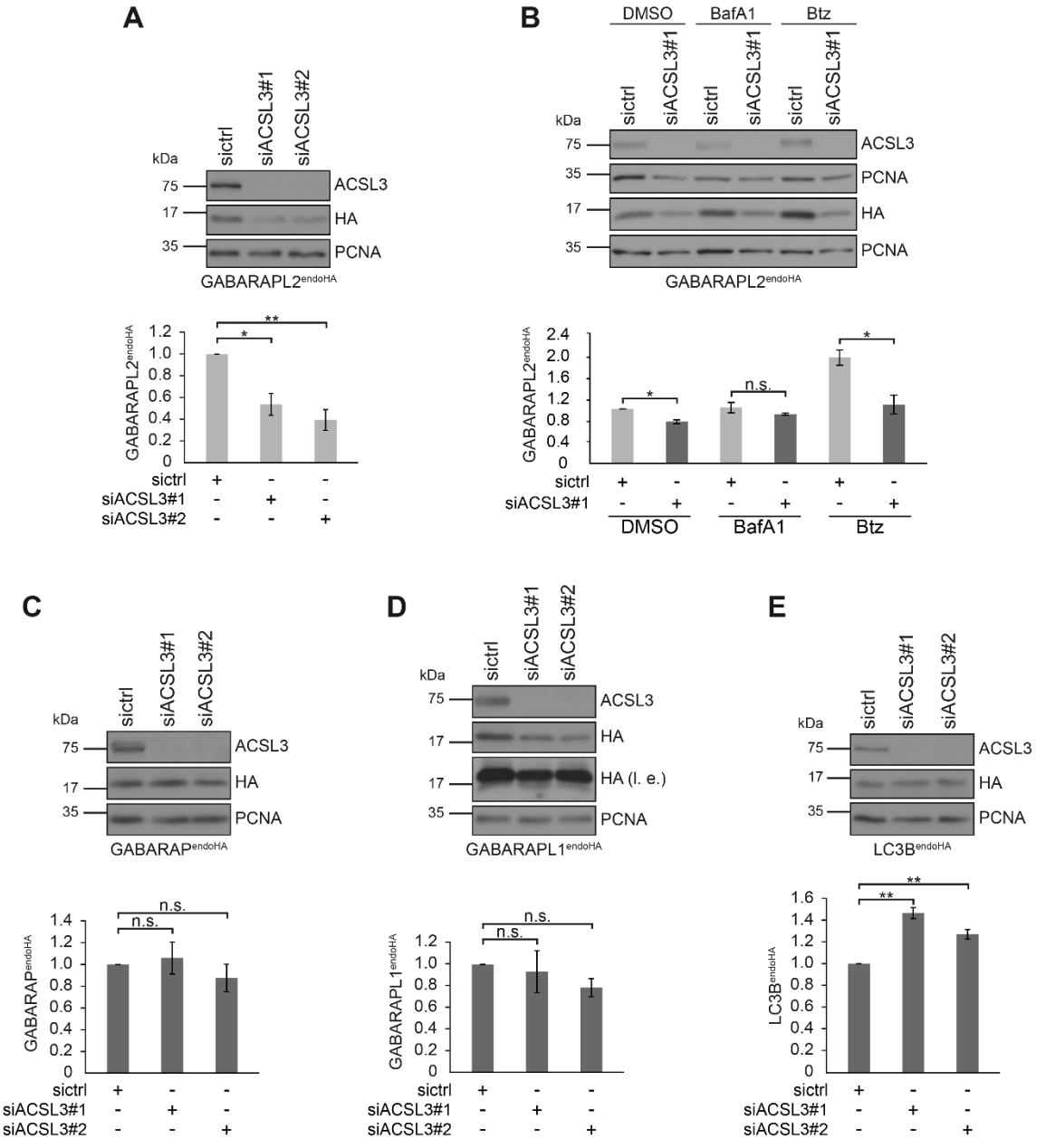

Figure 15: Stabilization of GABARAPL2 by ACSL3: (A-E) GABARAPL2^{endoHA} (**A&B**), GABARAP^{endoHA} (**C**), GABARAPL1^{endoHA} (**D**) and LC3B^{endoHA} (**E**) cells were reversely transfected with two different ACSL3 siRNAs and control siRNA followed by lysis, immunoblotting and analysis with indicated antibodies. Additionally to siRNA transfection, GABARAPL2^{endoHA} were treated with BafA1 or Btz (**B**). l.e. means long exposure. Data in bar diagrams represent quantitative analysis from four (**A,C-E**) or three (**B**) independent experiments as mean±sem. HA:PCNA ratio normalized to sictrl (**A,C-E**) or sictrl-DMSO (**B**) was statistically analyzed with Students t-test (*P<0.05, **P<0.01). n.s stands for not significant.

through proteasomal inhibition which indicates that GABARAPL2 is degraded through autophagy upon ACSL3 depletion (**Fig. 15 B**). Due to the high structural similarity between the hATG8 proteins, we also investigated the effects of ACSL3 depletion on GABARAP, GABARAPL1 and LC3B protein levels. Protein abundance of GABARAP and GABARAPL1 were not changed significantly (**Fig. 15 C&D**). Interestingly, LC3B protein levels significantly increased upon ACSL3 knockdown which might be a compensation for decreased GABARAPL2 protein levels (**Fig. 15 E**). In summary ACSL3 stabilizes GABARAPL2 but not GABARAP, GABARAPL1 or LC3B and thus, might serve as GABARAPL2 specific regulator.

Because ACSL3 is a single-pass type III ER membrane protein, we visualized ER morphology to rule out that ACSL3 depletion affected ER integrity. GABARAPL2^{endoHA} cells treated with siACSL3 were immunolabeled with ER membrane marker anti-Calnexin and ER-exit site marker anti-SEC13. Indeed, fluorescence microscopy showed that ER structure (**Fig. 16 A**) and ER exit sites (**Fig. 16 B**) were not obviously altered upon siACSL3 knockdown.

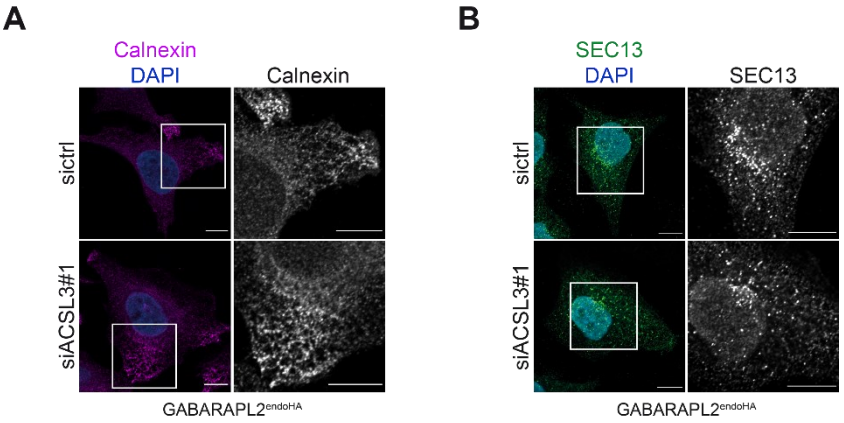

Figure 16: ER morphology upon ACSL3 depletion: (**A**&**B**) GABARAPL2^{endoHA} cells were treated as indicated, fixed and immunolabeled with anti-Calnexin (**A**) or anti-SEC13 (**B**). Scale bars: 10 µm.

5.3.3. Generation and validation of ACSL3^{NeonGreen} cell line with CRISPR-Cas9

To investigate the subcellular localization of GABARAPL2 and ACSL3, we sought to perform immunolabeling followed by confocal microscopy. Since we could not find a specific ACSL3 antibody for this approach, we tagged ACSL3 with NeonGreen in the GABARAPL2^{endoHA} cell line using CRISPR-Cas9. As the N-terminus helix region of ACSL3 is inserted into the outer ER leaflet, we tagged ACSL3 at the C-terminal end. We used the same procedure as described in 5.1.1 (**Fig. 7**) except that the DNA template started with the end section of the last exon of

ACSL3 followed by the NeonGreen gene, T2A, blasticidine-resistance gene and the 3'UTR of ACSL3 (**Fig. 17**). The stop codon of ACSL3 was removed at the original position and inserted after the blasticidine-resistance gene. Correct insertion of the tag was verified by Sanger sequencing (**Table 16**).

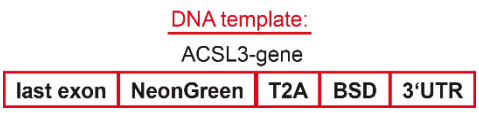

Figure 17: Schema of ACSL3 DNA-template: Schematic display of DNA-template used for endogenous, C-terminal NeonGreen tagging of ACSL3 with CRISPR-Cas9.

Table 16: Sequence of the C-terminal part of ACSL3^{NeonGreen}. Bold letters mark the integrated NeonGreen gene.

Cell lines	Sequences
GABARAPL2^{endoHA}/ ACSL3^{endoNeonGreen}	TATTTTTTTTTAATCATCTTAGCAAGTCTGGAAAAGTTTGAAATTCCAGTAAAAATTC GTTTGAGTCATGAACCGTGGACCCCTGAAACTGGTCTGGTGACAGATGCCTTCAA GCTGAAACGCAAAGAGCTTAAAACACATTACCAGGCGGACATTGAGCGAATGTATG GAAGAAAA**GCTGGCGGCATGGTGAGCAAGGGCGAGGAGGATAACATGGCCTCT CTCCCAGCGACACATGAGTTACACATCTTTGGCTCCATCAACGGTGTGGACTTTG ACATGGTGGGTCAGGGCACCGGCAATCCAAATGATGGTTATGAGGAGTTAAACC TGAAGTCCACCAAGGGTGACCTCCAGTTCTCCCCCTGGATTCTGGTCCCTCATAT CGGGTATGGCTTCCATCAGTACCTGCCCTACCCTGACGGGATGTCGCCTTTCCAG GCCGCCATGGTAGATGGCTCCGGATACCAAGTCCATCGCACAATGCAGTTTGAA GATGGTGCCT**

For further validation of the GABARAPL2^{endoHA}/ACSL3^{endoNeonGreen} cell line, we performed immunoblot analysis with anti-ACSL3, anti-NeonGreen and anti-HA antibodies. Parental GABARAPL2^{endoHA} cells and HeLa cells transiently transfected with TOMM20-NeonGreen served as controls. As expected, NeonGreen tagged ACSL3 migrated at the calculated size of approximately 106 kDa (ACSL3: 80 kDa; NeonGreen: 26kDa) (**Fig. 18 A**). To monitor the localization of ACSL3, we performed confocal LSM (**Fig. 18 B**) and super-resolution radial fluctuation imaging (SRRF) (**Fig. 18 C**). GABARAPL2^{endoHA}/ACSL3^{endoNeonGreen} cell were fixed prior to immunolabeling with anti-Calnexin and anti-NeonGreen (only for LSM) antibodies. SRRF imaging was always performed in collaboration with Santosh Phuyal and Hesso Farhan (University of Oslo). ACSL3 colocalized with the ER-membrane chaperone Calnexin indicating that ACSL3 localization at the ER membrane is unaffected by the NeonGreen tag (**Fig. 18 B**&**C**). To test the functionality of the ACSL3-NeonGreen fusion protein, we examined LD formation as ACSL3 is essential for LD biogenesis (155,225). To induce LD formation, GABARAPL2^{endoHA}/ACSL3^{endoNeonGreen} cells were treated with oleic acid or ethanol (EtOH) as control followed by fixation and staining of neutral lipids and phospholipids. As expected, ACSL3 colocalized with neutral lipids and phospholipids in control cells and relocated to LD

phospholipid monolayers around neutral lipid cores in oleic acid treated cells. Thus, enzymatic activity of ACSL3 in LD biogenesis is not affected by the NeonGreen tag (**Fig. 18 D**). Together,

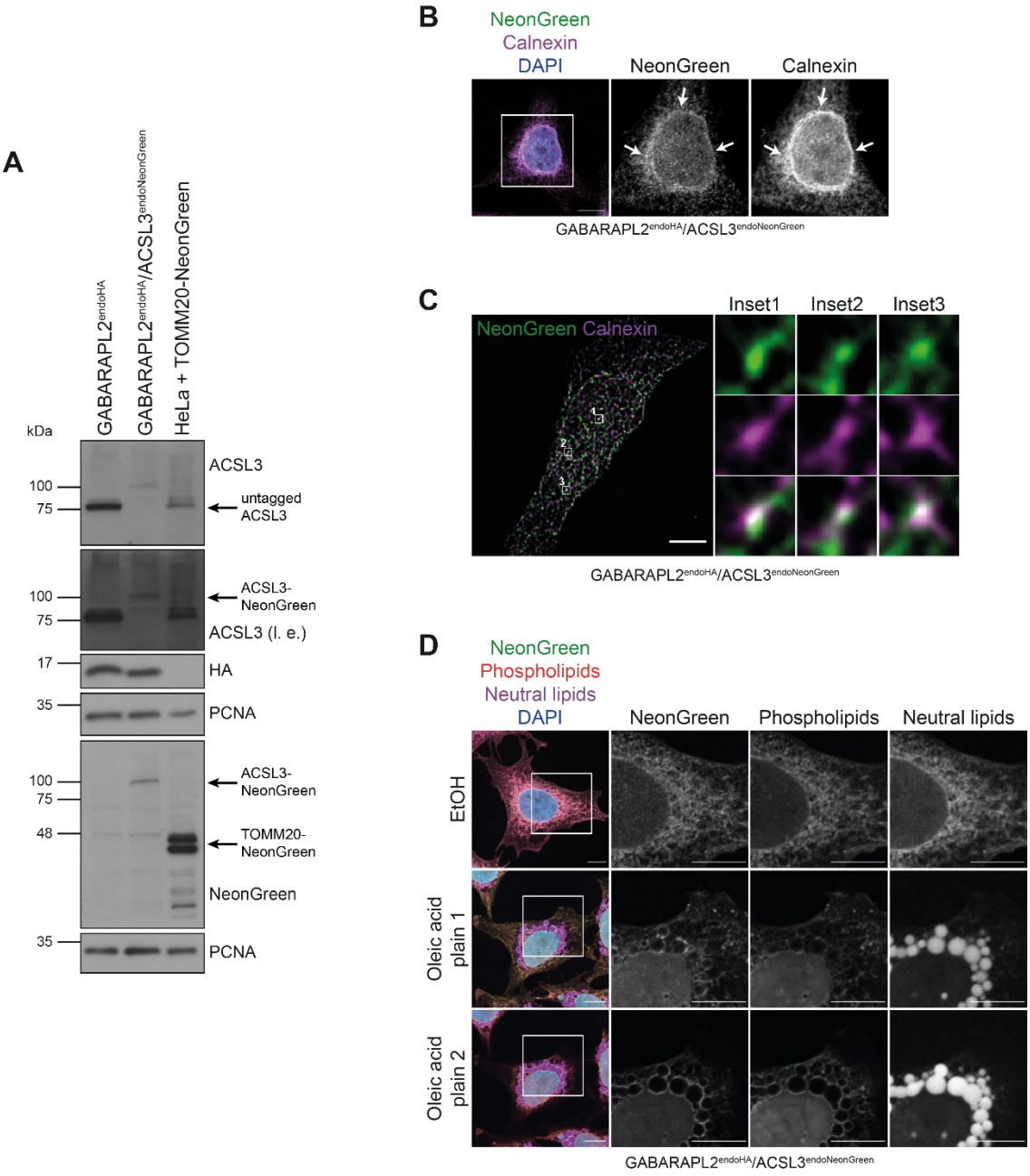

Figure 18: Validation of GABARAPL2^{endoHA}/ACSL3^{endoNeonGreen} cell line: (**A**) GABARAPL2^{endoHA}, GABARAPL2^{endoHA}/ACSL3^{endoNeonGreen} and Hela cells transfected with TOMM20-NeonGreen were lysed and subjected to immunoblotting with indicated antibodies. l.e. means long exposure. (**B&C**) GABARAPL2^{endoHA}/ACSL3^{endoNeonGreen} were fixed, immunolabeled as indicated and analyzed with confocal LSM (**B**) or SRRF(**C**). Magnified views (Insets) display colocalization events between ACSL3-NeonGreen and Calnexin. Arrows indicate colocalization events. (**D**) GABARAPL2^{endoHA}/ACSL3^{endoNeonGreen} treated with oleic acid or EtOH for 24 h were fixed prior to staining of neutral lipids and phospholipids. For oleic acid treatment two confocal planes are shown. Scale bars: 10 µm (**B**&**D**), 5 µm (**C**).

these results demonstrate that ACSL3 retains its functionality in the CRISPR-Cas9 generated GABARAPL2^{endoHA}/ACSL3^{endoNeonGreen} cell line.

To finally examine the localization of GABARAPL2 and ACSL3, we performed confocal LSM and SRRF imaging with the GABARAPL2^{endoHA}/ACSL3^{endoNeonGreen} cell line immunolabeled with anti-HA and anti-NeonGreen (only for LSM) antibodies. Partial colocalization of ACSL3 and GABARAPL2 confirmed our results from the biochemical binding experiments (**Fig. 19 A**&**B**).

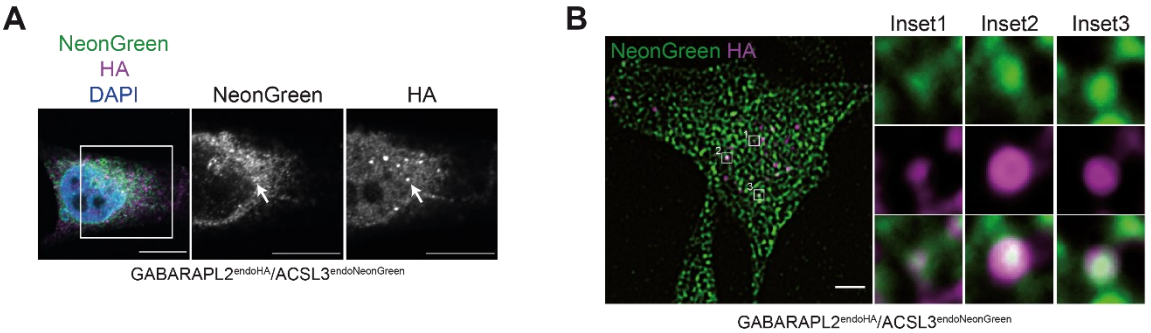

Figure 19: Subcellular localization of GABARAPL2 and ACSL3: (**A**&**B**) GABARAPL2^{endoHA}/ACSL3^{endoNeonGreen} cells, fixed and immunolabeled as indicated were imaged with LSM (**A**) or SRRF (**B**). Magnified views (Insets) display colocalization events between ACSL3-NeonGreen and GABARAPL2. Arrows indicate colocalization events. Scale bars: 10 µm (**A**), 5 µm (**B**).

5.3.4. Characterization of GABARAPL2-ACSL3 binding sites

To identify the interaction sites in ACSL3 and GABARAPL2 we focused on possible LIR (LC3-interacting region) and UIM (ubiquitin-interacting motif) binding motifs in ACSL3 and the two known binding sites LDS (LIR-docking site) and UDS (UIM-docking site) in GABARAPL2 (19-24). With the help of the online tool iLIR we identified four possible LIR motifs (LIR-1: 65–71, LIR-2: 135–140, LIR-3: 589–594, LIR-4: 643–648) and by manual inspection we found two possible UIM sites (UIM-A: 73-81, UIM-B: 663-670) in ACSL3 (**Fig. 20 A**). To investigate whether GABARAPL2 binds ACSL3 in a LIR- or UIM dependent manner, we purified GST-tagged wild-type and LIR- or UIM-binding deficient GABARAPL2 protein to perform pulldown assays. We obtain the LDS and UDS mutants of GABARAPL2 by replacing the relevant amino acids of either these binding motifs with alanine (ΔLDS: Y49A/L50A, ΔUDS: I76A/F77A/L78A/F79A). For the pulldown assays, we additionally prepared cell lines stably expressing HA-tagged, wild-type ACSL3 or truncated ACSL3 variants.

The short ACSL3 fragment comprised amino acids 1-85 including LIR-1 and UIM-A while the longer fragment included amino acids 86-718 with LIR-2, LIR-3, LIR-4 and UIM-B (**Fig. 20 A**). To control localization and expression of wild-type and fragmented ACSL3, fixed cells were immunolabeled with anti-HA antibody and analyzed by LSM. As expected, transmembrane domain containing ACSL3 1-85 accumulated around the nucleus, similar to wild-type ACSL3, and is probably integrated in the ER-membrane, while ACSL3 86-718 protein is distributed throughout the cytosol (**Fig. 20 B**). Finally, we performed pulldown assays with lysates from ACSL3 wild-type and fragment expressing cell lines and purified wild-type and mutant GST-GABARAPL2 protein followed by immunoblot analysis. Wild-type GABARAPL2 associated

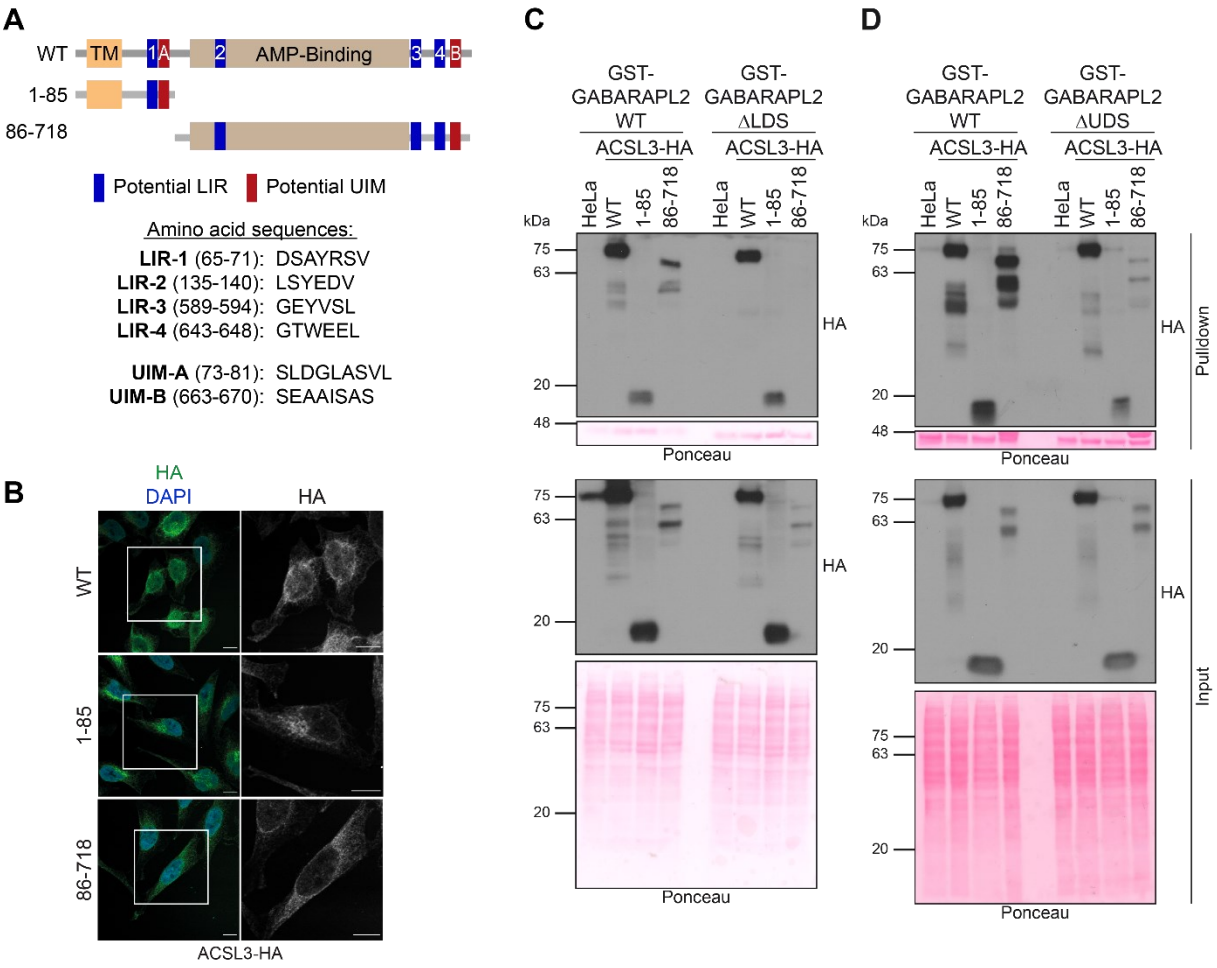

Figure 20: GABARAPL2 binds ACSL3 in a LIR-dependent manner: (**A**) Schematic display of potential LIRs and UIMs in wild type (WT) ACSL3 and fragments. (**B**) Cells expressing WT ACSL3 or fragments were fixed followed by immunolabeling with anti-HA. Scale bars: 10 µm. (**C**&**D**) Lysates driven from HeLa cells expressing WT ACSL3 or fragments were subjected to pulldown assays with WT and LIR (**C**) or UIM (**D**) binding deficient GST-GABARAPL2 proteins followed by immunoblot analysis. Ponceau staining was used as loading control.

with all ACSL3 variants, suggesting that both fragments contain at least one distinct GABARAPL2 binding site. Furthermore, immunoblot analysis showed binding of GABARAPL2 ΔLDS to full length and ACSL3 1-85 while it failed to bind ACSL3 86-718 (**Fig. 20 C**). Thus, ACSL3 exhibits a functional LIR binding motif in amino acid sequence 86-718. Interestingly, the UDS mutation in GABARAPL2 resulted in decreased binding to both ACSL3 fragments but did not affect the interaction with wild-type ACSL3 (**Fig. 20 D**). It was described that mutation of the phenylalanine at position 77 in GABARAPL2 is sufficient to prevent UDS-UIM binding (23). Hence, we performed an additional pulldown analysis with purified GST-GABARAPL2 F77A and wild-type and ACSL3-HA 1-85 expressing cells. However, in this setting we failed to detected a reduced GABARAPL2 binding of the ACSL3 1-85 fragment (**Fig. 21**).

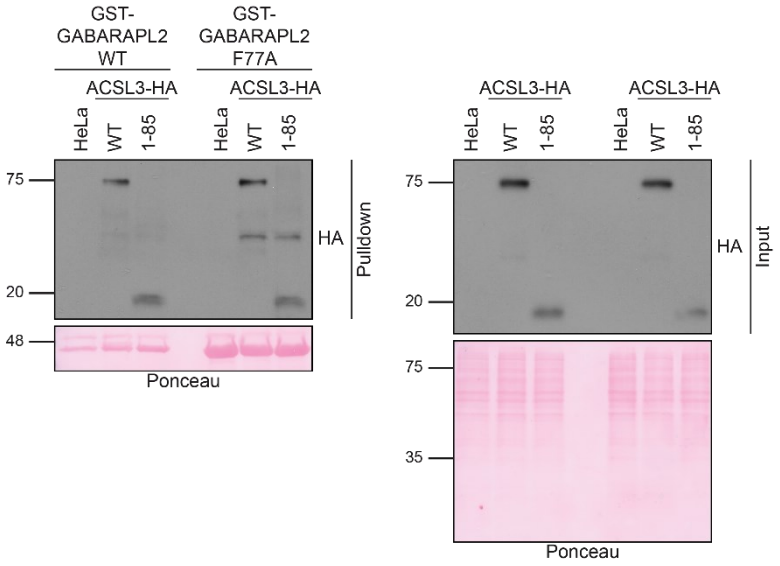

Figure 21: Second binding motif in ACSL3: Pulldown assay of purified GST-GABARAPL2 and GST-GABARAPL2 F77A incubated with wild type ACSL3-HA and 1-85 fragment. Immunoblot analysis was analyzed with HA antibody and Ponceau staining.

While the analysis of a potentially UDS-UIM driven GABARAPL2-ACSL3 interaction is not conclusive, these preliminary results indicated that either GABARAPL2 has a UIM binding motif in ACSL3 1-85 and the amino acids exchange in the ΔUDS is not sufficient to prevent the UDS-UIM interaction or GABARAPL2 contains a LIR- and UIM-unrelated binding motif.

Next, we examined the recruitment of GABARAPL2 to ACSL3 located at the ER with subcellular fractionation by differential centrifugation. Therefore, we gradually centrifuged HeLa cells stably expressing wild-type or LDS deficient HA-GABARAPL2 (**Fig. 22 A**) with increasing centrifugal force to obtain an enrichment of the ER. Fractions were analyzed by

immunoblotting with antibodies against HA, ACSL3, the nuclear marker Lamin A/C, the mitochondrial marker Cox, the microtubule marker α-Tubulin, the Golgi marker GM130 and the ER marker Calnexin. Wild-type GABARAPL2 cofractionated with the ER marker calnexin, while GABARAPL2 ΔLDS was not found in the ER-membrane fraction (**Fig. 22 B**). This result indicates that the recruitment of GABARAPL2 to the ER and its interaction with ACSL3 is LIR-dependent.

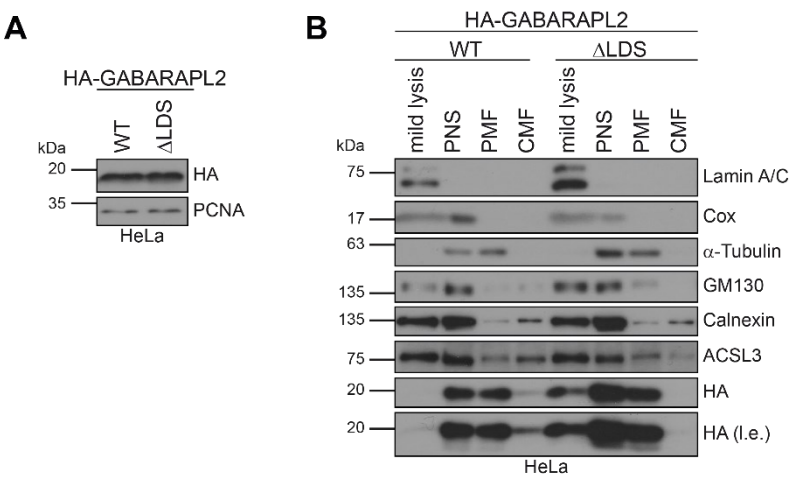

Figure 22: LDS of GABARAPL2 mediates ER recruitment: (**A**) Immunoblot analysis of HeLa cells stably expressing HA-tagged, WT or ΔLDS GABARAPL2. (**B**) HeLa cells stably expressing WT or ΔLDS GABARAPL2 were subjected to subcellular fractionation and analyzed by immunoblotting with indicated antibodies. l.e. means long exposure. Mild lysis: whole cell lysate; PNS: post nuclear fraction; PMF: post mitochondrial fraction; CMF: crude microsomal fraction.

To examine which of the four potential LIR motifs mediates the GABARAPL2-ACSL3 binding, we replaced the relevant amino acids of each motif with alanine and transiently expressed these mutant versions of ACSL3 in HeLa cells. However, immunoblot analysis of these ACSL3 variants revealed a strong variation in expression levels (**Fig. 23**). Mutation of LIR-1 did not affected expression of ACSL3 while deletion of LIR-2 and LIR-4 drastically decreased ACSL3 expression levels. ACSL3 ΔLIR3 expression was reduced compared to the wild type ACSL3

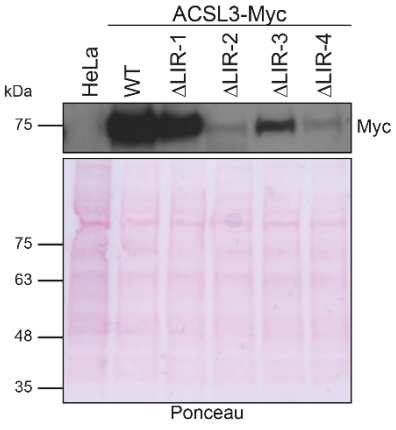

Figure 23: Expression levels of mutated ACSL3-Myc: Hela cells were transiently transfected with Myc-tagged WT and mutated ACSL3. Parental and transfected cells were analyzed with immunoblotting. Ponceau staining shows equal loading.

but still detectable (**Fig. 23**). Due to the strong deviations in expression levels, we did not proceed to perform pulldown assays with this experimental setup.

5.3.5. Localization of UBA5-ACSL3 interaction site

In our study we detected that UBA5 is also interacting with ACSL3. Thus, we purified GST-UBA5 and performed pulldown assays with wildtype and truncated ACSL3. Immunoblot analysis unveiled the presence of ACSL3 wild-type and 1-85 fragment in UBA5 pulldowns, indicating that the N-terminal part of ACSL3 is likely sufficient to mediate the binding between ACSL3 and UBA5. However, it is unclear if ACSL3 86-718 is also pulled down by GST-UBA5 as the bait exhibits the same size as the fragment (**Fig. 24**). To further clarify if there is a second binding site in ACSL3 86-718 and to confirm the detected binding region, UBA5 could be purified with a smaller tag such as 6xHIS.

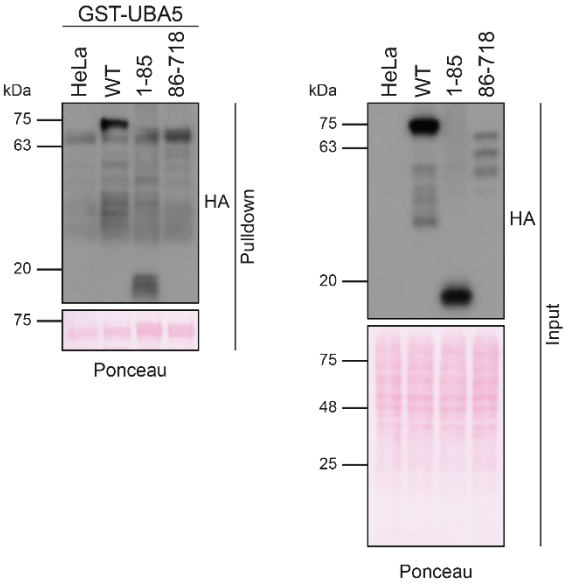

Figure 24: ACSL3-UBA5 interacting site: GST-UBA5 was incubated with WT and fragmented ACSL3-HA followed by GST-pulldown and immunoblot analysis with HA-antibody and Ponceau.

5.4. GABARAPL2 recruits UBA5 to the ER bound ACSL3

5.4.1. UBA5 is stabilized by interaction with ACSL3

To elucidate the biological function of the GABARAPL2-ACSL3 interaction, we turned our attention to GABARAPL2 and its known connections with the ER membrane. Since it was shown in a recent publication that GABARAPL2 recruits UBA5 to the ER membrane (95), we speculated whether ACSL3 might serve as an anchor site for UBA5 and GABARAPL2 at the ER. First, we confirmed the GABARAPL2-UBA5 interaction with HA IPs using cell lysates from parental and GABARAPL2^{endoHA} cells transiently transfected with Myc-UBA5 (**Fig. 25 A**).

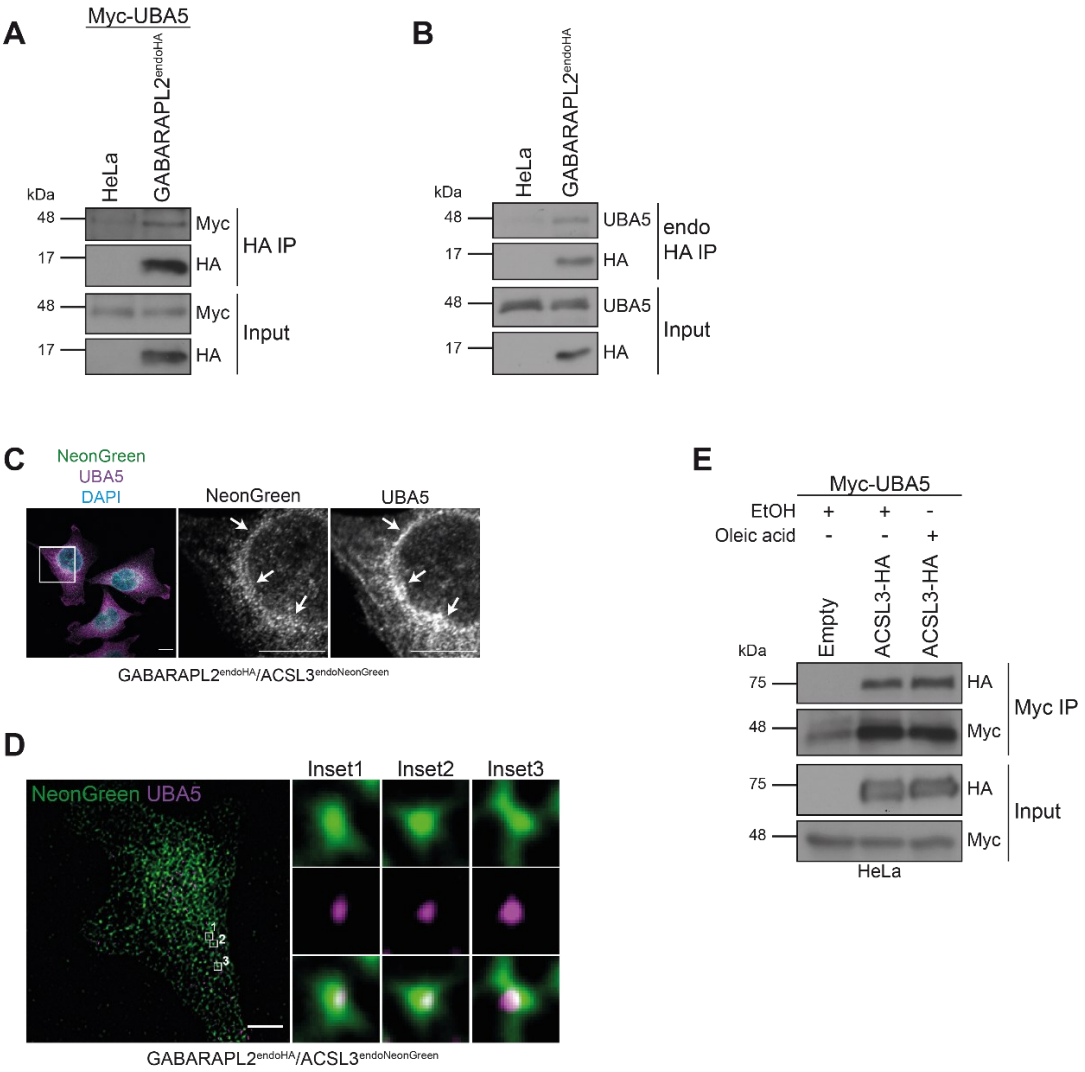

Figure 25: UBA5 interact with ACSL3: (**A**&**B**) GABARAPL2^{endoHA} cells, transfected with Myc-UBA5 (**A**) or left untreated (**B**) were subjected to HA IP and immunoblotting with indicated antibodies. (**C**&**D**) GABARAPL2^{endoHA} cells were fixed, immunolabeled as indicated and analyzed with confocal LSM (**C**) or SRRF (**D**). Scale bars: 10 µm (**C**), 5 µm (**D**). (**E**) Parental and ACSL3-HA expressing HeLa cells were transfected with Myc-UBA5 and treated for 24 h with oleic acid or EtOH followed by Myc IP and immunoblotting.

Furthermore, we provided evidence that both proteins also bind at endogenous expression levels by performing HA IPs with untreated HeLa and GABARAPL2^{endoHA} cells (**Fig. 25 B**). Next, we fixed GABARAPL2^{endoHA}/ACSL3^{endoNeonGreen} cells prior to immunolabeling with anti-UBA5 and anti-NeonGreen (only for LSM) antibodies and analysis by confocal LSM and SRRF (**Fig. 25 C**&**D**). With both microscopic techniques we could show partial colocalization of ACSL3 and UBA5. Therefore, we treated transiently transfected parental and ACSL3-HA expressing cells with EtOH or oleic acid and performed Myc IPs to examine whether UBA5 and ACSL3 also interact. Indeed, immunoblot analysis revealed binding between ACSL3 and UBA5 independent of oleic acid treatment (**Fig. 25 E**).

Due to the fact that GABARAPL2 is degraded upon ACSL3 depletion, we examined if UBA5 is also stabilized by ACSL3. Hence, GABARAPL2^{endoHA} cells reversely transfected with specific ACSL3 siRNA and treated with BafA1 or Btz were analyzed by immunoblotting. Similar to GABARAPL2, UBA5 protein abundance significantly decreased upon ACSL3 knockdown. However, UBA5 protein levels were not restored upon inhibition of autophagosomal or proteasomal degradation (**Fig. 26 A**). Additionally, we examined UBA5 protein abundance upon GABARAPL2 depletion to exclude indirect effects, due to decreased GABARAPL2 protein levels caused by ACSL3 knockdown. GABARAPL2^{endoHA} cells treated with siGABARAPL2 and analyzed by immunoblotting indeed showed no changes in UBA5 protein

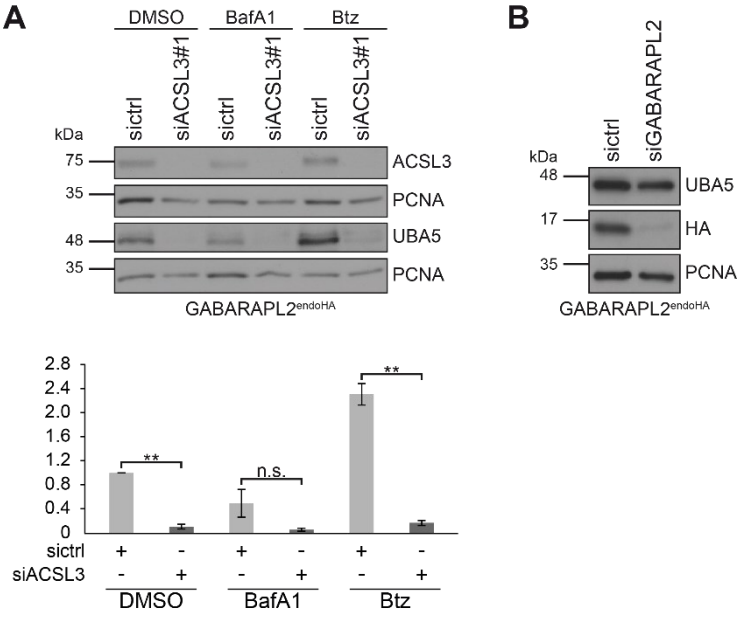

Figure 26: UBA5 is stabilized by ACSL3: (**A**) GABARAPL2^{endoHA} cells transfected with siACSL3 were treated with BafA1 or Btz and analyzed with immunoblotting and indicated antibodies. Quantitative analysis (n=3) is represented in the bar diagram as mean±sem. UBA5:PCNA ration normalized to sictrl-DMSO. Data was statistically analyzed with Students t-test (**P<0.01). n.s stands for not significant. (**B**) GABARAPL2^{endoHA} cells were reversely transfected with indicated siRNAs followed by immunoblotting.

levels (**Fig. 26 B**). Taken together, these results indicate that UBA5 associates with ACSL3 which also stabilizes UBA5.

5.4.2. UBA5-ACSL3 binding is mediated by GABARAPL2

The finding that UBA5 is recruited to the ER by GABARAPL2 and interacts with ACSL3 raises the question if the observed UBA5-ACSL3 binding is dependent on GABARAPL2. Therefore, we reversely transfected ACSL3-HA expressing HeLa cells with GABARAPL2 siRNA and Myc-UBA5. Lysates were subjected to IP with anti-Myc agarose. Immunoblot analysis exhibited decreased binding between ACSL3 and UBA5 upon GABARAPL2 depletion (**Fig. 27 A**). These data indicate that UBA5 is recruited to the ER by GABARAPL2 and together form a complex with ACSL3. This is further supported by SRRF imaging of GABARAPL2^{endoHA}/ ACSL3^{endoNeonGreen} cells immunolabeled with anti-HA and anti-UBA5 which showed that all three proteins colocalized (**Fig. 27 B**).

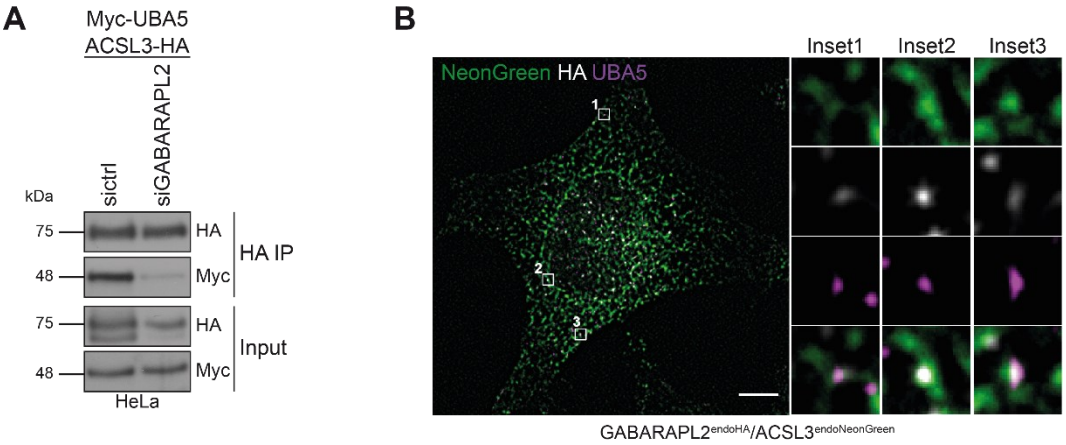

Figure 27: GABARAPL2 recruits UBA5 to ACSL3: (**A**) HeLa cells expressing ACSL3-HA were transfected with Myc-UBA5 and siRNA as indicated. Lysates were subjected to Myc IP and immunoblotting with anti-HA and anti-c-Myc antibodies. (**B**) GABARAPL2^{endoHA}/ACSL3^{endoNeonGreen} cells were fixed, immunolabeled with anti-UBA5 and anti-HA antibodies and analyzed with SRRF.

5.4.3. Ufmylation pathway components are affected by ACSL3 depletion

The E1 enzyme UBA5 is part of the UFM1 conjugation system and responsible for the very first step in the UFM1 protein conjugation cascade (89,90). Consequently, we examined if decreased UBA5 and ACSL3 protein abundance upon ACSL3 depletion influenced the other

pathway components involved in ufmylation. In three independent experiments GABARAPL2^{endoHA} cells were reversely transfected with ACSL3 specific and non-targeting siRNA and treated with DMSO, BafA or Btz followed by immunoblotting. Alike UBA5, protein levels of DDRGK1 and UFL1 were significantly decreased and not restored through blockage of the autophagosome or proteasome. In contrast UFC1 protein levels significantly increased in response to ACSL3 knockdown and UFM1 conjugation levels did not change (**Fig. 28 A&B**). Taken together, UBA5, UFL1 and DDRGK1 protein levels are decreased by ACSL3 depletion, possibly through transcriptional regulation. Thus, the UFM1 conjugation pathway seems to be regulated by ACSL3 in a direct or indirect manner.

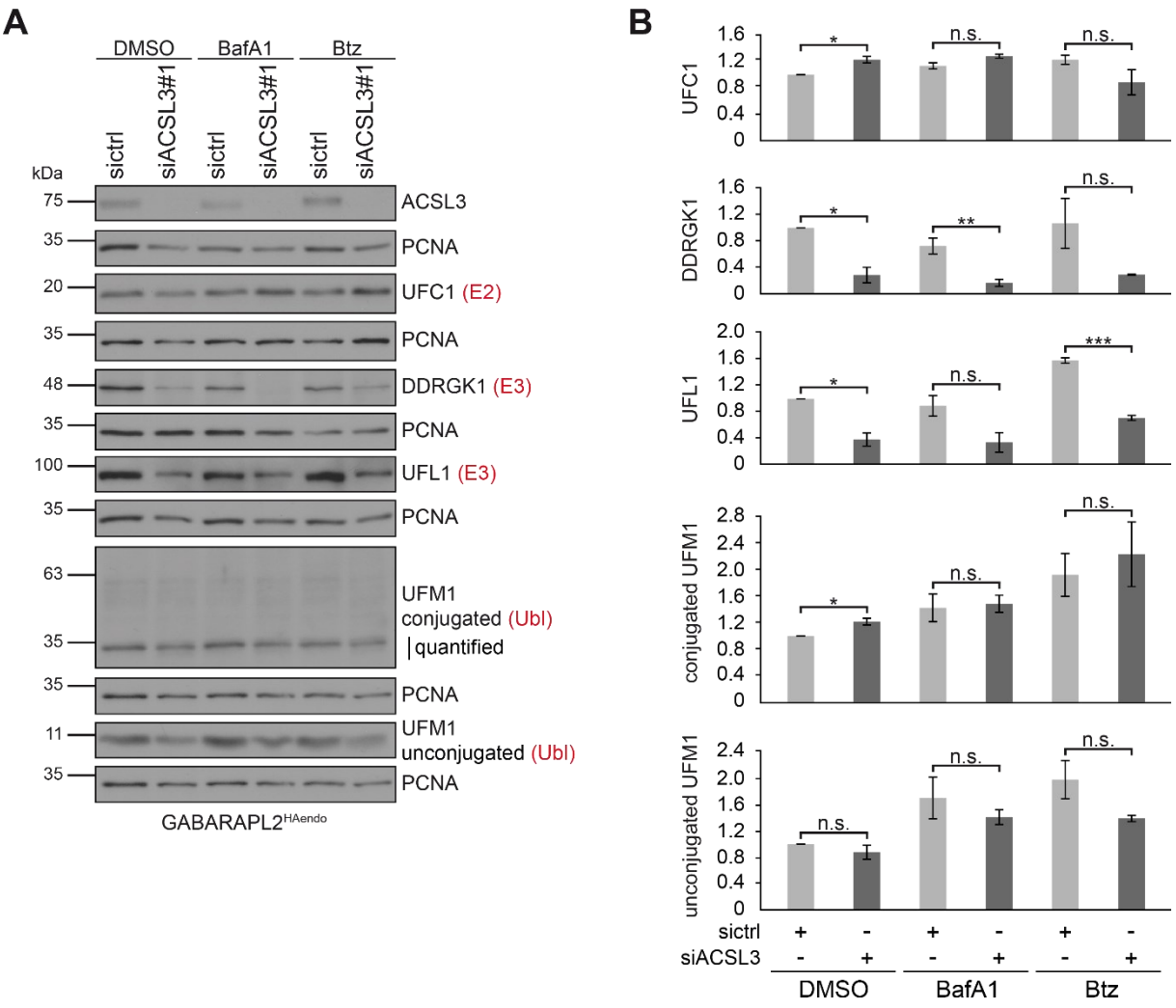

Figure 28: UFM1 conjugation system is regulated by ACSL3: (**A**) GABARAPL2^{endoHA} cells transfected with siACSL3 and non-targeting siRNA (sictrl) were treated with BafA1 or Btz. Cell lysates were subjected to immunoblotting with indicated antibodies. (**B**) Quantitative analysis from A and two additional experiments (n=3) is represented as mean±sem in bar diagrams. Protein:PCNA ratio was normalized to sictrl-DMSO and statistically analyzed with Students t-test (*P<0.05, **P<0.01, ***P<0.001). n.s stands for not significant.

5.4.4. Lipid droplet formation affects ufmylation

Since ACSL3 is essential for lipid droplet biogenesis, we investigated the effect of oleic acid treatment on ufmylation pathway components. GABARAPL2^{endoHA} cells were treated with oleic acid or EtOH for 0.5, 4 or 8 h to analyze different time point of lipid droplet formation (**Fig. 29 A**). Protein abundance of UBA5 significantly decreased within 8 h, while UFC1 levels were unchanged through oleic acid treatment. Already after 0.5 h we detected significantly less

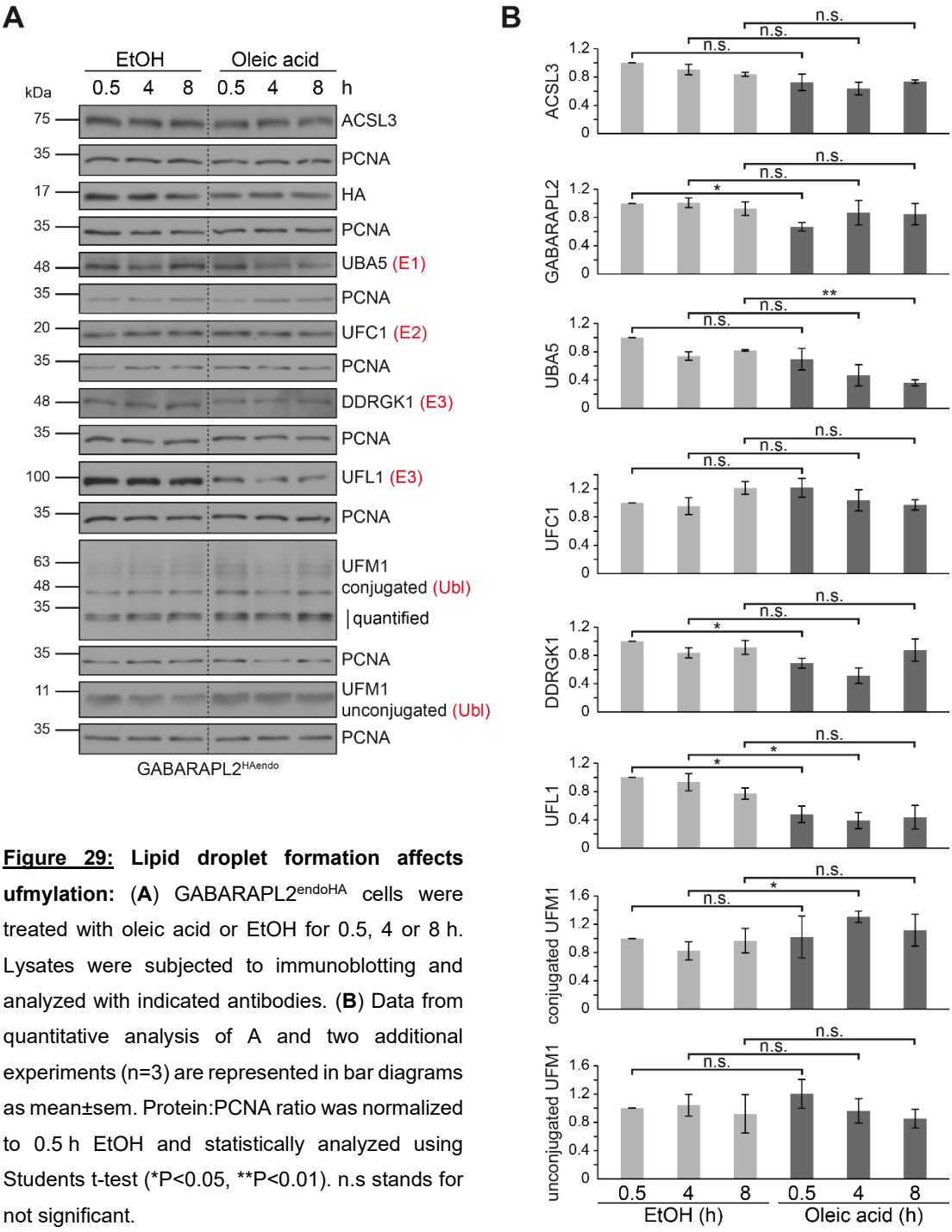

Figure 29: Lipid droplet formation affects ufmylation: (**A**) GABARAPL2^{endoHA} cells were treated with oleic acid or EtOH for 0.5, 4 or 8 h. Lysates were subjected to immunoblotting and analyzed with indicated antibodies. (**B**) Data from quantitative analysis of A and two additional experiments (n=3) are represented in bar diagrams as mean±sem. Protein:PCNA ratio was normalized to 0.5 h EtOH and statistically analyzed using Students t-test (*P<0.05, **P<0.01). n.s stands for not significant.

DDRGK1 and UFL1. Interestingly, UFL1 protein levels remained low whereas DDRGK1 protein abundance was restored after 8 h oleic acid treatment. In the contrary, conjugated UFM1 (~35 kDa) was significantly increased after 4 h incubation with oleic acid (**Fig. 29 B**). We suggest that this might be due to changes in UFM1 conjugation and deconjugation dynamics. Together, these results indicate that lipid droplet formation induced through oleic acid treatment negatively affects the ufmylation pathway.

5.4.5. ER-phagy is inhibited by induction of lipid droplet formation

The finding that the ufmylation pathway and in particular DDRGK1 are required for starvation induced autophagosomal degradation of ER-sheets (113) raises the question if lipid droplet formation affects ER-phagy similarly to DDRGK1 and other pathway components. Therefore, we used the ER autophagy tandem reporter system (309) in cooperation with Matthew D. Smith and Simon Wilkinson (University of Edinburgh). For this assay, HeLa cells were transfected with the tandem eGFP-mCherry-RAMP4 reporter, starved with Earle's balanced salt solution (EBSS) for 8 h and treated with oleic acid to induce LD formation or EtOH as control followed by fixation (**Fig. 30 A**). RAMP4 (Ribosome-attached membrane protein 4) is a subunit of the ER translocon complex and used as ER marker protein. eGFP exhibits a lower

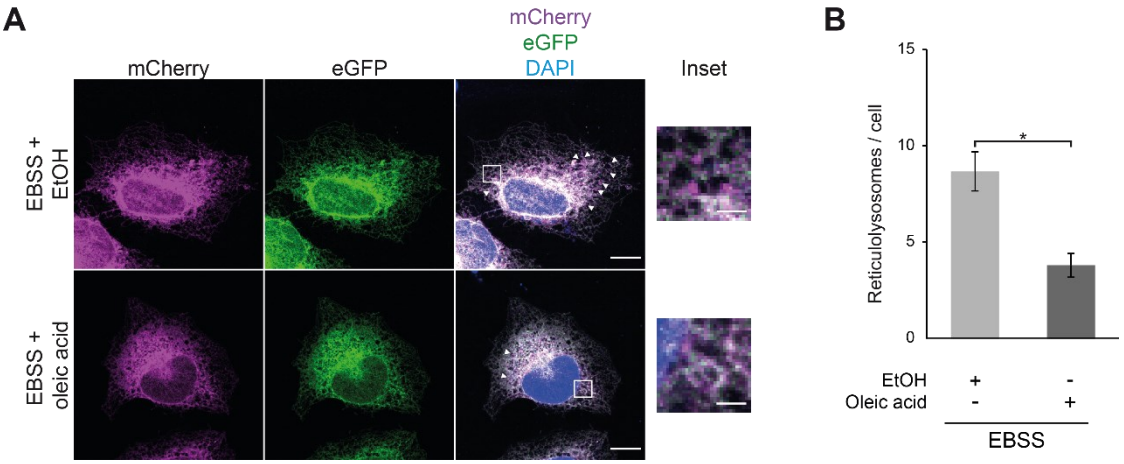

Figure 30: ER-phagy is inhibited by oleic acid treatment: (**A**) HeLa cells transfected with mCherry-eGFP-RAMP4 were starved with EBSS for 8 h and treated with oleic acid or EtOH. Purple-only puncta are reticulolysosomes. Arrowheads mark reticulolysosomes. Scale bars: 10 µm (main image), 2 µm (Inset). (**B**) Quantitative analysis of A. Reticulolysosomes per cell are represented in mean±sem. Data from three independent experiments were statistically analysis using students t-test (*P<0.05).

stability relative to mCherry. While both proteins are stable in the cytoplasm, eGFP loses fluorescence within lysosomes due to the acidic pH. Accordingly, colocalization of eGFP and mCherry display the ER in the cytosol whereas mCherry (purple-only) puncta indicate ER parts in lysosomes (reticulolysosomes). Interestingly, oleic acid treatment significantly decreased the number of reticulolysosomes (**Fig 30 B**). Taken together, ufmylation pathway is downregulated in response to LD formation and thus, remodeling of ER-sheets by ER-phagy is inhibited.

6. Discussion

6.1. Relevance of the hATG8^{endoHA} cell lines

From the mammalian ATG8 proteins LC3B is the most extensively studied protein in the context of autophagy. LC3B is historically considered to be the main autophagy marker, while the other hATG8 proteins are mostly neglected (310-312). In recent years, other ATG8 proteins gained focus in studies on hATG8 functions beyond autophagy. In this work we generated CRISPR/Cas9 knockin HeLa cell lines with an HA tag at the N-terminus of GABARAP, GABARAPL1, GABARAPL2, LC3B or LC3C as a tool to investigate isoform and protein specific functions of the hATG8 proteins. We could successfully show that all hATG8 proteins are still lipidated and provided data for correct localization upon autophagy induction for GABARAPL2. Furthermore, we proofed, with various experiments using mainly GABARAPL2^{endoHA} cells, that the tagged cell lines are very useful for many different applications such as immunoblotting, immunolabeling, immunoprecipitation and interactome analysis. Additionally to the hATG8^{endoHA} cell lines, we could successfully tag ACSL3 with NeonGreen in the GABARAPL2^{endoHA} cell line which allowed us to investigate the colocalization of the ACSL3 protein with GABARAPL2 and other proteins. This enormously facilitated the characterization of the GABARAPL2-ACSL3-UBA5 interaction axis. Together, the cell lines generated in this study are useful tools for further investigation and characterization of hATG8 interactors at endogenous level. Furthermore, these cell lines can be used to investigate whether functions annotated to GABARAPs and LC3s are isoform or subfamily specific or apply to all hATG8s.

6.2. Tagging of other cell lines with the established CRISPR/Cas9 method

For the CRISPR/Cas9 tagging, we used HeLa cells which are commonly used for studies of hATG8 proteins and autophagy (313-315). However, there are some disadvantages of HeLa cells as they exhibit a hypertriploid chromosome number and thus, it is more difficult to generate homozygous cell lines with CRISPR/Cas9 (316-318). With the help of PCR and

sequencing we found wild-type hATG8 DNA sequences in the corresponding hATG8^{endoHA} cell lines which demonstrates their heterozygosity. As consequence, it is not possible to make any conclusions about the total expression levels of the tagged proteins and to compare them (**Fig. 31**).

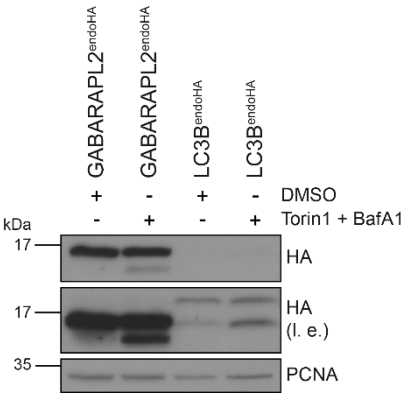

Figure 31: Protein levels of GABARAPL2 and LC3B: GABARAPL2^{endoHA} and LC3B^{endoHA} cells were treated as indicated and analyzed with immunoblotting. l.e. means long exposure.

Additionally, we were not able to tag LC3A in HeLa cells presumably as LC3A is not expressed in cancer cell lines (301). Therefore, the blasticidine resistant gene integrated in front of the LC3A gene was not expressed and cells died during selection. It is not essential to use homozygous cell lines in the context of studying the functions of the hATG8 proteins. However, it is of great interest to generate homozygous cell lines with HA-tagged hATG8s using the established CRISPR/Cas9 method to draw conclusions on expression pattern of ATG8 genes and how they differ in different cell types or tissues. Knockout or loss of function mutations of core ATG proteins in mice and other model organisms link impaired autophagy to many diseases such as neurodegeneration, infectious diseases, cancer and inflammatory disorder (319-323). But recent studies uncovered functions of ATG proteins including GABARAPs and LC3s in autophagy independent pathways. These pathways are often referred as non-canonical autophagy even though vesicles decorated with hATG8s are not typical autophagosomes as in LAP and the cargo of vesicles is not degraded by lysosomes as in secretory autophagy (**Table 17**) (11,324). Thus, researchers have to challenge if ATG-dependent phenotypes arise through impaired autophagy or other altered non-canonical autophagy pathways. For this reason, tagging of hATG8s or other ATG genes in cell lines from different tissues provide a tool to investigate cell or tissue specific functions of hATG8 and other core ATG proteins and their impact on disease phenotypes.

Table 17: Selected ATG8-dependent, non-canonical autophagy pathways

Pathway	Mechanism
Granule exocytosis	Paneth cells, located in small intestinal crypts, secret granules that contain antimicrobial peptides and enzymes and thus, balance the composition of the intestinal microbiome. Dysfunctional secretion in Paneth cells is associated with inflammatory bowel disease (325). Bacterial infection of Paneth cells triggers the secretion of lysozyme an antimicrobial enzyme. In dependency of ATG16L1 lysozyme is transported in LC3B positive vesicles to the plasma membrane and is released into the intestinal lumen (326).
Secretory lysosome exocytosis in osteoclasts	In osteoclasts the bone-apposed plasma membrane is termed ruffle boarder and a place of bone resorption. In dependency of the PE-ATG8 conjugation machinery lipidated LC3 is associated with ruffle boarders enabling their fusion with secretory lysosomes. Cysteine protease cathepsin K is released from the lysosome into the extracellular space resulting in osteal degradation (327).
Endosomal GLUT1 trafficking	Recycling of the glucose transporter GLUT1 from exosomes to the plasma membrane is mediated by the retromer complex which in turn is regulated by an inhibitory interaction with the RabGAP protein TBC1D5. Upon metabolic stress, TBC1D5 is sequestered by membrane associated LC3 enabling retromer dependent GLUT1 translocation to the plasma membrane (328).
Secretion of IL-1β	Upon lysosomal damage, interleukin IL-1β is secreted into the extracellular space. IL-1β is transported by TRIM16 to LC3B positive membranes and is captured in vesicles. The LC3B associated vesicles fuse with the plasma membrane and IL-1β is secreted. To date it is unknown if LC3B is needed for cargo recruitment or membrane fusion (329).
Replication inhibition of murine norovirus	Like other positive-sense RNA viruses, murine norovirus forms vacuole-like structures, termed replication complexes in the cytoplasm of host cells. In human and mice replication complexes are decorated with lipidated LC3 and are targeted by IFN-inducible GTPases which leads to membrane disruption and inhibition of viral replication (330).
Growth suppression of Toxoplasma gondii	Parasitic protozoan Toxoplasma gondii forms a surrounding parasitophorous vacuole membrane (PVM) out of the plasma cell membrane upon host cell infection. In interferon gamma activated human cells the PVM is ubiquitinated followed by recruitment of p62, NDP52 and LC3. LC3 positive PVMs are enclosed by several layers of host membranes restricting parasite growth but do not fuse with lysosomes (331).
LC3-dependent phagocytosis (LAP)	Described in 3.2.2.

6.3. Model of ACSL3 in the UFM1 conjugation pathway

In this study, we demonstrated that UBA5 is recruited by GABARAPL2 to ACSL3 which is located at the outer leaflet of the ER membrane and on LD surfaces (**Fig. 32**). We propose

that GABARAPL2 first interacts with the N-terminal domain of ACSL3 via UDS-UIM binding or a so far unknown interaction motif. Upon UBA5 dimerization, GABARAPL2 hands over UBA5 to ACSL3. The interaction is also mediated by a binding site within the N-terminal part of ACSL3. The binding motif in UBA5 could lie in a conserved and structural accessible region in the N-terminal part of UBA5. Loss as well as activation of ACSL3, induced through siRNA and oleic acid treatment respectively, led to downregulation of ufmylation pathway components UBA5, DDRGK1 and UFL1. Autophagosomal or proteasomal inhibition upon depletion of ACSL3 did not rescue protein abundance of UBA5, DDRGK1 and UFL1. Thus, we speculate that transcriptional regulation which might be induced through unconjugated UFM1 or unbound UFC1, decreased UBA5, DDRGK1 and UFL1 protein levels. However, in contrast to the assumption that ufmylation is downregulated upon lipid droplet biogenesis conjugated UFM1 significantly increased 4 h after oleic acid treatment. As treatment with oleic acid for 30 min or

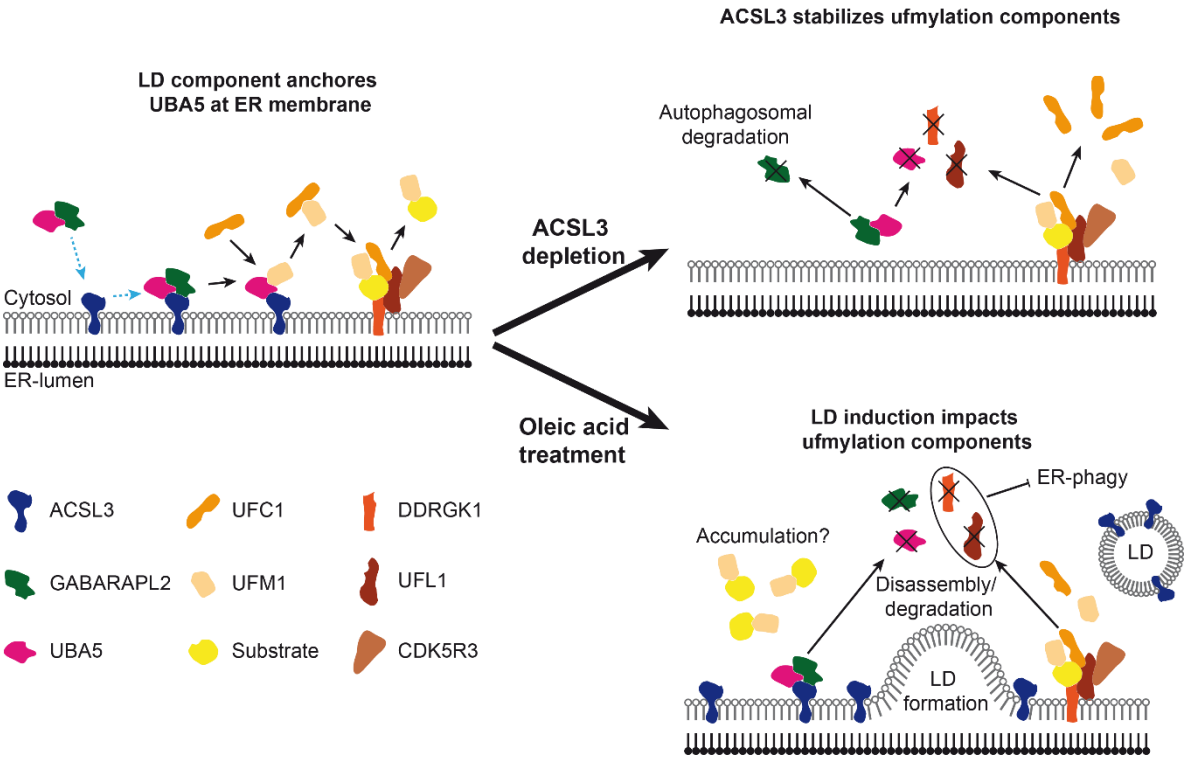

Figure 32: Working model: GABARAPL2 recruits UBA5 to the ER membrane where both interact with ACSL3. UBA5 activates UFM1 which is handed over via UFC1 to E3-ligase complex UFL1-DDRGK1-CDK5R3. UFM1 is covalently attached to target proteins. Upon ACSL3 depletion, GABARAPL2 protein abundance is diminished through autophagosomal degradation, while UBA5, UFL1 and DDRGK1 protein levels are decrease probably through transcriptional inhibition. Lipid droplet formation induced through oleic acid treatment inhibited ER-phagy presumably through reduced DDRGK1 and UFL1 protein levels. Botted blue arrows mark ER recruitment, black arrows indicate UFM1 conjugation cascade.

8 h has no significant effect on conjugated UFM1, we speculate that this is triggered by altered ufmylation and de-ufmylation dynamics. Furthermore, we provided evidence that the altered dynamics of the UFM1 conjugation system, triggered by oleic acid treatment and thus, LD biogenesis, inhibits starvation induced ER-phagy. It remains to be clarified if this downregulation is induced by the concentration of lipids in the cytosol, as LDs are also formed upon starvation but most likely do not affect ER-phagy in this context. Taken together, we showed that interaction between GABARAPL2, ACSL3 and UBA5 influences LD biogenesis-dependent regulation of the UFM1 conjugation machinery (**Fig. 32**).

6.4. Binding between GABARAPL2 - ACSL3 - UBA5

6.4.1. GABARAPL2 - ACSL3 binding

With IP-MS and IP-WB we identified ACSL3 as novel binding partner of GABARAPL2. According to the current perception, interactions between ATG8s and their binding partners occur through LDS-LIR or UDS-UIM binding. The data from our binding studies indicate that interaction between GABARAPL2 and ACSL3 is mediated by LDS-LIR binding and another LIR-independent binding motif (**Fig. 33**).

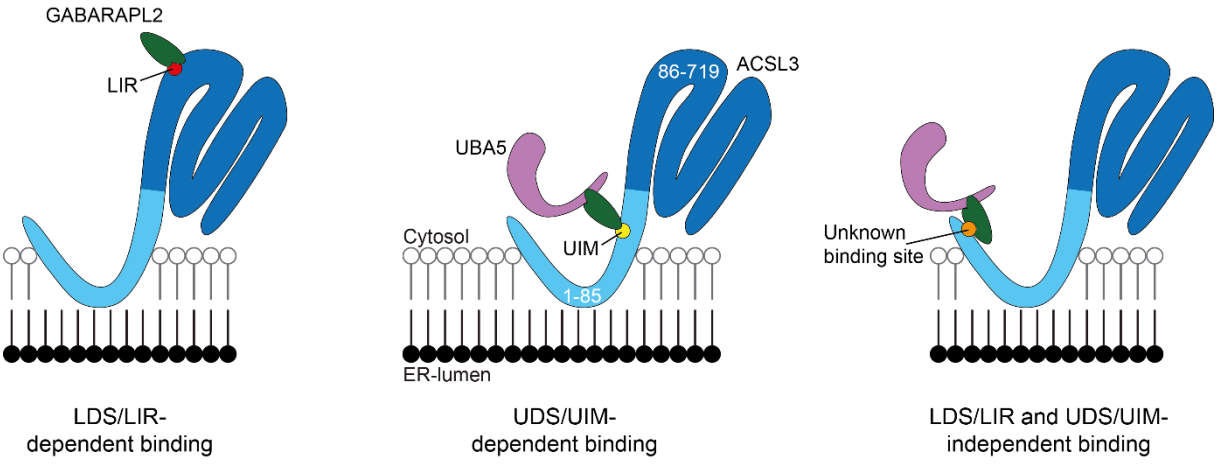

Figure 33: Possible binding scenarios between GABARAPL2 and ACSL3: LDS-LIR dependent binding between GABARAPL2 and ACSL3 86-718 exclude simultaneous interaction between GABARAPL2 and UBA5. The UDS motif could mediate binding between GABARAPL2 and N-terminal ACSL3. A so far unknow binding motif within the amino acid 1-85 in ACSL3 could be responsible for GABARAPL2-ACSL3 interaction.

A LIR motif typically consists of the core consensus sequence W/F/Y-x-x-L/I/V (x = any amino acid). In ACSL3 we detected four potential LIR motifs with iLIR which is an algorithmic search tool for potential functional LIR sites. Pulldown assays using purified GABARAPL2 protein with a deletion of the LDS site showed that the LIR binding site is in the ACSL3 sequence 78-718 which excludes LIR-1. However, when we tried to transiently express LIR deficient ACSL3 we observed strong variations in protein abundance of ACSL3. In the database of Swiss-Model we found a predicted protein structure of ACSL3 79-719 which is based on homology modelling (**Fig. 34**). According to this prediction LIR-2 is located at the beginning of a helical structure.

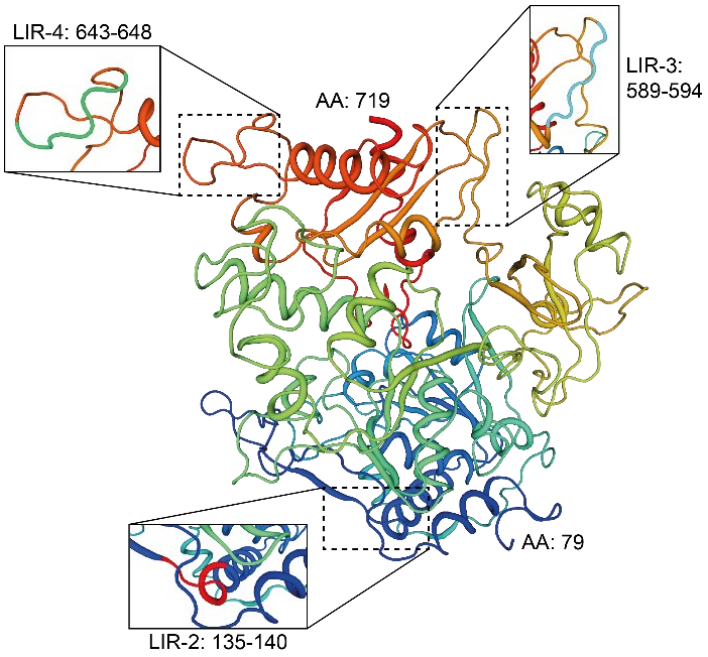

Figure 34: Predicted ACSL3 structure from SwissModel: Protein structure from ACSL3 79-719 modeled by Swiss-Model. Magnifications show the potential LIR binding sites. AA stands for amino acid.

In this case the amino acid changes in LIR-2 to alanine might have disrupted the protein structure and led to degradation of misfolded ACSL3. As LIR-2 is embedded in the helical structure, it is mostly likely not the LIR motif mediating binding between ACSL3 and GABARAPL2. In accordance with this model LIR-3 and LIR-4 are located in a more open structure and not in the AMP binding site as LIR-2 and thus, might be accessible for GABARAPL2. However, this predicted model is based on structures of other proteins which exhibit sequence similarity to ACSL3 and might not be correct in all aspects. Thus, to identify the actual LIR motif in ACSL3, more sophisticated mutagenesis of the LIR sites which does not disrupt the protein fold of ACSL3 is necessary.

As mentioned, a second mode of interaction of ATG8s with binding partners through UDS-UIM sites was recently discovered in Arabidopsis. According to this study, the UIM binding motif has the consensus sequence ψ-ζ-X-A-ψ-X-X-S (ψ = hydrophobic residues, ζ = hydrophilic residues, X = any amino acid) (23). We detected a possible inverted UIM motif in ACSL3 1-85. However, it does not exhibit all features of the proposed consensus sequence (**Fig. 35**). Interestingly, two recently published studies identified UDS dependent binding between LC3B-CCDC50 (Coiled-coil domain-containing protein 50) and GABARAP-CALCOCO1 (Calcium-binding and coiled-coil domain-containing protein 1). However, there is no sequence that exactly fits to the proposed consensus sequence of UIM in the relevant domains of CCDC50 and CALCOCO1 (332,333). For UIM mediated LC3B-CCDC50 interaction, Hou and colleagues identified the amino acid motif A-R-K-L in the CCDC50 sequence as essential for LC3B binding. Intriguingly, this motif exhibits the same features that we found in the ACSL3 UIM motif (**Fig. 35**). Thus, the UIM consensus motif in humans is probably different than the suggested consensus motif in Arabidopsis.

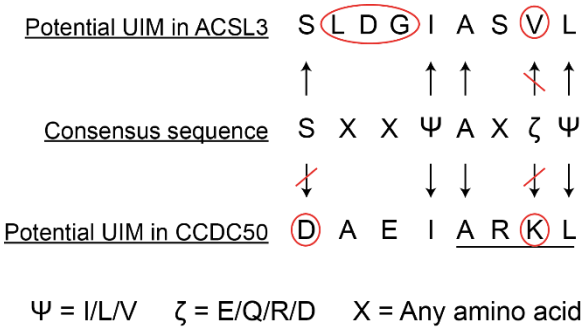

Figure 35: UIM consensus sequence: Comparison of the potential UIMs in ACSL3 and CCDC50 with the proposed consensus motif. The relevant amino acids according to Hou and colleagues are underlined. Ψ, ζ and X stands for hydrophobic, hydrophilic residues or any amino acid, respectively.

However, in the pulldown assay with GABARAPL2 ΔUDS we also detected ACSL3 1-85 which suggests a so far unknown, UDS-UIM independent interaction motif between GABARAPL2 and ACSL3. On the other hand, mutagenesis of UDS and F77 through alanine in GABARAPL2 might not be sufficient to prevent binding between ACSL3 and GABARAPL2. Interestingly, the amino acids within the UDS site of GABARAPL2 exhibit hydrophobic site changes just as alanine. It might be worth a try to exchange the amino acids in the UDS binding motif with ones that have neutral or hydrophobic site changes to change the overall hydrophobicity on the GABARAPL2 UDS surface. Furthermore, sequence alignments of human ACSL3 with the

homologs of mouse, chicken, zebrafish and frog revealed that the potential inverted UIM motif is conserved between these species and thus, might be relevant for the protein function or interaction with other proteins (**Fig. 36**).

Figure 36: Multiple sequence alignment of ACSL3: The human ACSL3 protein sequence was aligned with homologs from Mus musculus (mouse), Gallus gallus (chicken), Danio rerio (zebrafish) and Xenopus laevis (frog) using ClustalW. Asterisks mark conserved amino acids, double and single dots indicate strong or weakly similar conserved amino acids respectively, according to ClustalW calculations. The transmembrane domain is marked in blue, the potential UIM site in green and the AMP-binding site in grey.

6.4.2. UBA5 - ACSL3 binding

In our work, we provide evidence that a binding site in ACSL3 1-85 mediates interaction between UBA5 and ACSL3. However, we could not exclude a second binding site in amino acid region 86-718 of ACSL3 as GST-UBA5 migrates at the same size as the ACSL3 fragment. With multiple sequence alignments we sought to identified highly conserved regions in UBA5 in order to identify potential amino acids stretches that could mediate binding between UBA5 and ACSL3. Besides the mostly conserved adenylation domain (AD, amino acid: 57-329) and C-terminal UIS site we identified a highly conserved amino acid stretch from amino acid 44-56 in the N-terminal region of human UBA5 (**Fig. 37 A**).

A

```
      A. thaliana     -MEV-------GFKALLDDLDVLEKSLSDPALINKLRSHVENLATLSKCNPHRRSKVKEL  52
        C. elegans    MSDEQIDKLVSRLDGALNRLGNVKKDHPLESSSN------SKPTHQPKSPAPYRQKIEKL  54
    D. melanogaster   -MSHAIDELQAII-------ADLKTELETEP---------KSSGGVASNSRLARDRIDRM  43
          D. rerio    --MATVEELKLRI-------RELENELIKSK---------QKQ---SDAEHNIRPKIEQM  39
         X. laevis    -MEGLIEELRSRV-------RELEEELDR---------------VRNGQHEGHRTKIEKM  37
         G. gallus    -MAERVELLERRV-------RELERELELAR----------------GGRASARARIETM  36
        H. sapiens    -MAESVERLQQRV-------QELERELAQER---------SLQVPRSGDGGGGRVRIEKM  43
                                 .        :: .                              * ::. :

      A. thaliana     SSEVVDSNPYSRLMALQRMGIVDNYERIREFSVAIVGIGGVGSVAAEMLTRCGIGRLLLY  112
        C. elegans    SAEVVDSNPYSRLMALQRMGIVNEYERIREKTVAVVGVGGVGSVVAEMLTRCGIGKLILF  114
    D. melanogaster   SAEVVDSNPYSRLMALQRMNIVKDYERIRYKAVAIVGVGGVGSVTADMLTRCGIGKLILF  103
          D. rerio    SAEVVDSNPYSRLMALKRMGIVQDYEKIRSFAVAVVGVGGVGSVTAEMLTRCGIGKLLLF  99
         X. laevis    SAEVVDSNPYSRLMALKRMGIVKDYEKIRTFTVAVVGVGGVGSVTAEMLTRCGIGKLLLF  97
         G. gallus    SPEVTDSNPYSRLMALKRMGIVKDYEKIRTFTVAIVGVGGVGSVTAEMLTRCGIGKLLLF  96
        H. sapiens    SSEVVDSNPYSRLMALKRMGIVSDYEKIRTFAVAIVGVGGVGSVTAEMLTRCGIGKLLLF  103
                      * **.**********:**.**.:**:**  :**:**:******.*:********:*:*:
                                    UDS
      A. thaliana     DYDTVELANMNRLFFRPDQVGMTKTDAAVQTLAEINPDVVLESFTMNITTVQGFETFTSS  172
        C. elegans    DYDKVEIANMNRLFYQPNQAGLSKVEAARDTLIHVNPDVQIEVHNFNITTMDNFDTFVNR  174
    D. melanogaster   DYDKVELANMNRLFFTPDQAGLSKVAAAAATLSFINPDVEIETHNYNITTVENFDRFLDT  163
          D. rerio    DYDKVELANMNRLFFQPHQAGLSKVEAAQHTLRNINPDVAFETHNYNITTMDNFTHFMDR  159
         X. laevis    DYDKVELANMNRLFFQPHQAGLSKVEAAQHTLRNINPDVAFETHNYNITTMDNFTHFMDR  157
         G. gallus    DYDKVELANMNRLFFQPHQAGLSKVQAAEHTLRNINPDVQFEVHNYNITTLDNFEHFMDR  156
        H. sapiens    DYDKVELANMNRLFFQPHQAGLSKVQAAEHTLRNINPDVLFEVHNYNITTVENFQHFMDR  163
                      ***.**:*******: *.*.*::.*. **  **  :**** :* .. ****::.*  * .

      A. thaliana     LTNKSFCPSKEGGSGVDLVLSCVDNYEARMAVNQACNELRQTWMESGVSEDAVSGHIQLL  232
        C. elegans    IRKGS----LTDGK-IDLVLSCVDNFEARMAVNMACNEENQIWMESGVSENAVSGHIQYI  229
    D. melanogaster   ISQGG----RIAGQPVDLVLSCVDNFEARMAINAACNERNLNWFESGVSENAVSGHIQFI  219
          D. rerio    VSHGG----LEEGKPVDLILSCVDNFEARMAINTACNELGQIWMESGVSENAVSGHIQLI  215
         X. laevis    ISKGG----LKEGSPVDLVLSCVDNFEARMAINTACNELGQVWMESGVSENAVSGHIQLI  213
         G. gallus    ISNGA----LEEGKPVDLVLSCVDNFEARMAINTACNELGQIWMESGVSENAVSGHIQLI  212
        H. sapiens    ISNGG----LEEGKPVDLVLSCVDNFEARMTINTACNELGQTWMESGVSENAVSGHIQLI  219
                      : : .      *. :**:******:****::* ****    *:******:******* :

      A. thaliana     VPGETACFACAPPLVVASGIDERTLKREGVCAASLPTTMGVVAGLLVQNSLKFLLNFGEV  292
        C. elegans    EPGKTACFACVPPLVVASGIDERTLKRDGVCAASLPTTMAVVAGFLVMNTLKYLLNFGEV  289
    D. melanogaster   RPGDTACFACAPPLVVAENIDEKTLKREGVCAASLPTTMGITAGFLVQNALKYLLNFGEV  279
          D. rerio    IPGETACFACAPPLVVAANIDEKTLKRDGVCAASLPTTMGVVAGLLVQNVLKYLLGFGTV  275
         X. laevis    KPGETACFACAPPLVVAANIDEKTLKREGVCAASLPTTMGVVAGILVQNVLKYLLNFGTV  273
         G. gallus    IPGESACFACAPPLVVAANIDEKTLKREGVCAASLPTTMGVVAGILVQNVLKYLLNFGTY  272
        H. sapiens    IPGESACFACAPPLVVAANIDEKTLKREGVCAASLPTTMGVVAGILVQNVLKFLLNFGTV  279
                       **.:*****.****** .***:****:**********.:.**:** * **:**.** *

      A. thaliana     SPYLGYNSLKDFFPTMKMRPNPQCSNVACLERQKEYMLAKPERDAAAKAKMEADASTTID  352
        C. elegans    SQYVGYNALSDFFPRDSIKPNPYCDDSHCLQRQKEYEEKVANQPVD------LEVEVPEE  343
    D. melanogaster   SDYLGYNALSDFFPKMTLKPNPQCDDRNCLVRQKEFQARPKPVLIE------EK---AVS  330
          D. rerio    SYYLGYNAMQDFFPSMAMKANPQCDDRHCRRQQDEYKKKEAERPKQ------EV-V-QEE  327
         X. laevis    SFYLGYNAMQDFFPTMAMKPNPQCDDKYCRKQQEEFKLKEAAKPKQ------ET-VVVEE  326
         G. gallus    SYYLGYNAMQDFFPTMAMKPNPQCSDQNCRKQQENYKIKEAAQPKQ------EE-I-HQE  324
        H. sapiens    SFYLGYNAMQDFFPTMSMKPNPQCDDRNCRKQQEEYKKKVAALPKQ------EV-I-QEE  331
                      * *:***::.****   :: ** *.:  *  :*.::                      .

      A. thaliana     EGPLHDDNEWNISVVDDENEKDTTKAASSSDTLPEGLTRELPVADEYEKAIAIASGSGET  412
        C. elegans    ETVVHEDNEWGIELVNESEPSAEQS---SSLNAGTGLKFAYEPIKRDAQTEL-SP-----  394
    D. melanogaster   EEPLHATNEWGIELVAEDAPES-NTTPAETPVMGEGLRLAYEAPEKSSETSE-ETVSAAT  388
          D. rerio    EEVVHEDNEWGIELVSEVTEAELQDASGPIPDLPEGITVAYTIPEKDG--GS-GE--TVE  382
         X. laevis    EEVVHEDNDWGIELVSEVSEEELKAASGPVPDLPEGIKVAYTIPITKP--TS-GF--TVE  381
         G. gallus    EEIVHEDNDWGIELVSETTEDELKAASGPVPDLPVGITVAYTIPNKEENLTA-EE--TVA  381
        H. sapiens    EEIIHEDNEWGIELVSEVSEEELKNFSGPVPDLPEGITVAYTIPKKQEDSVT-EL--TVE  388
                      *  :*  *:*.*.:* :                  *:

      A. thaliana     EEEDDLEDLKKQLEALNAA-------  431
        C. elegans    -AQAATHDFMKSIKDKLVEEAQNKGK  419
    D. melanogaster   ADETSLEDLMAQMKSM----------  404
          D. rerio    ETEQSLEELMAQMKKI----------  398
         X. laevis    DSEQSLDELMAQMKNL----------  397
         G. gallus    ESEESLEDLMAKMRNL----------  397
        H. sapiens    DSGESLEDLMAKMKNM----------  404
                           .::  .:.
```

B

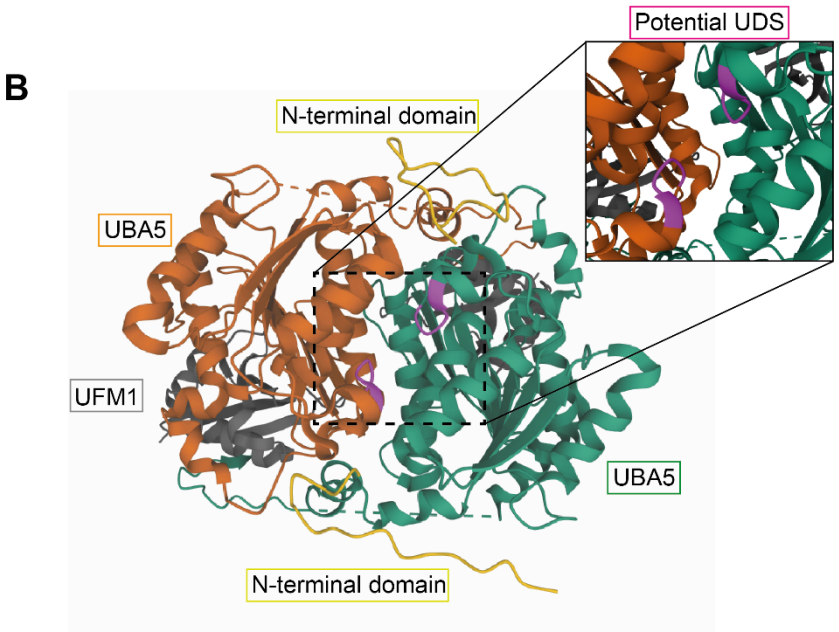

Figure 37: Analysis of UBA5 sequence and structure: (**A**) The sequence of human UBA5 was aligned with the homologs of Arabidopsis thaliana, Caenorhabditis elegans, Drosophila Melanogaster (fruit fly), Danio rerio, Xenopus laevis and Gallus gallus using ClustalW. Conserved amino acids are marked with asterisks. Strongly or weakly similar conserved amino acids are marked with double or single dots respectively, according to the criteria of ClustalW. The highly conserved N-terminal region is coloured in yellow, the UDS site is highlighted in purple and the UIS site is marked in blue. (**B**) Protein structure of UBA5 homodimer (orange and green) associated with UFM1 (grey) obtained from the RCSB protein data bank (PDB) (deposited by Souhda and colleagues). Potential UDS sites are coloured in purple, N-terminal domains from amino acids 36-52 are coloured in yellow.

The protein structure of dimerized UBA5, deposited by Souhda and colleagues at the RCSB protein data bank (PDB), revealed that the N-terminal part from amino acid 36-52 is exposed on the surface of UBA5 (**Fig. 37 B**) (334). The high conservation and accessibility of the amino acid stretch 44-52 make this part of UBA5 a strong candidate for an ACSL3 binding site. Furthermore, we detected a potential UDS motif in the AD of UBA5 by manual sequence inspection. This site stretches from amino acid 116 to 119 which is partially conserved amongst the compared species (**Fig. 37 A**). The detected motif L-F-F-Q does not exhibit an aromatic amino acid or a threonine (T) at the last position as in the suggested consensus motif of the UDS site ψ-F-ψ-$\frac{\Omega}{T}$ (ψ = hydrophobic residues, Ω = aromatic residues) (23). However, glutamine (Q) is a polar amino acid with uncharged site chains as threonine and thus, the identified motif could very well be a UDS binding site. Examination of the protein structure showed that the potential UDS motifs from the UBA5 homodimers lie across from each other close to the protein surface (**Fig. 37 B**). To identify whether the binding motif in UBA5 is within the N-terminal conserved region, pulldown assays with purified UBA5, missing the N-terminal 1-56 amino acid stretch, could be performed with ACSL3-HA cell lysates. To examine whether the potential UDS is essential for UBA5-ACSL3 interaction, the relevant amino acids could be mutagenized without disturbing the fold of UBA5.

6.5. Function of GABARAPL2 - ACSL3 - UBA5 interaction

Our data supports a model in which ACSL3 binds UBA5 in dependency of GABARAPL2. The ACSL3-GABARAPL2 interaction is mediated by two binding sites and ACSL3-UBA5 association is possibly dependent on amino acids 1-85 in ACSL3. Our findings arise the question how binding between these three proteins occurs and which functions it serves.

The mode of interaction between UBA5 and its known interacting partners GABARAPL2, UFM1 and UFC1 are well studied. UBA5 interacts with GABARAPL2 or UFM1 via an atypical LIR interaction motif termed UIS which is located C-terminally to the UBA5 AD (**Fig. 38 A**) (94,95,98). Recently, it was shown that UBA5 is recruited to the ER by GABARAPs, and ufmylation is inhibited upon knockdown of all GABARAP proteins. Furthermore, UBA5 binds

either GABARAPL2 or UFM1 but not both at the same time (95). Interestingly, two UBA5 proteins form a homodimer which is enhanced through the presence of UFM1. Moreover, homodimerization is essential for UBA5-ATP binding and adenylation of UFM1. Activation of UFM1 occurs in a trans-binding mechanism which means that one subunit of an UBA5 dimer binds to UFM1 while the other subunit adenylates UFM1 (**Fig. 38 B**) (96,97). Interaction between the E2 enzyme of the UFM1 conjugation machinery UFC1 and UBA5 is promoted by the UFC1 binding sequence (UBS) located at the C-terminal end of UBA5. Transfer of UFM1 to UFC1 is also mediated in a trans-binding mechanism which means that UFC1 binding to UBA5 receives UFM1 from the other UBA5 subunit (**Fig. 38 B**) (97,335).

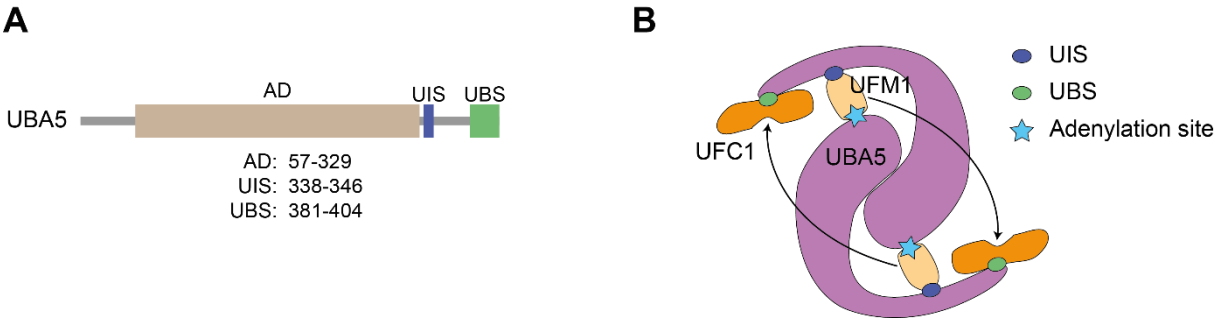

Figure 38: Model of UFM1 adenylation by UBA5: (**A**) Schematic display of UBA5 interacting regions UIS and UBS and adenylation domain (AD). (**B**) Current status of UFM1 activation by UBA5 and hand-over to UFC1.

Taken together, UFM1 conjugation is dependent on UBA5 recruitment to the ER-membrane by GABARAPL2. Furthermore, UBA5, DDRGK1 and UFL1 are stabilized by ACSL3, and UFM1 conjugation to substrates takes place at the ER-membrane. Thus, it is tempting to speculated that UBA5 is anchored to the ER-membrane by ACSL3 throughout UFM1 activation. Possibly GABARAPL2 binds ACSL3 through an UIM or another, so far unknown, interacting motif in the N-terminal part of ACSL3 as the LDS domain is blocked by UBA5 (**Fig. 39**). In presence of UFM1, UBA5 might be handed over to ACSL3 and potentially binds to amino acid 1-85. We found GABARAPL2 recruitment to the ER in dependency of the functional LDS interacting region which suggests that after releasing UBA5, GABARAPL2 might interact with a LIR motif in ACSL3 86-718. On the other hand, GABARAPL2 relocalization to the ER membrane could also be induced through LDS-LIR interaction with UBA5 and consequently GABARAPL2 would not necessarily bind to a LIR motif in ACSL3.

However, it is currently unknown whether two ACSL3 molecules are required to bind an UBA5 dimer, and whether ACSL3-bound UBA5 carries an activated UFM1 (**Fig. 39**). Together, we propose that UBA5 is anchored by ACSL3 at the ER-membrane during UFM1 conjugation.

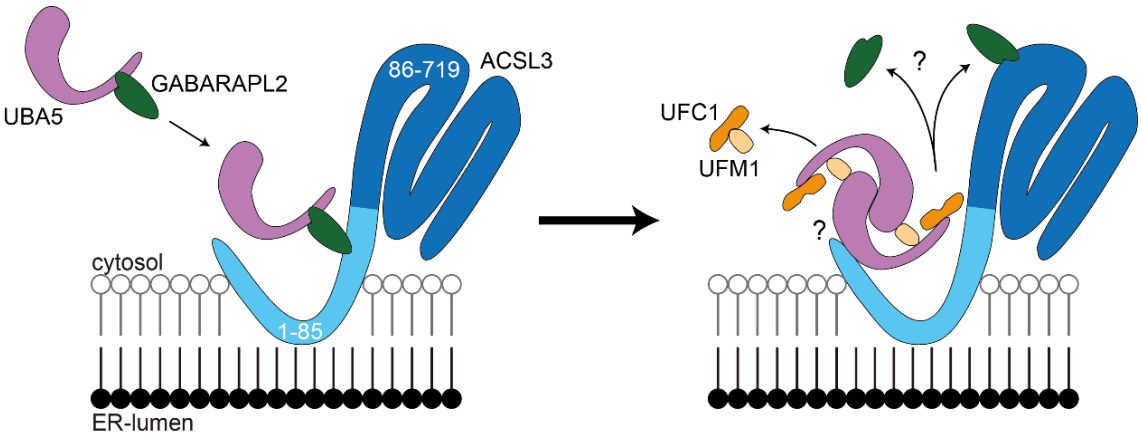

Figure 39: Interacting model of GABARAPL2-ACSL3-UBA5: GABARAPL2 interacting with UBA5 through LDS-LIR binding recruits UBA5 to the ER-membrane. GABARAPL2 binds to ACSL3 within amino acid 1-85 via UDS-UIM binding or a so far unknown interacting motif. Upon presence of UFM1 GABARAPL2 hands over UBA5 to ACSL3 and either interacts with ACSL3 within amino acids 86-719 in a LIR dependent manner or dissociates. UBA5 dimerizes and interacts with UFM1 and UFC1 followed by UFM1 activation.

6.6. Connections between LD-biogenesis and ufmylation

In our study, we identified a regulatory connection between the UFM1 conjugation machinery and LD biogenesis. Both pathways are tightly connected to the ER membrane through the localization of pathway components at the ER and their cellular function. Ufmylation is dependent on ER membrane localization of UBA5 and the E3 enzyme complex formed of DDRGK1, UFL1 and CDK5RAP3 (95,103,112). The functional role of UFM1 conjugation is not completely understood. However, ufmylation is connected to ER stress response and maintenance of ER homeostasis (113,114,124). Furthermore, current studies link UFM1 substrate conjugation to ER-phagy and clearance of ribosomes stalled at the ER membrane (102,111,113,124). LD biogenesis mainly takes place at the ER through accumulation of neutral lipids between the ER leaflets which leads to LD formation and budding (136). Proteins participating in LD biogenesis such as Seipins, FIT1 and 2 and ACSL3 are located at the ER membrane (169,210,222). Like ufmylation, LD formation is connected to the UPR. Upon ER

stress, LD are formed as a downstream effect and dysfunctional LD biogenesis induces ER stress (148,150). However, the exact mechanism of the interplay between these two pathways, both contributing to ER homeostasis, remains elusive.

In our study, we provide initial evidence that lipid droplet formation which is dependent on ACSL3 affects the abundance of ufmylation pathway components. The protein abundance of UBA5, DDRGK1 and UFL1 are decreased upon lipid stress in a similar manner than in response to ACSL3 depletion. This raises the question how activation or depletion of ACSL3 affects protein levels of these UFM1 pathway components. We observed that after 30 min and 24 h oleic acid treatment UBA5 was still able to interact with ACSL3 but, upon 8 h oleic acid treatment, UBA5 protein levels were significantly decreased. However, 30 min after induction of LD biogenesis through oleic acid treatment DDRGK1 and UFL1 protein levels were already significantly decreased. Thus, it is tempting to speculate that activation of ACSL3 might not prevent UBA5 interaction at first but might inhibit UBA5 dimerization and thus, UFM1 transfer to UFC1 (**Fig. 40**). This in turn could trigger downregulation of DDRGK1 and UFL1 at the transcriptional level. Along these lines, depletion of ACSL3 would also prevent UFM1-UFC1 conjugation as UBA5 is not anchored to the ER membrane by ACSL3. To gain further insight

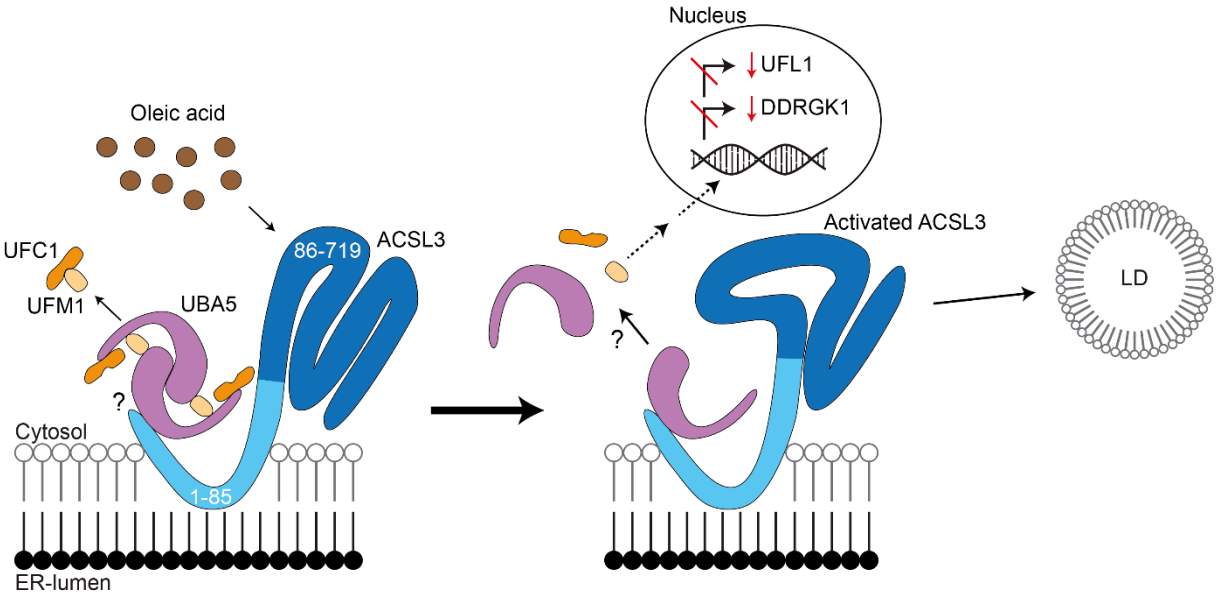

Figure 40: Activation of ACSL3 and its potential consequences on ufmylation pathway: Oleic acid treatment leads to activation of ACSL3 which might inhibit UBA5 dimerization and transfer of UFM1 to UFC1. Transcriptional inhibition might be induced through unconjugated UFM1 or UFC1. Dotted arrows indicate involvement of unknown intermediate steps.

in the regulatory effects of ACSL3 activation on the ufmylation pathway, it would be necessary to extend the treatment times with oleic acid. Additionally, experiments performed with long fatty acyl CoA synthetase inhibitor Triacsin C would help to clarify the role of ACSL3 activity in anchoring UBA5 to the ER membrane and in regulating ufmylation.

In consistency with the downregulation of amino acid starvation induced ER-phagy upon depletion of DDRGK1 or UFL1, we showed that induction of LD biogenesis also inhibits ER-phagy. In our experiments, we induced LD formation through a lipid overload which provides the cells with nutrients in form of fatty acids. Interestingly, LD biogenesis is also stimulated by amino acid starvation as it triggers bulk autophagy and thus, fatty acids are released through degradation of organelle membranes (137,147). However, LD biogenesis induced through amino acid starvation most likely does not inhibit starvation induced ER-phagy. This raises the question if the amount of available fatty acids in the cytosol affects the regulation of ufmylation and ER-phagy by LD formation. Treatment of cells with a lower concentration of oleic acid as we used in our experiments might downregulate ufmylation and ER-phagy to a lower extend or not at all. It is tempting to speculate, that high concentrations of lipids lead to excessive ER rearrangements through LD biogenesis and thus, remodeling of ER membranes through ER-phagy might be inhibited to prevent disintegration of the ER. Analysis of DDRGK1, UFL1 and UBA5 protein abundance with different oleic acid concentrations would give further insights in the regulatory mechanism on ufmylation through ACSL3 and LD formation.

Another connection between the UFM1 conjugation pathway and ACSL3 was recently discovered in a MS approach which identified RPL26 as novel ufmylation target. This unbased large-scale data indicate that ACSL3 is a potential UFM1 substrate (111). In general, post-translational modification of proteins by conjugation with Ub or Ubls enable the reversible regulation of protein functions. This includes the activation of enzymes, targeting of proteins to proteasomal or autophagosomal degradation, conformational changes of the modified protein or initiation of an interaction to other proteins (336). Thus, one possible scenario could be that UFM1 conjugation to ACSL3 serves as feedback regulation of the ufmylation system. A

conformational change of ACSL3 induced through modification by UFM1 could inhibit binding of GABARAPL2 and/or UBA5 to ACSL3 or dimerization of UBA5. Consequentially, activation of UFM1 and thus, conjugation to targets would be stopped to possibly prevent excessive ufmylation. The deconjugation of UFM1 from ACSL3 by UFSP2 would then reestablish UFM1 conjugation to other targets (**Fig. 41**). Another possibility could be that conjugation of UFM1 to ACSL3 is mediated by the presence of lipids in the cytosol which then induces the activity of ACSL3 and LD biogenesis. As a consequence, the ufmylation pathway would be downregulated (**Fig. 41**). However, there are also many other possible scenarios and it remains to be clarified if ACSL3 is ufmylated at all.

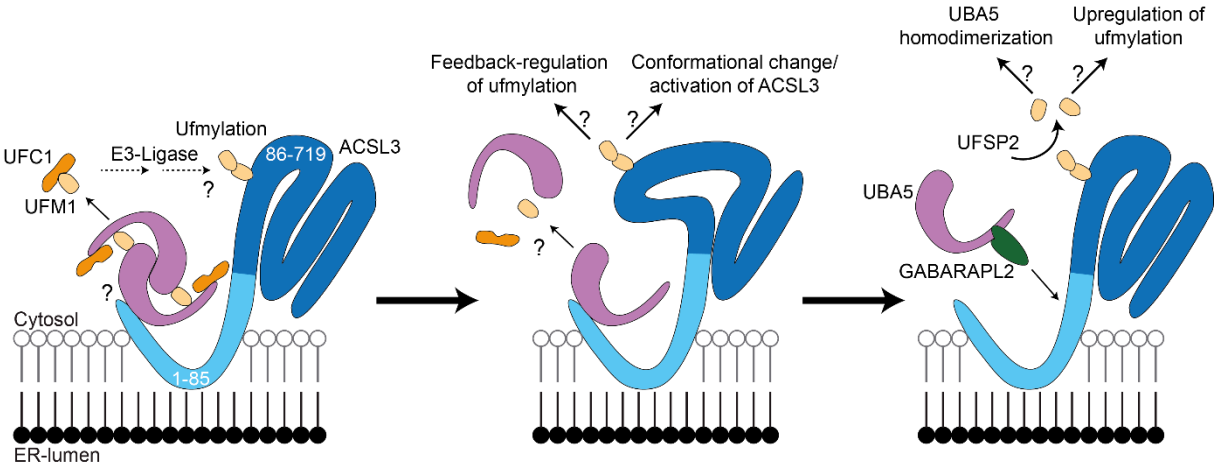

Figure 41: Modification of ACSL3 by UFM1: Ufmylation of ACSL3 could induce a conformational change or activation of ACSL3 followed by disassemble of UBA5 homodimer and thus, a feedback regulation of the UFM1 conjugation machinery. Cleavage of UFM1 from ACSL3 by UFSP2 could reverse the conformational change or deactivate ACSL3 and thus, enable binding and homodimerization of UBA5. Dotted arrows mark the DDRGK1-UFL1-dependent UFM1 conjugation step.

7. References

1. Clausen, L., Abildgaard, A.B., Gersing, S.K., Stein, A., Lindorff-Larsen, K. and Hartmann-Petersen, R. (2019) Protein stability and degradation in health and disease. *Adv Protein Chem Struct Biol*, **114**, 61-83.
2. Dikic, I. (2017) Proteasomal and Autophagic Degradation Systems. *Annu Rev Biochem*, **86**, 193-224.
3. Zientara-Rytter, K. and Subramani, S. (2019) The Roles of Ubiquitin-Binding Protein Shuttles in the Degradative Fate of Ubiquitinated Proteins in the Ubiquitin-Proteasome System and Autophagy. *Cells*, **8**.
4. Liu, W.J., Ye, L., Huang, W.F., Guo, L.J., Xu, Z.G., Wu, H.L., Yang, C. and Liu, H.F. (2016) p62 links the autophagy pathway and the ubiqutin-proteasome system upon ubiquitinated protein degradation. *Cell Mol Biol Lett*, **21**, 29.
5. Pohl, C. and Dikic, I. (2019) Cellular quality control by the ubiquitin-proteasome system and autophagy. *Science*, **366**, 818-822.
6. Danieli, A. and Martens, S. (2018) p62-mediated phase separation at the intersection of the ubiquitin-proteasome system and autophagy. *J Cell Sci*, **131**.
7. Kerscher, O., Felberbaum, R. and Hochstrasser, M. (2006) Modification of proteins by ubiquitin and ubiquitin-like proteins. *Annu Rev Cell Dev Biol*, **22**, 159-180.
8. Cohen-Kaplan, V., Livneh, I., Avni, N., Cohen-Rosenzweig, C. and Ciechanover, A. (2016) The ubiquitin-proteasome system and autophagy: Coordinated and independent activities. *Int J Biochem Cell Biol*, **79**, 403-418.
9. Dikic, I. and Elazar, Z. (2018) Mechanism and medical implications of mammalian autophagy. *Nat Rev Mol Cell Biol*, **19**, 349-364.
10. Kirkin, V. and Rogov, V.V. (2019) A Diversity of Selective Autophagy Receptors Determines the Specificity of the Autophagy Pathway. *Mol Cell*, **76**, 268-285.
11. Levine, B. and Kroemer, G. (2019) Biological Functions of Autophagy Genes: A Disease Perspective. *Cell*, **176**, 11-42.
12. Meijer, W.H., van der Klei, I.J., Veenhuis, M. and Kiel, J.A. (2007) ATG genes involved in non-selective autophagy are conserved from yeast to man, but the selective Cvt and pexophagy pathways also require organism-specific genes. *Autophagy*, **3**, 106-116.
13. Ohsumi, Y. (2014) Historical landmarks of autophagy research. *Cell Res*, **24**, 9-23.
14. Tsukada, M. and Ohsumi, Y. (1993) Isolation and characterization of autophagy-defective mutants of Saccharomyces cerevisiae. *FEBS Lett*, **333**, 169-174.
15. Mizushima, N., Yoshimori, T. and Ohsumi, Y. (2011) The role of Atg proteins in autophagosome formation. *Annu Rev Cell Dev Biol*, **27**, 107-132.
16. Lystad, A.H. and Simonsen, A. (2019) Mechanisms and Pathophysiological Roles of the ATG8 Conjugation Machinery. *Cells*, **8**.
17. Shpilka, T., Weidberg, H., Pietrokovski, S. and Elazar, Z. (2011) Atg8: an autophagy-related ubiquitin-like protein family. *Genome Biol*, **12**, 226.
18. Slobodkin, M.R. and Elazar, Z. (2013) The Atg8 family: multifunctional ubiquitin-like key regulators of autophagy. *Essays Biochem*, **55**, 51-64.
19. Noda, N.N., Kumeta, H., Nakatogawa, H., Satoo, K., Adachi, W., Ishii, J., Fujioka, Y., Ohsumi, Y. and Inagaki, F. (2008) Structural basis of target recognition by Atg8/LC3 during selective autophagy. *Genes Cells*, **13**, 1211-1218.
20. Pankiv, S., Clausen, T.H., Lamark, T., Brech, A., Bruun, J.A., Outzen, H., Overvatn, A., Bjorkoy, G. and Johansen, T. (2007) p62/SQSTM1 binds directly to Atg8/LC3 to facilitate degradation of ubiquitinated protein aggregates by autophagy. *J Biol Chem*, **282**, 24131-24145.
21. Rogov, V., Dotsch, V., Johansen, T. and Kirkin, V. (2014) Interactions between autophagy receptors and ubiquitin-like proteins form the molecular basis for selective autophagy. *Mol Cell*, **53**, 167-178.
22. Birgisdottir, A.B., Lamark, T. and Johansen, T. (2013) The LIR motif - crucial for selective autophagy. *J Cell Sci*, **126**, 3237-3247.

23. Marshall, R.S., Hua, Z., Mali, S., McLoughlin, F. and Vierstra, R.D. (2019) ATG8-Binding UIM Proteins Define a New Class of Autophagy Adaptors and Receptors. *Cell*, **177**, 766-781 e724.
24. Marshall, R.S., Li, F., Gemperline, D.C., Book, A.J. and Vierstra, R.D. (2015) Autophagic Degradation of the 26S Proteasome Is Mediated by the Dual ATG8/Ubiquitin Receptor RPN10 in Arabidopsis. *Mol Cell*, **58**, 1053-1066.
25. Mizushima, N. (2020) The ATG conjugation systems in autophagy. *Curr Opin Cell Biol*, **63**, 1-10.
26. Ichimura, Y., Kirisako, T., Takao, T., Satomi, Y., Shimonishi, Y., Ishihara, N., Mizushima, N., Tanida, I., Kominami, E., Ohsumi, M. *et al.* (2000) A ubiquitin-like system mediates protein lipidation. *Nature*, **408**, 488-492.
27. Kirisako, T., Ichimura, Y., Okada, H., Kabeya, Y., Mizushima, N., Yoshimori, T., Ohsumi, M., Takao, T., Noda, T. and Ohsumi, Y. (2000) The reversible modification regulates the membrane-binding state of Apg8/Aut7 essential for autophagy and the cytoplasm to vacuole targeting pathway. *J Cell Biol*, **151**, 263-276.
28. Mizushima, N., Noda, T., Yoshimori, T., Tanaka, Y., Ishii, T., George, M.D., Klionsky, D.J., Ohsumi, M. and Ohsumi, Y. (1998) A protein conjugation system essential for autophagy. *Nature*, **395**, 395-398.
29. Hanada, T., Noda, N.N., Satomi, Y., Ichimura, Y., Fujioka, Y., Takao, T., Inagaki, F. and Ohsumi, Y. (2007) The Atg12-Atg5 conjugate has a novel E3-like activity for protein lipidation in autophagy. *J Biol Chem*, **282**, 37298-37302.
30. Alemu, E.A., Lamark, T., Torgersen, K.M., Birgisdottir, A.B., Larsen, K.B., Jain, A., Olsvik, H., Overvatn, A., Kirkin, V. and Johansen, T. (2012) ATG8 family proteins act as scaffolds for assembly of the ULK complex: sequence requirements for LC3-interacting region (LIR) motifs. *J Biol Chem*, **287**, 39275-39290.
31. Joachim, J., Jefferies, H.B., Razi, M., Frith, D., Snijders, A.P., Chakravarty, P., Judith, D. and Tooze, S.A. (2015) Activation of ULK Kinase and Autophagy by GABARAP Trafficking from the Centrosome Is Regulated by WAC and GM130. *Mol Cell*, **60**, 899-913.
32. Kim, J., Kundu, M., Viollet, B. and Guan, K.L. (2011) AMPK and mTOR regulate autophagy through direct phosphorylation of Ulk1. *Nat Cell Biol*, **13**, 132-141.
33. Shang, L., Chen, S., Du, F., Li, S., Zhao, L. and Wang, X. (2011) Nutrient starvation elicits an acute autophagic response mediated by Ulk1 dephosphorylation and its subsequent dissociation from AMPK. *Proc Natl Acad Sci U S A*, **108**, 4788-4793.
34. Hosokawa, N., Hara, T., Kaizuka, T., Kishi, C., Takamura, A., Miura, Y., Iemura, S., Natsume, T., Takehana, K., Yamada, N. *et al.* (2009) Nutrient-dependent mTORC1 association with the ULK1-Atg13-FIP200 complex required for autophagy. *Mol Biol Cell*, **20**, 1981-1991.
35. Hara, T., Takamura, A., Kishi, C., Iemura, S., Natsume, T., Guan, J.L. and Mizushima, N. (2008) FIP200, a ULK-interacting protein, is required for autophagosome formation in mammalian cells. *J Cell Biol*, **181**, 497-510.
36. Hosokawa, N., Sasaki, T., Iemura, S., Natsume, T., Hara, T. and Mizushima, N. (2009) Atg101, a novel mammalian autophagy protein interacting with Atg13. *Autophagy*, **5**, 973-979.
37. Kaufmann, A., Beier, V., Franquelim, H.G. and Wollert, T. (2014) Molecular mechanism of autophagic membrane-scaffold assembly and disassembly. *Cell*, **156**, 469-481.
38. Weidberg, H., Shvets, E., Shpilka, T., Shimron, F., Shinder, V. and Elazar, Z. (2010) LC3 and GATE-16/GABARAP subfamilies are both essential yet act differently in autophagosome biogenesis. *EMBO J*, **29**, 1792-1802.
39. Xie, Z., Nair, U. and Klionsky, D.J. (2008) Atg8 controls phagophore expansion during autophagosome formation. *Mol Biol Cell*, **19**, 3290-3298.
40. Weidberg, H., Shpilka, T., Shvets, E., Abada, A., Shimron, F. and Elazar, Z. (2011) LC3 and GATE-16 N termini mediate membrane fusion processes required for autophagosome biogenesis. *Dev Cell*, **20**, 444-454.
41. Carra, S., Seguin, S.J. and Landry, J. (2008) HspB8 and Bag3: a new chaperone complex targeting misfolded proteins to macroautophagy. *Autophagy*, **4**, 237-239.

42. Filimonenko, M., Isakson, P., Finley, K.D., Anderson, M., Jeong, H., Melia, T.J., Bartlett, B.J., Myers, K.M., Birkeland, H.C., Lamark, T. *et al.* (2010) The selective macroautophagic degradation of aggregated proteins requires the PI3P-binding protein Alfy. *Mol Cell*, **38**, 265-279.
43. Korac, J., Schaeffer, V., Kovacevic, I., Clement, A.M., Jungblut, B., Behl, C., Terzic, J. and Dikic, I. (2013) Ubiquitin-independent function of optineurin in autophagic clearance of protein aggregates. *J Cell Sci*, **126**, 580-592.
44. Novak, I., Kirkin, V., McEwan, D.G., Zhang, J., Wild, P., Rozenknop, A., Rogov, V., Lohr, F., Popovic, D., Occhipinti, A. *et al.* (2010) Nix is a selective autophagy receptor for mitochondrial clearance. *EMBO Rep*, **11**, 45-51.
45. Richter, B., Sliter, D.A., Herhaus, L., Stolz, A., Wang, C., Beli, P., Zaffagnini, G., Wild, P., Martens, S., Wagner, S.A. *et al.* (2016) Phosphorylation of OPTN by TBK1 enhances its binding to Ub chains and promotes selective autophagy of damaged mitochondria. *Proc Natl Acad Sci U S A*, **113**, 4039-4044.
46. von Muhlinen, N., Akutsu, M., Ravenhill, B.J., Foeglein, A., Bloor, S., Rutherford, T.J., Freund, S.M., Komander, D. and Randow, F. (2012) LC3C, bound selectively by a noncanonical LIR motif in NDP52, is required for antibacterial autophagy. *Mol Cell*, **48**, 329-342.
47. Wild, P., Farhan, H., McEwan, D.G., Wagner, S., Rogov, V.V., Brady, N.R., Richter, B., Korac, J., Waidmann, O., Choudhary, C. *et al.* (2011) Phosphorylation of the autophagy receptor optineurin restricts Salmonella growth. *Science*, **333**, 228-233.
48. Le Guerroue, F., Eck, F., Jung, J., Starzetz, T., Mittelbronn, M., Kaulich, M. and Behrends, C. (2017) Autophagosomal Content Profiling Reveals an LC3C-Dependent Piecemeal Mitophagy Pathway. *Mol Cell*, **68**, 786-796 e786.
49. Stolz, A., Ernst, A. and Dikic, I. (2014) Cargo recognition and trafficking in selective autophagy. *Nat Cell Biol*, **16**, 495-501.
50. Kabeya, Y., Mizushima, N., Yamamoto, A., Oshitani-Okamoto, S., Ohsumi, Y. and Yoshimori, T. (2004) LC3, GABARAP and GATE16 localize to autophagosomal membrane depending on form-II formation. *J Cell Sci*, **117**, 2805-2812.
51. Furuta, N., Fujita, N., Noda, T., Yoshimori, T. and Amano, A. (2010) Combinational soluble N-ethylmaleimide-sensitive factor attachment protein receptor proteins VAMP8 and Vti1b mediate fusion of antimicrobial and canonical autophagosomes with lysosomes. *Mol Biol Cell*, **21**, 1001-1010.
52. Itakura, E., Kishi-Itakura, C. and Mizushima, N. (2012) The hairpin-type tail-anchored SNARE syntaxin 17 targets to autophagosomes for fusion with endosomes/lysosomes. *Cell*, **151**, 1256-1269.
53. Jager, S., Bucci, C., Tanida, I., Ueno, T., Kominami, E., Saftig, P. and Eskelinen, E.L. (2004) Role for Rab7 in maturation of late autophagic vacuoles. *J Cell Sci*, **117**, 4837-4848.
54. Tanaka, Y., Guhde, G., Suter, A., Eskelinen, E.L., Hartmann, D., Lullmann-Rauch, R., Janssen, P.M., Blanz, J., von Figura, K. and Saftig, P. (2000) Accumulation of autophagic vacuoles and cardiomyopathy in LAMP-2-deficient mice. *Nature*, **406**, 902-906.
55. McEwan, D.G., Popovic, D., Gubas, A., Terawaki, S., Suzuki, H., Stadel, D., Coxon, F.P., Miranda de Stegmann, D., Bhogaraju, S., Maddi, K. *et al.* (2015) PLEKHM1 regulates autophagosome-lysosome fusion through HOPS complex and LC3/GABARAP proteins. *Mol Cell*, **57**, 39-54.
56. Nguyen, T.N., Padman, B.S., Usher, J., Oorschot, V., Ramm, G. and Lazarou, M. (2016) Atg8 family LC3/GABARAP proteins are crucial for autophagosome-lysosome fusion but not autophagosome formation during PINK1/Parkin mitophagy and starvation. *J Cell Biol*, **215**, 857-874.
57. Wang, H., Bedford, F.K., Brandon, N.J., Moss, S.J. and Olsen, R.W. (1999) GABA(A)-receptor-associated protein links GABA(A) receptors and the cytoskeleton. *Nature*, **397**, 69-72.
58. Sieghart, W. and Sperk, G. (2002) Subunit composition, distribution and function of GABA(A) receptor subtypes. *Curr Top Med Chem*, **2**, 795-816.

59. Jacob, T.C., Moss, S.J. and Jurd, R. (2008) GABA(A) receptor trafficking and its role in the dynamic modulation of neuronal inhibition. *Nat Rev Neurosci*, **9**, 331-343.
60. Leil, T.A., Chen, Z.W., Chang, C.S. and Olsen, R.W. (2004) GABAA receptor-associated protein traffics GABAA receptors to the plasma membrane in neurons. *J Neurosci*, **24**, 11429-11438.
61. Chen, Z.W. and Olsen, R.W. (2007) GABAA receptor associated proteins: a key factor regulating GABAA receptor function. *J Neurochem*, **100**, 279-294.
62. Legesse-Miller, A., Sagiv, Y., Porat, A. and Elazar, Z. (1998) Isolation and characterization of a novel low molecular weight protein involved in intra-Golgi traffic. *J Biol Chem*, **273**, 3105-3109.
63. Muller, J.M., Shorter, J., Newman, R., Deinhardt, K., Sagiv, Y., Elazar, Z., Warren, G. and Shima, D.T. (2002) Sequential SNARE disassembly and GATE-16-GOS-28 complex assembly mediated by distinct NSF activities drives Golgi membrane fusion. *J Cell Biol*, **157**, 1161-1173.
64. Sollner, T., Bennett, M.K., Whiteheart, S.W., Scheller, R.H. and Rothman, J.E. (1993) A protein assembly-disassembly pathway in vitro that may correspond to sequential steps of synaptic vesicle docking, activation, and fusion. *Cell*, **75**, 409-418.
65. Nickel, W., Weber, T., McNew, J.A., Parlati, F., Sollner, T.H. and Rothman, J.E. (1999) Content mixing and membrane integrity during membrane fusion driven by pairing of isolated v-SNAREs and t-SNAREs. *Proc Natl Acad Sci U S A*, **96**, 12571-12576.
66. Mayer, A., Wickner, W. and Haas, A. (1996) Sec18p (NSF)-driven release of Sec17p (alpha-SNAP) can precede docking and fusion of yeast vacuoles. *Cell*, **85**, 83-94.
67. Otto, H., Hanson, P.I. and Jahn, R. (1997) Assembly and disassembly of a ternary complex of synaptobrevin, syntaxin, and SNAP-25 in the membrane of synaptic vesicles. *Proc Natl Acad Sci U S A*, **94**, 6197-6201.
68. Ungermann, C., Sato, K. and Wickner, W. (1998) Defining the functions of trans-SNARE pairs. *Nature*, **396**, 543-548.
69. Elazar, Z., Scherz-Shouval, R. and Shorer, H. (2003) Involvement of LMA1 and GATE-16 family members in intracellular membrane dynamics. *Biochim Biophys Acta*, **1641**, 145-156.
70. Sagiv, Y., Legesse-Miller, A., Porat, A. and Elazar, Z. (2000) GATE-16, a membrane transport modulator, interacts with NSF and the Golgi v-SNARE GOS-28. *EMBO J*, **19**, 1494-1504.
71. Meyer, H.H. (2005) Golgi reassembly after mitosis: the AAA family meets the ubiquitin family. *Biochim Biophys Acta*, **1744**, 481-492.
72. Stadel, D., Millarte, V., Tillmann, K.D., Huber, J., Tamin-Yecheskel, B.C., Akutsu, M., Demishtein, A., Ben-Zeev, B., Anikster, Y., Perez, F. *et al.* (2015) TECPR2 Cooperates with LC3C to Regulate COPII-Dependent ER Export. *Mol Cell*, **60**, 89-104.
73. McCaughey, J. and Stephens, D.J. (2018) COPII-dependent ER export in animal cells: adaptation and control for diverse cargo. *Histochem Cell Biol*, **150**, 119-131.
74. Baisamy, L., Cavin, S., Jurisch, N. and Diviani, D. (2009) The ubiquitin-like protein LC3 regulates the Rho-GEF activity of AKAP-Lbc. *J Biol Chem*, **284**, 28232-28242.
75. Genau, H.M., Huber, J., Baschieri, F., Akutsu, M., Dotsch, V., Farhan, H., Rogov, V. and Behrends, C. (2015) CUL3-KBTBD6/KBTBD7 ubiquitin ligase cooperates with GABARAP proteins to spatially restrict TIAM1-RAC1 signaling. *Mol Cell*, **57**, 995-1010.
76. Jaffe, A.B. and Hall, A. (2005) Rho GTPases: biochemistry and biology. *Annu Rev Cell Dev Biol*, **21**, 247-269.
77. Hordijk, P.L., ten Klooster, J.P., van der Kammen, R.A., Michiels, F., Oomen, L.C. and Collard, J.G. (1997) Inhibition of invasion of epithelial cells by Tiam1-Rac signaling. *Science*, **278**, 1464-1466.
78. Ridley, A.J. (2015) Rho GTPase signalling in cell migration. *Curr Opin Cell Biol*, **36**, 103-112.
79. Florey, O., Kim, S.E., Sandoval, C.P., Haynes, C.M. and Overholtzer, M. (2011) Autophagy machinery mediates macroendocytic processing and entotic cell death by targeting single membranes. *Nat Cell Biol*, **13**, 1335-1343.

80. Gluschko, A., Herb, M., Wiegmann, K., Krut, O., Neiss, W.F., Utermohlen, O., Kronke, M. and Schramm, M. (2018) The beta2 Integrin Mac-1 Induces Protective LC3-Associated Phagocytosis of Listeria monocytogenes. *Cell Host Microbe*, **23**, 324-337 e325.
81. Henault, J., Martinez, J., Riggs, J.M., Tian, J., Mehta, P., Clarke, L., Sasai, M., Latz, E., Brinkmann, M.M., Iwasaki, A. *et al.* (2012) Noncanonical autophagy is required for type I interferon secretion in response to DNA-immune complexes. *Immunity*, **37**, 986-997.
82. Huang, J., Canadien, V., Lam, G.Y., Steinberg, B.E., Dinauer, M.C., Magalhaes, M.A., Glogauer, M., Grinstein, S. and Brumell, J.H. (2009) Activation of antibacterial autophagy by NADPH oxidases. *Proc Natl Acad Sci U S A*, **106**, 6226-6231.
83. Martinez, J., Cunha, L.D., Park, S., Yang, M., Lu, Q., Orchard, R., Li, Q.Z., Yan, M., Janke, L., Guy, C. *et al.* (2016) Noncanonical autophagy inhibits the autoinflammatory, lupus-like response to dying cells. *Nature*, **533**, 115-119.
84. Martinez, J., Almendinger, J., Oberst, A., Ness, R., Dillon, C.P., Fitzgerald, P., Hengartner, M.O. and Green, D.R. (2011) Microtubule-associated protein 1 light chain 3 alpha (LC3)-associated phagocytosis is required for the efficient clearance of dead cells. *Proc Natl Acad Sci U S A*, **108**, 17396-17401.
85. Freeman, S.A. and Grinstein, S. (2014) Phagocytosis: receptors, signal integration, and the cytoskeleton. *Immunol Rev*, **262**, 193-215.
86. Herb, M., Gluschko, A. and Schramm, M. (2020) LC3-associated phagocytosis - The highway to hell for phagocytosed microbes. *Semin Cell Dev Biol*, **101**, 68-76.
87. Martinez, J., Malireddi, R.K., Lu, Q., Cunha, L.D., Pelletier, S., Gingras, S., Orchard, R., Guan, J.L., Tan, H., Peng, J. *et al.* (2015) Molecular characterization of LC3-associated phagocytosis reveals distinct roles for Rubicon, NOX2 and autophagy proteins. *Nat Cell Biol*, **17**, 893-906.
88. Sanjuan, M.A., Dillon, C.P., Tait, S.W., Moshiach, S., Dorsey, F., Connell, S., Komatsu, M., Tanaka, K., Cleveland, J.L., Withoff, S. *et al.* (2007) Toll-like receptor signalling in macrophages links the autophagy pathway to phagocytosis. *Nature*, **450**, 1253-1257.
89. Komatsu, M., Chiba, T., Tatsumi, K., Iemura, S., Tanida, I., Okazaki, N., Ueno, T., Kominami, E., Natsume, T. and Tanaka, K. (2004) A novel protein-conjugating system for Ufm1, a ubiquitin-fold modifier. *EMBO J*, **23**, 1977-1986.
90. Gerakis, Y., Quintero, M., Li, H. and Hetz, C. (2019) The UFMylation System in Proteostasis and Beyond. *Trends Cell Biol*, **29**, 974-986.
91. Sasakawa, H., Sakata, E., Yamaguchi, Y., Komatsu, M., Tatsumi, K., Kominami, E., Tanaka, K. and Kato, K. (2006) Solution structure and dynamics of Ufm1, a ubiquitin-fold modifier 1. *Biochem Biophys Res Commun*, **343**, 21-26.
92. Kang, S.H., Kim, G.R., Seong, M., Baek, S.H., Seol, J.H., Bang, O.S., Ovaa, H., Tatsumi, K., Komatsu, M., Tanaka, K. *et al.* (2007) Two novel ubiquitin-fold modifier 1 (Ufm1)-specific proteases, UfSP1 and UfSP2. *J Biol Chem*, **282**, 5256-5262.
93. Gavin, J.M., Hoar, K., Xu, Q., Ma, J., Lin, Y., Chen, J., Chen, W., Bruzzese, F.J., Harrison, S., Mallender, W.D. *et al.* (2014) Mechanistic study of Uba5 enzyme and the Ufm1 conjugation pathway. *J Biol Chem*, **289**, 22648-22658.
94. Habisov, S., Huber, J., Ichimura, Y., Akutsu, M., Rogova, N., Loehr, F., McEwan, D.G., Johansen, T., Dikic, I., Doetsch, V. *et al.* (2016) Structural and Functional Analysis of a Novel Interaction Motif within UFM1-activating Enzyme 5 (UBA5) Required for Binding to Ubiquitin-like Proteins and Ufmylation. *J Biol Chem*, **291**, 9025-9041.
95. Huber, J., Obata, M., Gruber, J., Akutsu, M., Lohr, F., Rogova, N., Guntert, P., Dikic, I., Kirkin, V., Komatsu, M. *et al.* (2020) An atypical LIR motif within UBA5 (ubiquitin like modifier activating enzyme 5) interacts with GABARAP proteins and mediates membrane localization of UBA5. *Autophagy*, **16**, 256-270.
96. Mashahreh, B., Hassouna, F., Soudah, N., Cohen-Kfir, E., Strulovich, R., Haitin, Y. and Wiener, R. (2018) Trans-binding of UFM1 to UBA5 stimulates UBA5 homodimerization and ATP binding. *FASEB J*, **32**, 2794-2802.

97. Oweis, W., Padala, P., Hassouna, F., Cohen-Kfir, E., Gibbs, D.R., Todd, E.A., Berndsen, C.E. and Wiener, R. (2016) Trans-Binding Mechanism of Ubiquitin-like Protein Activation Revealed by a UBA5-UFM1 Complex. *Cell Rep*, **16**, 3113-3120.
98. Padala, P., Oweis, W., Mashahreh, B., Soudah, N., Cohen-Kfir, E., Todd, E.A., Berndsen, C.E. and Wiener, R. (2017) Novel insights into the interaction of UBA5 with UFM1 via a UFM1-interacting sequence. *Sci Rep*, **7**, 508.
99. Tatsumi, K., Sou, Y.S., Tada, N., Nakamura, E., Iemura, S., Natsume, T., Kang, S.H., Chung, C.H., Kasahara, M., Kominami, E. *et al.* (2010) A novel type of E3 ligase for the Ufm1 conjugation system. *J Biol Chem*, **285**, 5417-5427.
100. Cappadocia, L. and Lima, C.D. (2018) Ubiquitin-like Protein Conjugation: Structures, Chemistry, and Mechanism. *Chem Rev*, **118**, 889-918.
101. Lemaire, K., Moura, R.F., Granvik, M., Igoillo-Esteve, M., Hohmeier, H.E., Hendrickx, N., Newgard, C.B., Waelkens, E., Cnop, M. and Schuit, F. (2011) Ubiquitin fold modifier 1 (UFM1) and its target UFBP1 protect pancreatic beta cells from ER stress-induced apoptosis. *PLoS One*, **6**, e18517.
102. Stephani, M., Picchianti, L., Gajic, A., Beveridge, R., Skarwan, E., Sanchez de Medina Hernandez, V., Mohseni, A., Clavel, M., Zeng, Y., Naumann, C. *et al.* (2020) A cross-kingdom conserved ER-phagy receptor maintains endoplasmic reticulum homeostasis during stress. *Elife*, **9**.
103. Wu, J., Lei, G., Mei, M., Tang, Y. and Li, H. (2010) A novel C53/LZAP-interacting protein regulates stability of C53/LZAP and DDRGK domain-containing Protein 1 (DDRGK1) and modulates NF-kappaB signaling. *J Biol Chem*, **285**, 15126-15136.
104. Zhang, Y., Zhang, M., Wu, J., Lei, G. and Li, H. (2012) Transcriptional regulation of the Ufm1 conjugation system in response to disturbance of the endoplasmic reticulum homeostasis and inhibition of vesicle trafficking. *PLoS One*, **7**, e48587.
105. Liu, J., Wang, Y., Song, L., Zeng, L., Yi, W., Liu, T., Chen, H., Wang, M., Ju, Z. and Cong, Y.S. (2017) A critical role of DDRGK1 in endoplasmic reticulum homoeostasis via regulation of IRE1alpha stability. *Nat Commun*, **8**, 14186.
106. Zhu, Y., Lei, Q., Li, D., Zhang, Y., Jiang, X., Hu, Z. and Xu, G. (2018) Proteomic and Biochemical Analyses Reveal a Novel Mechanism for Promoting Protein Ubiquitination and Degradation by UFBP1, a Key Component of Ufmylation. *J Proteome Res*, **17**, 1509-1520.
107. Ching, Y.P., Qi, Z. and Wang, J.H. (2000) Cloning of three novel neuronal Cdk5 activator binding proteins. *Gene*, **242**, 285-294.
108. Jiang, H., Luo, S. and Li, H. (2005) Cdk5 activator-binding protein C53 regulates apoptosis induced by genotoxic stress via modulating the G2/M DNA damage checkpoint. *J Biol Chem*, **280**, 20651-20659.
109. Jiang, H., Wu, J., He, C., Yang, W. and Li, H. (2009) Tumor suppressor protein C53 antagonizes checkpoint kinases to promote cyclin-dependent kinase 1 activation. *Cell Res*, **19**, 458-468.
110. Wang, J., He, X., Luo, Y. and Yarbrough, W.G. (2006) A novel ARF-binding protein (LZAP) alters ARF regulation of HDM2. *Biochem J*, **393**, 489-501.
111. Walczak, C.P., Leto, D.E., Zhang, L., Riepe, C., Muller, R.Y., DaRosa, P.A., Ingolia, N.T., Elias, J.E. and Kopito, R.R. (2019) Ribosomal protein RPL26 is the principal target of UFMylation. *Proc Natl Acad Sci U S A*, **116**, 1299-1308.
112. Yang, R., Wang, H., Kang, B., Chen, B., Shi, Y., Yang, S., Sun, L., Liu, Y., Xiao, W., Zhang, T. *et al.* (2019) CDK5RAP3, a UFL1 substrate adaptor, is crucial for liver development. *Development*, **146**.
113. Liang, J.R., Lingeman, E., Luong, T., Ahmed, S., Muhar, M., Nguyen, T., Olzmann, J.A. and Corn, J.E. (2020) A Genome-wide ER-phagy Screen Highlights Key Roles of Mitochondrial Metabolism and ER-Resident UFMylation. *Cell*, **180**, 1160-1177 e1120.
114. DeJesus, R., Moretti, F., McAllister, G., Wang, Z., Bergman, P., Liu, S., Frias, E., Alford, J., Reece-Hoyes, J.S., Lindeman, A. *et al.* (2016) Functional CRISPR screening identifies the ufmylation pathway as a regulator of SQSTM1/p62. *Elife*, **5**.

115. Wang, Z., Gong, Y., Peng, B., Shi, R., Fan, D., Zhao, H., Zhu, M., Zhang, H., Lou, Z., Zhou, J. *et al.* (2019) MRE11 UFMylation promotes ATM activation. *Nucleic Acids Res*, **47**, 4124-4135.
116. Cai, Y., Pi, W., Sivaprakasam, S., Zhu, X., Zhang, M., Chen, J., Makala, L., Lu, C., Wu, J., Teng, Y. *et al.* (2015) UFBP1, a Key Component of the Ufm1 Conjugation System, Is Essential for Ufmylation-Mediated Regulation of Erythroid Development. *PLoS Genet*, **11**, e1005643.
117. Hu, X., Pang, Q., Shen, Q., Liu, H., He, J., Wang, J., Xiong, J., Zhang, H. and Chen, F. (2014) Ubiquitin-fold modifier 1 inhibits apoptosis by suppressing the endoplasmic reticulum stress response in Raw264.7 cells. *Int J Mol Med*, **33**, 1539-1546.
118. Lin, J.X., Xie, X.S., Weng, X.F., Qiu, S.L., Yoon, C., Lian, N.Z., Xie, J.W., Wang, J.B., Lu, J., Chen, Q.Y. *et al.* (2019) UFM1 suppresses invasive activities of gastric cancer cells by attenuating the expres7sion of PDK1 through PI3K/AKT signaling. *J Exp Clin Cancer Res*, **38**, 410.
119. Liu, J., Guan, D., Dong, M., Yang, J., Wei, H., Liang, Q., Song, L., Xu, L., Bai, J., Liu, C. *et al.* (2020) UFMylation maintains tumour suppressor p53 stability by antagonizing its ubiquitination. *Nat Cell Biol*, **22**, 1056-1063.
120. Yoo, H.M., Kang, S.H., Kim, J.Y., Lee, J.E., Seong, M.W., Lee, S.W., Ka, S.H., Sou, Y.S., Komatsu, M., Tanaka, K. *et al.* (2014) Modification of ASC1 by UFM1 is crucial for ERalpha transactivation and breast cancer development. *Mol Cell*, **56**, 261-274.
121. Karagoz, G.E., Acosta-Alvear, D. and Walter, P. (2019) The Unfolded Protein Response: Detecting and Responding to Fluctuations in the Protein-Folding Capacity of the Endoplasmic Reticulum. *Cold Spring Harb Perspect Biol*, **11**.
122. Zhu, H., Bhatt, B., Sivaprakasam, S., Cai, Y., Liu, S., Kodeboyina, S.K., Patel, N., Savage, N.M., Sharma, A., Kaufman, R.J. *et al.* (2019) Ufbp1 promotes plasma cell development and ER expansion by modulating distinct branches of UPR. *Nat Commun*, **10**, 1084.
123. Chino, H. and Mizushima, N. (2020) ER-Phagy: Quality Control and Turnover of Endoplasmic Reticulum. *Trends Cell Biol*, **30**, 384-398.
124. Wang, L., Xu, Y., Rogers, H., Saidi, L., Noguchi, C.T., Li, H., Yewdell, J.W., Guydosh, N.R. and Ye, Y. (2020) UFMylation of RPL26 links translocation-associated quality control to endoplasmic reticulum protein homeostasis. *Cell Res*, **30**, 5-20.
125. Ruggiano, A., Foresti, O. and Carvalho, P. (2014) Quality control: ER-associated degradation: protein quality control and beyond. *J Cell Biol*, **204**, 869-879.
126. Osborne, C.K. and Schiff, R. (2011) Mechanisms of endocrine resistance in breast cancer. *Annu Rev Med*, **62**, 233-247.
127. Kastenhuber, E.R. and Lowe, S.W. (2017) Putting p53 in Context. *Cell*, **170**, 1062-1078.
128. Qin, B., Yu, J., Nowsheen, S., Wang, M., Tu, X., Liu, T., Li, H., Wang, L. and Lou, Z. (2019) UFL1 promotes histone H4 ufmylation and ATM activation. *Nat Commun*, **10**, 1242.
129. Qin, B., Yu, J., Nowsheen, S., Zhao, F., Wang, L. and Lou, Z. (2020) STK38 promotes ATM activation by acting as a reader of histone H4 ufmylation. *Sci Adv*, **6**, eaax8214.
130. Fang, Z. and Pan, Z. (2019) Essential Role of Ubiquitin-Fold Modifier 1 Conjugation in DNA Damage Response. *DNA Cell Biol*, **38**, 1030-1039.
131. Lee, J.H., Ghirlando, R., Bhaskara, V., Hoffmeyer, M.R., Gu, J. and Paull, T.T. (2003) Regulation of Mre11/Rad50 by Nbs1: effects on nucleotide-dependent DNA binding and association with ataxia-telangiectasia-like disorder mutant complexes. *J Biol Chem*, **278**, 45171-45181.
132. Uziel, T., Lerenthal, Y., Moyal, L., Andegeko, Y., Mittelman, L. and Shiloh, Y. (2003) Requirement of the MRN complex for ATM activation by DNA damage. *EMBO J*, **22**, 5612-5621.
133. Dzierzak, E. and Philipsen, S. (2013) Erythropoiesis: development and differentiation. *Cold Spring Harb Perspect Med*, **3**, a011601.

134. Tatsumi, K., Yamamoto-Mukai, H., Shimizu, R., Waguri, S., Sou, Y.S., Sakamoto, A., Taya, C., Shitara, H., Hara, T., Chung, C.H. *et al.* (2011) The Ufm1-activating enzyme Uba5 is indispensable for erythroid differentiation in mice. *Nat Commun*, **2**, 181.
135. Zhang, M., Zhu, X., Zhang, Y., Cai, Y., Chen, J., Sivaprakasam, S., Gurav, A., Pi, W., Makala, L., Wu, J. *et al.* (2015) RCAD/Ufl1, a Ufm1 E3 ligase, is essential for hematopoietic stem cell function and murine hematopoiesis. *Cell Death Differ*, **22**, 1922-1934.
136. Olzmann, J.A. and Carvalho, P. (2019) Dynamics and functions of lipid droplets. *Nat Rev Mol Cell Biol*, **20**, 137-155.
137. Rambold, A.S., Cohen, S. and Lippincott-Schwartz, J. (2015) Fatty acid trafficking in starved cells: regulation by lipid droplet lipolysis, autophagy, and mitochondrial fusion dynamics. *Dev Cell*, **32**, 678-692.
138. Murphy, D.J. (2001) The biogenesis and functions of lipid bodies in animals, plants and microorganisms. *Prog Lipid Res*, **40**, 325-438.
139. Igal, R.A. and Coleman, R.A. (1996) Acylglycerol recycling from triacylglycerol to phospholipid, not lipase activity, is defective in neutral lipid storage disease fibroblasts. *J Biol Chem*, **271**, 16644-16651.
140. Markgraf, D.F., Klemm, R.W., Junker, M., Hannibal-Bach, H.K., Ejsing, C.S. and Rapoport, T.A. (2014) An ER protein functionally couples neutral lipid metabolism on lipid droplets to membrane lipid synthesis in the ER. *Cell Rep*, **6**, 44-55.
141. Herms, A., Bosch, M., Reddy, B.J., Schieber, N.L., Fajardo, A., Ruperez, C., Fernandez-Vidal, A., Ferguson, C., Rentero, C., Tebar, F. *et al.* (2015) AMPK activation promotes lipid droplet dispersion on detyrosinated microtubules to increase mitochondrial fatty acid oxidation. *Nat Commun*, **6**, 7176.
142. Liu, P., Bartz, R., Zehmer, J.K., Ying, Y.S., Zhu, M., Serrero, G. and Anderson, R.G. (2007) Rab-regulated interaction of early endosomes with lipid droplets. *Biochim Biophys Acta*, **1773**, 784-793.
143. Miyanari, Y., Atsuzawa, K., Usuda, N., Watashi, K., Hishiki, T., Zayas, M., Bartenschlager, R., Wakita, T., Hijikata, M. and Shimotohno, K. (2007) The lipid droplet is an important organelle for hepatitis C virus production. *Nat Cell Biol*, **9**, 1089-1097.
144. Hartman, I.Z., Liu, P., Zehmer, J.K., Luby-Phelps, K., Jo, Y., Anderson, R.G. and DeBose-Boyd, R.A. (2010) Sterol-induced dislocation of 3-hydroxy-3-methylglutaryl coenzyme A reductase from endoplasmic reticulum membranes into the cytosol through a subcellular compartment resembling lipid droplets. *J Biol Chem*, **285**, 19288-19298.
145. Olzmann, J.A., Richter, C.M. and Kopito, R.R. (2013) Spatial regulation of UBXD8 and p97/VCP controls ATGL-mediated lipid droplet turnover. *Proc Natl Acad Sci U S A*, **110**, 1345-1350.
146. Listenberger, L.L., Han, X., Lewis, S.E., Cases, S., Farese, R.V., Jr., Ory, D.S. and Schaffer, J.E. (2003) Triglyceride accumulation protects against fatty acid-induced lipotoxicity. *Proc Natl Acad Sci U S A*, **100**, 3077-3082.
147. Nguyen, T.B., Louie, S.M., Daniele, J.R., Tran, Q., Dillin, A., Zoncu, R., Nomura, D.K. and Olzmann, J.A. (2017) DGAT1-Dependent Lipid Droplet Biogenesis Protects Mitochondrial Function during Starvation-Induced Autophagy. *Dev Cell*, **42**, 9-21 e25.
148. Fei, W., Wang, H., Fu, X., Bielby, C. and Yang, H. (2009) Conditions of endoplasmic reticulum stress stimulate lipid droplet formation in Saccharomyces cerevisiae. *Biochem J*, **424**, 61-67.
149. Hapala, I., Marza, E. and Ferreira, T. (2011) Is fat so bad? Modulation of endoplasmic reticulum stress by lipid droplet formation. *Biol Cell*, **103**, 271-285.
150. Jarc, E. and Petan, T. (2019) Lipid Droplets and the Management of Cellular Stress. *Yale J Biol Med*, **92**, 435-452.
151. Welte, M.A. and Gould, A.P. (2017) Lipid droplet functions beyond energy storage. *Biochim Biophys Acta Mol Cell Biol Lipids*, **1862**, 1260-1272.
152. Onal, G., Kutlu, O., Gozuacik, D. and Dokmeci Emre, S. (2017) Lipid Droplets in Health and Disease. *Lipids Health Dis*, **16**, 128.

153. Filipe, A. and McLauchlan, J. (2015) Hepatitis C virus and lipid droplets: finding a niche. *Trends Mol Med*, **21**, 34-42.
154. Marshall, L.L., Stimpson, S.E., Hyland, R., Coorssen, J.R. and Myers, S.J. (2014) Increased lipid droplet accumulation associated with a peripheral sensory neuropathy. *J Chem Biol*, **7**, 67-76.
155. Pol, A., Gross, S.P. and Parton, R.G. (2014) Review: biogenesis of the multifunctional lipid droplet: lipids, proteins, and sites. *J Cell Biol*, **204**, 635-646.
156. Thiam, A.R. and Foret, L. (2016) The physics of lipid droplet nucleation, growth and budding. *Biochim Biophys Acta*, **1861**, 715-722.
157. Binns, D., Januszewski, T., Chen, Y., Hill, J., Markin, V.S., Zhao, Y., Gilpin, C., Chapman, K.D., Anderson, R.G. and Goodman, J.M. (2006) An intimate collaboration between peroxisomes and lipid bodies. *J Cell Biol*, **173**, 719-731.
158. Kong, J., Ji, Y., Jeon, Y.G., Han, J.S., Han, K.H., Lee, J.H., Lee, G., Jang, H., Choe, S.S., Baes, M. *et al.* (2020) Spatiotemporal contact between peroxisomes and lipid droplets regulates fasting-induced lipolysis via PEX5. *Nat Commun*, **11**, 578.
159. Valm, A.M., Cohen, S., Legant, W.R., Melunis, J., Hershberg, U., Wait, E., Cohen, A.R., Davidson, M.W., Betzig, E. and Lippincott-Schwartz, J. (2017) Applying systems-level spectral imaging and analysis to reveal the organelle interactome. *Nature*, **546**, 162-167.
160. Wang, H., Sreenivasan, U., Hu, H., Saladino, A., Polster, B.M., Lund, L.M., Gong, D.W., Stanley, W.C. and Sztalryd, C. (2011) Perilipin 5, a lipid droplet-associated protein, provides physical and metabolic linkage to mitochondria. *J Lipid Res*, **52**, 2159-2168.
161. Prinz, W.A. (2014) Bridging the gap: membrane contact sites in signaling, metabolism, and organelle dynamics. *J Cell Biol*, **205**, 759-769.
162. Choudhary, V., Ojha, N., Golden, A. and Prinz, W.A. (2015) A conserved family of proteins facilitates nascent lipid droplet budding from the ER. *J Cell Biol*, **211**, 261-271.
163. Duelund, L., Jensen, G.V., Hannibal-Bach, H.K., Ejsing, C.S., Pedersen, J.S., Pakkanen, K.I. and Ipsen, J.H. (2013) Composition, structure and properties of POPC-triolein mixtures. Evidence of triglyceride domains in phospholipid bilayers. *Biochim Biophys Acta*, **1828**, 1909-1917.
164. Khandelia, H., Duelund, L., Pakkanen, K.I. and Ipsen, J.H. (2010) Triglyceride blisters in lipid bilayers: implications for lipid droplet biogenesis and the mobile lipid signal in cancer cell membranes. *PLoS One*, **5**, e12811.
165. Renne, M.F., Klug, Y.A. and Carvalho, P. (2020) Lipid droplet biogenesis: A mystery "unmixing"? *Semin Cell Dev Biol*.
166. Tauchi-Sato, K., Ozeki, S., Houjou, T., Taguchi, R. and Fujimoto, T. (2002) The surface of lipid droplets is a phospholipid monolayer with a unique Fatty Acid composition. *J Biol Chem*, **277**, 44507-44512.
167. Ben M'barek, K., Ajjaji, D., Chorlay, A., Vanni, S., Foret, L. and Thiam, A.R. (2017) ER Membrane Phospholipids and Surface Tension Control Cellular Lipid Droplet Formation. *Dev Cell*, **41**, 591-604 e597.
168. Choudhary, V., Golani, G., Joshi, A.S., Cottier, S., Schneiter, R., Prinz, W.A. and Kozlov, M.M. (2018) Architecture of Lipid Droplets in Endoplasmic Reticulum Is Determined by Phospholipid Intrinsic Curvature. *Curr Biol*, **28**, 915-926 e919.
169. Kassan, A., Herms, A., Fernandez-Vidal, A., Bosch, M., Schieber, N.L., Reddy, B.J., Fajardo, A., Gelabert-Baldrich, M., Tebar, F., Enrich, C. *et al.* (2013) Acyl-CoA synthetase 3 promotes lipid droplet biogenesis in ER microdomains. *J Cell Biol*, **203**, 985-1001.
170. Salo, V.T., Belevich, I., Li, S., Karhinen, L., Vihinen, H., Vigouroux, C., Magre, J., Thiele, C., Holtta-Vuori, M., Jokitalo, E. *et al.* (2016) Seipin regulates ER-lipid droplet contacts and cargo delivery. *EMBO J*, **35**, 2699-2716.
171. Salo, V.T., Li, S., Vihinen, H., Holtta-Vuori, M., Szkalisity, A., Horvath, P., Belevich, I., Peranen, J., Thiele, C., Somerharju, P. *et al.* (2019) Seipin Facilitates Triglyceride Flow to Lipid Droplet and Counteracts Droplet Ripening via Endoplasmic Reticulum Contact. *Dev Cell*, **50**, 478-493 e479.

172. Wilfling, F., Wang, H., Haas, J.T., Krahmer, N., Gould, T.J., Uchida, A., Cheng, J.X., Graham, M., Christiano, R., Frohlich, F. *et al.* (2013) Triacylglycerol synthesis enzymes mediate lipid droplet growth by relocalizing from the ER to lipid droplets. *Dev Cell*, **24**, 384-399.
173. Wang, C.W. (2016) Lipid droplets, lipophagy, and beyond. *Biochim Biophys Acta*, **1861**, 793-805.
174. Gong, J., Sun, Z., Wu, L., Xu, W., Schieber, N., Xu, D., Shui, G., Yang, H., Parton, R.G. and Li, P. (2011) Fsp27 promotes lipid droplet growth by lipid exchange and transfer at lipid droplet contact sites. *J Cell Biol*, **195**, 953-963.
175. Jambunathan, S., Yin, J., Khan, W., Tamori, Y. and Puri, V. (2011) FSP27 promotes lipid droplet clustering and then fusion to regulate triglyceride accumulation. *PLoS One*, **6**, e28614.
176. Jenkins, C.M., Mancuso, D.J., Yan, W., Sims, H.F., Gibson, B. and Gross, R.W. (2004) Identification, cloning, expression, and purification of three novel human calcium-independent phospholipase A2 family members possessing triacylglycerol lipase and acylglycerol transacylase activities. *J Biol Chem*, **279**, 48968-48975.
177. Kraemer, F.B. and Shen, W.J. (2002) Hormone-sensitive lipase: control of intracellular tri-(di-)acylglycerol and cholesteryl ester hydrolysis. *J Lipid Res*, **43**, 1585-1594.
178. Singh, R., Kaushik, S., Wang, Y., Xiang, Y., Novak, I., Komatsu, M., Tanaka, K., Cuervo, A.M. and Czaja, M.J. (2009) Autophagy regulates lipid metabolism. *Nature*, **458**, 1131-1135.
179. Villena, J.A., Roy, S., Sarkadi-Nagy, E., Kim, K.H. and Sul, H.S. (2004) Desnutrin, an adipocyte gene encoding a novel patatin domain-containing protein, is induced by fasting and glucocorticoids: ectopic expression of desnutrin increases triglyceride hydrolysis. *J Biol Chem*, **279**, 47066-47075.
180. Zimmermann, R., Strauss, J.G., Haemmerle, G., Schoiswohl, G., Birner-Gruenberger, R., Riederer, M., Lass, A., Neuberger, G., Eisenhaber, F., Hermetter, A. *et al.* (2004) Fat mobilization in adipose tissue is promoted by adipose triglyceride lipase. *Science*, **306**, 1383-1386.
181. Haemmerle, G., Zimmermann, R., Hayn, M., Theussl, C., Waeg, G., Wagner, E., Sattler, W., Magin, T.M., Wagner, E.F. and Zechner, R. (2002) Hormone-sensitive lipase deficiency in mice causes diglyceride accumulation in adipose tissue, muscle, and testis. *J Biol Chem*, **277**, 4806-4815.
182. Schweiger, M., Schreiber, R., Haemmerle, G., Lass, A., Fledelius, C., Jacobsen, P., Tornqvist, H., Zechner, R. and Zimmermann, R. (2006) Adipose triglyceride lipase and hormone-sensitive lipase are the major enzymes in adipose tissue triacylglycerol catabolism. *J Biol Chem*, **281**, 40236-40241.
183. Taschler, U., Radner, F.P., Heier, C., Schreiber, R., Schweiger, M., Schoiswohl, G., Preiss-Landl, K., Jaeger, D., Reiter, B., Koefeler, H.C. *et al.* (2011) Monoglyceride lipase deficiency in mice impairs lipolysis and attenuates diet-induced insulin resistance. *J Biol Chem*, **286**, 17467-17477.
184. Kounakis, K., Chaniotakis, M., Markaki, M. and Tavernarakis, N. (2019) Emerging Roles of Lipophagy in Health and Disease. *Front Cell Dev Biol*, **7**, 185.
185. Lizaso, A., Tan, K.T. and Lee, Y.H. (2013) beta-adrenergic receptor-stimulated lipolysis requires the RAB7-mediated autolysosomal lipid degradation. *Autophagy*, **9**, 1228-1243.
186. Schroeder, B., Schulze, R.J., Weller, S.G., Sletten, A.C., Casey, C.A. and McNiven, M.A. (2015) The small GTPase Rab7 as a central regulator of hepatocellular lipophagy. *Hepatology*, **61**, 1896-1907.
187. Khan, S.A., Sathyanarayan, A., Mashek, M.T., Ong, K.T., Wollaston-Hayden, E.E. and Mashek, D.G. (2015) ATGL-catalyzed lipolysis regulates SIRT1 to control PGC-1alpha/PPAR-alpha signaling. *Diabetes*, **64**, 418-426.
188. Lee, I.H., Cao, L., Mostoslavsky, R., Lombard, D.B., Liu, J., Bruns, N.E., Tsokos, M., Alt, F.W. and Finkel, T. (2008) A role for the NAD-dependent deacetylase Sirt1 in the regulation of autophagy. *Proc Natl Acad Sci U S A*, **105**, 3374-3379.

189. Sathyanarayan, A., Mashek, M.T. and Mashek, D.G. (2017) ATGL Promotes Autophagy/Lipophagy via SIRT1 to Control Hepatic Lipid Droplet Catabolism. *Cell Rep*, **19**, 1-9.
190. Schott, M.B., Weller, S.G., Schulze, R.J., Krueger, E.W., Drizyte-Miller, K., Casey, C.A. and McNiven, M.A. (2019) Lipid droplet size directs lipolysis and lipophagy catabolism in hepatocytes. *J Cell Biol*, **218**, 3320-3335.
191. Zechner, R., Madeo, F. and Kratky, D. (2017) Cytosolic lipolysis and lipophagy: two sides of the same coin. *Nat Rev Mol Cell Biol*, **18**, 671-684.
192. Beilstein, F., Bouchoux, J., Rousset, M. and Demignot, S. (2013) Proteomic analysis of lipid droplets from Caco-2/TC7 enterocytes identifies novel modulators of lipid secretion. *PLoS One*, **8**, e53017.
193. Bersuker, K., Peterson, C.W.H., To, M., Sahl, S.J., Savikhin, V., Grossman, E.A., Nomura, D.K. and Olzmann, J.A. (2018) A Proximity Labeling Strategy Provides Insights into the Composition and Dynamics of Lipid Droplet Proteomes. *Dev Cell*, **44**, 97-112 e117.
194. Brasaemle, D.L., Dolios, G., Shapiro, L. and Wang, R. (2004) Proteomic analysis of proteins associated with lipid droplets of basal and lipolytically stimulated 3T3-L1 adipocytes. *J Biol Chem*, **279**, 46835-46842.
195. Krahmer, N., Hilger, M., Kory, N., Wilfling, F., Stoehr, G., Mann, M., Farese, R.V., Jr. and Walther, T.C. (2013) Protein correlation profiles identify lipid droplet proteins with high confidence. *Mol Cell Proteomics*, **12**, 1115-1126.
196. Larsson, S., Resjo, S., Gomez, M.F., James, P. and Holm, C. (2012) Characterization of the lipid droplet proteome of a clonal insulin-producing beta-cell line (INS-1 832/13). *J Proteome Res*, **11**, 1264-1273.
197. Zhang, H., Wang, Y., Li, J., Yu, J., Pu, J., Li, L., Zhang, H., Zhang, S., Peng, G., Yang, F. *et al.* (2011) Proteome of skeletal muscle lipid droplet reveals association with mitochondria and apolipoprotein a-I. *J Proteome Res*, **10**, 4757-4768.
198. Dhiman, R., Caesar, S., Thiam, A.R. and Schrul, B. (2020) Mechanisms of protein targeting to lipid droplets: A unified cell biological and biophysical perspective. *Semin Cell Dev Biol*.
199. Ingelmo-Torres, M., Gonzalez-Moreno, E., Kassan, A., Hanzal-Bayer, M., Tebar, F., Herms, A., Grewal, T., Hancock, J.F., Enrich, C., Bosch, M. *et al.* (2009) Hydrophobic and basic domains target proteins to lipid droplets. *Traffic*, **10**, 1785-1801.
200. Rowe, E.R., Mimmack, M.L., Barbosa, A.D., Haider, A., Isaac, I., Ouberai, M.M., Thiam, A.R., Patel, S., Saudek, V., Siniossoglou, S. *et al.* (2016) Conserved Amphipathic Helices Mediate Lipid Droplet Targeting of Perilipins 1-3. *J Biol Chem*, **291**, 6664-6678.
201. Sztalryd, C. and Brasaemle, D.L. (2017) The perilipin family of lipid droplet proteins: Gatekeepers of intracellular lipolysis. *Biochim Biophys Acta Mol Cell Biol Lipids*, **1862**, 1221-1232.
202. Zhang, P., Meng, L., Song, L., Du, J., Du, S., Cui, W., Liu, C. and Li, F. (2018) Roles of Perilipins in Diseases and Cancers. *Curr Genomics*, **19**, 247-257.
203. Granneman, J.G., Moore, H.P., Krishnamoorthy, R. and Rathod, M. (2009) Perilipin controls lipolysis by regulating the interactions of AB-hydrolase containing 5 (Abhd5) and adipose triglyceride lipase (Atgl). *J Biol Chem*, **284**, 34538-34544.
204. Granneman, J.G., Moore, H.P., Mottillo, E.P., Zhu, Z. and Zhou, L. (2011) Interactions of perilipin-5 (Plin5) with adipose triglyceride lipase. *J Biol Chem*, **286**, 5126-5135.
205. Wang, H., Hu, L., Dalen, K., Dorward, H., Marcinkiewicz, A., Russell, D., Gong, D., Londos, C., Yamaguchi, T., Holm, C. *et al.* (2009) Activation of hormone-sensitive lipase requires two steps, protein phosphorylation and binding to the PAT-1 domain of lipid droplet coat proteins. *J Biol Chem*, **284**, 32116-32125.
206. Gemmink, A., Daemen, S., Kuijpers, H.J.H., Schaart, G., Duimel, H., Lopez-Iglesias, C., van Zandvoort, M., Knoops, K. and Hesselink, M.K.C. (2018) Super-resolution microscopy localizes perilipin 5 at lipid droplet-mitochondria interaction sites and at lipid droplets juxtaposing to perilipin 2. *Biochim Biophys Acta Mol Cell Biol Lipids*, **1863**, 1423-1432.

207. Boutant, M., Kulkarni, S.S., Joffraud, M., Ratajczak, J., Valera-Alberni, M., Combe, R., Zorzano, A. and Canto, C. (2017) Mfn2 is critical for brown adipose tissue thermogenic function. *EMBO J*, **36**, 1543-1558.
208. Bulankina, A.V., Deggerich, A., Wenzel, D., Mutenda, K., Wittmann, J.G., Rudolph, M.G., Burger, K.N. and Honing, S. (2009) TIP47 functions in the biogenesis of lipid droplets. *J Cell Biol*, **185**, 641-655.
209. Copic, A., Antoine-Bally, S., Gimenez-Andres, M., La Torre Garay, C., Antonny, B., Manni, M.M., Pagnotta, S., Guihot, J. and Jackson, C.L. (2018) A giant amphipathic helix from a perilipin that is adapted for coating lipid droplets. *Nat Commun*, **9**, 1332.
210. Cartwright, B.R., Binns, D.D., Hilton, C.L., Han, S., Gao, Q. and Goodman, J.M. (2015) Seipin performs dissectible functions in promoting lipid droplet biogenesis and regulating droplet morphology. *Mol Biol Cell*, **26**, 726-739.
211. Pagac, M., Cooper, D.E., Qi, Y., Lukmantara, I.E., Mak, H.Y., Wu, Z., Tian, Y., Liu, Z., Lei, M., Du, X. *et al.* (2016) SEIPIN Regulates Lipid Droplet Expansion and Adipocyte Development by Modulating the Activity of Glycerol-3-phosphate Acyltransferase. *Cell Rep*, **17**, 1546-1559.
212. Wang, H., Becuwe, M., Housden, B.E., Chitraju, C., Porras, A.J., Graham, M.M., Liu, X.N., Thiam, A.R., Savage, D.B., Agarwal, A.K. *et al.* (2016) Seipin is required for converting nascent to mature lipid droplets. *Elife*, **5**.
213. Puri, V., Konda, S., Ranjit, S., Aouadi, M., Chawla, A., Chouinard, M., Chakladar, A. and Czech, M.P. (2007) Fat-specific protein 27, a novel lipid droplet protein that enhances triglyceride storage. *J Biol Chem*, **282**, 34213-34218.
214. Puri, V., Ranjit, S., Konda, S., Nicoloro, S.M., Straubhaar, J., Chawla, A., Chouinard, M., Lin, C., Burkart, A., Corvera, S. *et al.* (2008) Cidea is associated with lipid droplets and insulin sensitivity in humans. *Proc Natl Acad Sci U S A*, **105**, 7833-7838.
215. Xu, W., Wu, L., Yu, M., Chen, F.J., Arshad, M., Xia, X., Ren, H., Yu, J., Xu, L., Xu, D. *et al.* (2016) Differential Roles of Cell Death-inducing DNA Fragmentation Factor-alpha-like Effector (CIDE) Proteins in Promoting Lipid Droplet Fusion and Growth in Subpopulations of Hepatocytes. *J Biol Chem*, **291**, 4282-4293.
216. Ye, J., Li, J.Z., Liu, Y., Li, X., Yang, T., Ma, X., Li, Q., Yao, Z. and Li, P. (2009) Cideb, an ER- and lipid droplet-associated protein, mediates VLDL lipidation and maturation by interacting with apolipoprotein B. *Cell Metab*, **9**, 177-190.
217. Chen, F.J., Yin, Y., Chua, B.T. and Li, P. (2020) CIDE family proteins control lipid homeostasis and the development of metabolic diseases. *Traffic*, **21**, 94-105.
218. Grahn, T.H., Zhang, Y., Lee, M.J., Sommer, A.G., Mostoslavsky, G., Fried, S.K., Greenberg, A.S. and Puri, V. (2013) FSP27 and PLIN1 interaction promotes the formation of large lipid droplets in human adipocytes. *Biochem Biophys Res Commun*, **432**, 296-301.
219. Grahn, T.H., Kaur, R., Yin, J., Schweiger, M., Sharma, V.M., Lee, M.J., Ido, Y., Smas, C.M., Zechner, R., Lass, A. *et al.* (2014) Fat-specific protein 27 (FSP27) interacts with adipose triglyceride lipase (ATGL) to regulate lipolysis and insulin sensitivity in human adipocytes. *J Biol Chem*, **289**, 12029-12039.
220. Singh, M., Kaur, R., Lee, M.J., Pickering, R.T., Sharma, V.M., Puri, V. and Kandror, K.V. (2014) Fat-specific protein 27 inhibits lipolysis by facilitating the inhibitory effect of transcription factor Egr1 on transcription of adipose triglyceride lipase. *J Biol Chem*, **289**, 14481-14487.
221. Gross, D.A., Snapp, E.L. and Silver, D.L. (2010) Structural insights into triglyceride storage mediated by fat storage-inducing transmembrane (FIT) protein 2. *PLoS One*, **5**, e10796.
222. Kadereit, B., Kumar, P., Wang, W.J., Miranda, D., Snapp, E.L., Severina, N., Torregroza, I., Evans, T. and Silver, D.L. (2008) Evolutionarily conserved gene family important for fat storage. *Proc Natl Acad Sci U S A*, **105**, 94-99.
223. Becuwe, M., Bond, L.M., Pinto, A.F.M., Boland, S., Mejhert, N., Elliott, S.D., Cicconet, M., Graham, M.M., Liu, X.N., Ilkayeva, O. *et al.* (2020) FIT2 is an acyl-coenzyme A diphosphatase crucial for endoplasmic reticulum homeostasis. *J Cell Biol*, **219**.

224. Hayes, M., Choudhary, V., Ojha, N., Shin, J.J., Han, G.S., Carman, G.M., Loewen, C.J., Prinz, W.A. and Levine, T. (2017) Fat storage-inducing transmembrane (FIT or FITM) proteins are related to lipid phosphatase/phosphotransferase enzymes. *Microb Cell*, **5**, 88-103.
225. Mashek, D.G., Li, L.O. and Coleman, R.A. (2007) Long-chain acyl-CoA synthetases and fatty acid channeling. *Future Lipidol*, **2**, 465-476.
226. Fujimoto, Y., Itabe, H., Kinoshita, T., Homma, K.J., Onoduka, J., Mori, M., Yamaguchi, S., Makita, M., Higashi, Y., Yamashita, A. *et al.* (2007) Involvement of ACSL in local synthesis of neutral lipids in cytoplasmic lipid droplets in human hepatocyte HuH7. *J Lipid Res*, **48**, 1280-1292.
227. Jung, H.S., Shimizu-Albergine, M., Shen, X., Kramer, F., Shao, D., Vivekanandan-Giri, A., Pennathur, S., Tian, R., Kanter, J.E. and Bornfeldt, K.E. (2020) TNF-alpha induces acyl-CoA synthetase 3 to promote lipid droplet formation in human endothelial cells. *J Lipid Res*, **61**, 33-44.
228. Poppelreuther, M., Sander, S., Minden, F., Dietz, M.S., Exner, T., Du, C., Zhang, I., Ehehalt, F., Knuppel, L., Domschke, S. *et al.* (2018) The metabolic capacity of lipid droplet localized acyl-CoA synthetase 3 is not sufficient to support local triglyceride synthesis independent of the endoplasmic reticulum in A431 cells. *Biochim Biophys Acta Mol Cell Biol Lipids*, **1863**, 614-624.
229. Fujimoto, Y., Itabe, H., Sakai, J., Makita, M., Noda, J., Mori, M., Higashi, Y., Kojima, S. and Takano, T. (2004) Identification of major proteins in the lipid droplet-enriched fraction isolated from the human hepatocyte cell line HuH7. *Biochim Biophys Acta*, **1644**, 47-59.
230. Poppelreuther, M., Rudolph, B., Du, C., Grossmann, R., Becker, M., Thiele, C., Ehehalt, R. and Fullekrug, J. (2012) The N-terminal region of acyl-CoA synthetase 3 is essential for both the localization on lipid droplets and the function in fatty acid uptake. *J Lipid Res*, **53**, 888-900.
231. Kimura, H., Arasaki, K., Ohsaki, Y., Fujimoto, T., Ohtomo, T., Yamada, J. and Tagaya, M. (2018) Syntaxin 17 promotes lipid droplet formation by regulating the distribution of acyl-CoA synthetase 3. *J Lipid Res*, **59**, 805-819.
232. Grissa, I., Vergnaud, G. and Pourcel, C. (2007) The CRISPRdb database and tools to display CRISPRs and to generate dictionaries of spacers and repeats. *BMC Bioinformatics*, **8**, 172.
233. Jansen, R., Embden, J.D., Gaastra, W. and Schouls, L.M. (2002) Identification of genes that are associated with DNA repeats in prokaryotes. *Mol Microbiol*, **43**, 1565-1575.
234. Bolotin, A., Quinquis, B., Sorokin, A. and Ehrlich, S.D. (2005) Clustered regularly interspaced short palindrome repeats (CRISPRs) have spacers of extrachromosomal origin. *Microbiology (Reading)*, **151**, 2551-2561.
235. Mojica, F.J., Diez-Villasenor, C., Garcia-Martinez, J. and Soria, E. (2005) Intervening sequences of regularly spaced prokaryotic repeats derive from foreign genetic elements. *J Mol Evol*, **60**, 174-182.
236. Pourcel, C., Salvignol, G. and Vergnaud, G. (2005) CRISPR elements in Yersinia pestis acquire new repeats by preferential uptake of bacteriophage DNA, and provide additional tools for evolutionary studies. *Microbiology (Reading)*, **151**, 653-663.
237. Barrangou, R., Fremaux, C., Deveau, H., Richards, M., Boyaval, P., Moineau, S., Romero, D.A. and Horvath, P. (2007) CRISPR provides acquired resistance against viruses in prokaryotes. *Science*, **315**, 1709-1712.
238. Cong, L., Ran, F.A., Cox, D., Lin, S., Barretto, R., Habib, N., Hsu, P.D., Wu, X., Jiang, W., Marraffini, L.A. *et al.* (2013) Multiplex genome engineering using CRISPR/Cas systems. *Science*, **339**, 819-823.
239. Jinek, M., Chylinski, K., Fonfara, I., Hauer, M., Doudna, J.A. and Charpentier, E. (2012) A programmable dual-RNA-guided DNA endonuclease in adaptive bacterial immunity. *Science*, **337**, 816-821.
240. Jinek, M., East, A., Cheng, A., Lin, S., Ma, E. and Doudna, J. (2013) RNA-programmed genome editing in human cells. *Elife*, **2**, e00471.

241. Mali, P., Yang, L., Esvelt, K.M., Aach, J., Guell, M., DiCarlo, J.E., Norville, J.E. and Church, G.M. (2013) RNA-guided human genome engineering via Cas9. *Science*, **339**, 823-826.
242. Qi, L.S., Larson, M.H., Gilbert, L.A., Doudna, J.A., Weissman, J.S., Arkin, A.P. and Lim, W.A. (2013) Repurposing CRISPR as an RNA-guided platform for sequence-specific control of gene expression. *Cell*, **152**, 1173-1183.
243. Ishino, Y., Shinagawa, H., Makino, K., Amemura, M. and Nakata, A. (1987) Nucleotide sequence of the iap gene, responsible for alkaline phosphatase isozyme conversion in Escherichia coli, and identification of the gene product. *J Bacteriol*, **169**, 5429-5433.
244. Amitai, G. and Sorek, R. (2016) CRISPR-Cas adaptation: insights into the mechanism of action. *Nat Rev Microbiol*, **14**, 67-76.
245. Hille, F. and Charpentier, E. (2016) CRISPR-Cas: biology, mechanisms and relevance. *Philos Trans R Soc Lond B Biol Sci*, **371**.
246. Makarova, K.S., Haft, D.H., Barrangou, R., Brouns, S.J., Charpentier, E., Horvath, P., Moineau, S., Mojica, F.J., Wolf, Y.I., Yakunin, A.F. *et al.* (2011) Evolution and classification of the CRISPR-Cas systems. *Nat Rev Microbiol*, **9**, 467-477.
247. Makarova, K.S., Wolf, Y.I., Alkhnbashi, O.S., Costa, F., Shah, S.A., Saunders, S.J., Barrangou, R., Brouns, S.J., Charpentier, E., Haft, D.H. *et al.* (2015) An updated evolutionary classification of CRISPR-Cas systems. *Nat Rev Microbiol*, **13**, 722-736.
248. Makarova, K.S., Wolf, Y.I., Iranzo, J., Shmakov, S.A., Alkhnbashi, O.S., Brouns, S.J.J., Charpentier, E., Cheng, D., Haft, D.H., Horvath, P. *et al.* (2020) Evolutionary classification of CRISPR-Cas systems: a burst of class 2 and derived variants. *Nat Rev Microbiol*, **18**, 67-83.
249. Wang, J., Li, J., Zhao, H., Sheng, G., Wang, M., Yin, M. and Wang, Y. (2015) Structural and Mechanistic Basis of PAM-Dependent Spacer Acquisition in CRISPR-Cas Systems. *Cell*, **163**, 840-853.
250. Yosef, I., Goren, M.G. and Qimron, U. (2012) Proteins and DNA elements essential for the CRISPR adaptation process in Escherichia coli. *Nucleic Acids Res*, **40**, 5569-5576.
251. Horvath, P., Romero, D.A., Coute-Monvoisin, A.C., Richards, M., Deveau, H., Moineau, S., Boyaval, P., Fremaux, C. and Barrangou, R. (2008) Diversity, activity, and evolution of CRISPR loci in Streptococcus thermophilus. *J Bacteriol*, **190**, 1401-1412.
252. Mojica, F.J.M., Diez-Villasenor, C., Garcia-Martinez, J. and Almendros, C. (2009) Short motif sequences determine the targets of the prokaryotic CRISPR defence system. *Microbiology (Reading)*, **155**, 733-740.
253. Nunez, J.K., Lee, A.S., Engelman, A. and Doudna, J.A. (2015) Integrase-mediated spacer acquisition during CRISPR-Cas adaptive immunity. *Nature*, **519**, 193-198.
254. Deltcheva, E., Chylinski, K., Sharma, C.M., Gonzales, K., Chao, Y., Pirzada, Z.A., Eckert, M.R., Vogel, J. and Charpentier, E. (2011) CRISPR RNA maturation by trans-encoded small RNA and host factor RNase III. *Nature*, **471**, 602-607.
255. Shmakov, S., Abudayyeh, O.O., Makarova, K.S., Wolf, Y.I., Gootenberg, J.S., Semenova, E., Minakhin, L., Joung, J., Konermann, S., Severinov, K. *et al.* (2015) Discovery and Functional Characterization of Diverse Class 2 CRISPR-Cas Systems. *Mol Cell*, **60**, 385-397.
256. Zetsche, B., Gootenberg, J.S., Abudayyeh, O.O., Slaymaker, I.M., Makarova, K.S., Essletzbichler, P., Volz, S.E., Joung, J., van der Oost, J., Regev, A. *et al.* (2015) Cpf1 is a single RNA-guided endonuclease of a class 2 CRISPR-Cas system. *Cell*, **163**, 759-771.
257. Carte, J., Wang, R., Li, H., Terns, R.M. and Terns, M.P. (2008) Cas6 is an endoribonuclease that generates guide RNAs for invader defense in prokaryotes. *Genes Dev*, **22**, 3489-3496.
258. Garneau, J.E., Dupuis, M.E., Villion, M., Romero, D.A., Barrangou, R., Boyaval, P., Fremaux, C., Horvath, P., Magadan, A.H. and Moineau, S. (2010) The CRISPR/Cas bacterial immune system cleaves bacteriophage and plasmid DNA. *Nature*, **468**, 67-71.
259. Makarova, K.S., Grishin, N.V., Shabalina, S.A., Wolf, Y.I. and Koonin, E.V. (2006) A putative RNA-interference-based immune system in prokaryotes: computational

analysis of the predicted enzymatic machinery, functional analogies with eukaryotic RNAi, and hypothetical mechanisms of action. *Biol Direct*, **1**, 7.
260. Marraffini, L.A. and Sontheimer, E.J. (2008) CRISPR interference limits horizontal gene transfer in staphylococci by targeting DNA. *Science*, **322**, 1843-1845.
261. Plagens, A., Richter, H., Charpentier, E. and Randau, L. (2015) DNA and RNA interference mechanisms by CRISPR-Cas surveillance complexes. *FEMS Microbiol Rev*, **39**, 442-463.
262. Chen, J.S., Ma, E., Harrington, L.B., Da Costa, M., Tian, X., Palefsky, J.M. and Doudna, J.A. (2018) CRISPR-Cas12a target binding unleashes indiscriminate single-stranded DNase activity. *Science*, **360**, 436-439.
263. Brouns, S.J., Jore, M.M., Lundgren, M., Westra, E.R., Slijkhuis, R.J., Snijders, A.P., Dickman, M.J., Makarova, K.S., Koonin, E.V. and van der Oost, J. (2008) Small CRISPR RNAs guide antiviral defense in prokaryotes. *Science*, **321**, 960-964.
264. Haft, D.H., Selengut, J., Mongodin, E.F. and Nelson, K.E. (2005) A guild of 45 CRISPR-associated (Cas) protein families and multiple CRISPR/Cas subtypes exist in prokaryotic genomes. *PLoS Comput Biol*, **1**, e60.
265. Hale, C.R., Zhao, P., Olson, S., Duff, M.O., Graveley, B.R., Wells, L., Terns, R.M. and Terns, M.P. (2009) RNA-guided RNA cleavage by a CRISPR RNA-Cas protein complex. *Cell*, **139**, 945-956.
266. Abudayyeh, O.O., Gootenberg, J.S., Essletzbichler, P., Han, S., Joung, J., Belanto, J.J., Verdine, V., Cox, D.B.T., Kellner, M.J., Regev, A. *et al.* (2017) RNA targeting with CRISPR-Cas13. *Nature*, **550**, 280-284.
267. Gao, P., Yang, H., Rajashankar, K.R., Huang, Z. and Patel, D.J. (2016) Type V CRISPR-Cas Cpf1 endonuclease employs a unique mechanism for crRNA-mediated target DNA recognition. *Cell Res*, **26**, 901-913.
268. Jiang, W., Bikard, D., Cox, D., Zhang, F. and Marraffini, L.A. (2013) RNA-guided editing of bacterial genomes using CRISPR-Cas systems. *Nat Biotechnol*, **31**, 233-239.
269. Kim, D., Kim, J., Hur, J.K., Been, K.W., Yoon, S.H. and Kim, J.S. (2016) Genome-wide analysis reveals specificities of Cpf1 endonucleases in human cells. *Nat Biotechnol*, **34**, 863-868.
270. Kim, H., Kim, S.T., Ryu, J., Kang, B.C., Kim, J.S. and Kim, S.G. (2017) CRISPR/Cpf1-mediated DNA-free plant genome editing. *Nat Commun*, **8**, 14406.
271. Moreno-Mateos, M.A., Fernandez, J.P., Rouet, R., Vejnar, C.E., Lane, M.A., Mis, E., Khokha, M.K., Doudna, J.A. and Giraldez, A.J. (2017) CRISPR-Cpf1 mediates efficient homology-directed repair and temperature-controlled genome editing. *Nat Commun*, **8**, 2024.
272. Tang, X., Lowder, L.G., Zhang, T., Malzahn, A.A., Zheng, X., Voytas, D.F., Zhong, Z., Chen, Y., Ren, Q., Li, Q. *et al.* (2017) A CRISPR-Cpf1 system for efficient genome editing and transcriptional repression in plants. *Nat Plants*, **3**, 17103.
273. Zetsche, B., Heidenreich, M., Mohanraju, P., Fedorova, I., Kneppers, J., DeGennaro, E.M., Winblad, N., Choudhury, S.R., Abudayyeh, O.O., Gootenberg, J.S. *et al.* (2017) Multiplex gene editing by CRISPR-Cpf1 using a single crRNA array. *Nat Biotechnol*, **35**, 31-34.
274. Platt, R.J., Chen, S., Zhou, Y., Yim, M.J., Swiech, L., Kempton, H.R., Dahlman, J.E., Parnas, O., Eisenhaure, T.M., Jovanovic, M. *et al.* (2014) CRISPR-Cas9 knockin mice for genome editing and cancer modeling. *Cell*, **159**, 440-455.
275. Sternberg, S.H., Redding, S., Jinek, M., Greene, E.C. and Doudna, J.A. (2014) DNA interrogation by the CRISPR RNA-guided endonuclease Cas9. *Nature*, **507**, 62-67.
276. Pawelczak, K.S., Gavande, N.S., VanderVere-Carozza, P.S. and Turchi, J.J. (2018) Modulating DNA Repair Pathways to Improve Precision Genome Engineering. *ACS Chem Biol*, **13**, 389-396.
277. Chang, H.H.Y., Pannunzio, N.R., Adachi, N. and Lieber, M.R. (2017) Non-homologous DNA end joining and alternative pathways to double-strand break repair. *Nat Rev Mol Cell Biol*, **18**, 495-506.
278. Fellmann, C., Gowen, B.G., Lin, P.C., Doudna, J.A. and Corn, J.E. (2017) Cornerstones of CRISPR-Cas in drug discovery and therapy. *Nat Rev Drug Discov*, **16**, 89-100.

279. Knott, G.J. and Doudna, J.A. (2018) CRISPR-Cas guides the future of genetic engineering. *Science*, **361**, 866-869.
280. Gilbert, L.A., Horlbeck, M.A., Adamson, B., Villalta, J.E., Chen, Y., Whitehead, E.H., Guimaraes, C., Panning, B., Ploegh, H.L., Bassik, M.C. *et al.* (2014) Genome-Scale CRISPR-Mediated Control of Gene Repression and Activation. *Cell*, **159**, 647-661.
281. Kasap, C., Elemento, O. and Kapoor, T.M. (2014) DrugTargetSeqR: a genomics- and CRISPR-Cas9-based method to analyze drug targets. *Nat Chem Biol*, **10**, 626-628.
282. Shalem, O., Sanjana, N.E., Hartenian, E., Shi, X., Scott, D.A., Mikkelson, T., Heckl, D., Ebert, B.L., Root, D.E., Doench, J.G. *et al.* (2014) Genome-scale CRISPR-Cas9 knockout screening in human cells. *Science*, **343**, 84-87.
283. Shi, J., Wang, E., Milazzo, J.P., Wang, Z., Kinney, J.B. and Vakoc, C.R. (2015) Discovery of cancer drug targets by CRISPR-Cas9 screening of protein domains. *Nat Biotechnol*, **33**, 661-667.
284. Gootenberg, J.S., Abudayyeh, O.O., Kellner, M.J., Joung, J., Collins, J.J. and Zhang, F. (2018) Multiplexed and portable nucleic acid detection platform with Cas13, Cas12a, and Csm6. *Science*, **360**, 439-444.
285. Gootenberg, J.S., Abudayyeh, O.O., Lee, J.W., Essletzbichler, P., Dy, A.J., Joung, J., Verdine, V., Donghia, N., Daringer, N.M., Freije, C.A. *et al.* (2017) Nucleic acid detection with CRISPR-Cas13a/C2c2. *Science*, **356**, 438-442.
286. Myhrvold, C., Freije, C.A., Gootenberg, J.S., Abudayyeh, O.O., Metsky, H.C., Durbin, A.F., Kellner, M.J., Tan, A.L., Paul, L.M., Parham, L.A. *et al.* (2018) Field-deployable viral diagnostics using CRISPR-Cas13. *Science*, **360**, 444-448.
287. Gaj, T., Ojala, D.S., Ekman, F.K., Byrne, L.C., Limsirichai, P. and Schaffer, D.V. (2017) In vivo genome editing improves motor function and extends survival in a mouse model of ALS. *Sci Adv*, **3**, eaar3952.
288. Ma, H., Marti-Gutierrez, N., Park, S.W., Wu, J., Lee, Y., Suzuki, K., Koski, A., Ji, D., Hayama, T., Ahmed, R. *et al.* (2017) Correction of a pathogenic gene mutation in human embryos. *Nature*, **548**, 413-419.
289. Staahl, B.T., Benekareddy, M., Coulon-Bainier, C., Banfal, A.A., Floor, S.N., Sabo, J.K., Urnes, C., Munares, G.A., Ghosh, A. and Doudna, J.A. (2017) Efficient genome editing in the mouse brain by local delivery of engineered Cas9 ribonucleoprotein complexes. *Nat Biotechnol*, **35**, 431-434.
290. Zhang, Y., Long, C., Li, H., McAnally, J.R., Baskin, K.K., Shelton, J.M., Bassel-Duby, R. and Olson, E.N. (2017) CRISPR-Cpf1 correction of muscular dystrophy mutations in human cardiomyocytes and mice. *Sci Adv*, **3**, e1602814.
291. Zuo, E., Huo, X., Yao, X., Hu, X., Sun, Y., Yin, J., He, B., Wang, X., Shi, L., Ping, J. *et al.* (2017) CRISPR/Cas9-mediated targeted chromosome elimination. *Genome Biol*, **18**, 224.
292. Long, C., Li, H., Tiburcy, M., Rodriguez-Caycedo, C., Kyrychenko, V., Zhou, H., Zhang, Y., Min, Y.L., Shelton, J.M., Mammen, P.P.A. *et al.* (2018) Correction of diverse muscular dystrophy mutations in human engineered heart muscle by single-site genome editing. *Sci Adv*, **4**, eaap9004.
293. Behrends, C., Sowa, M.E., Gygi, S.P. and Harper, J.W. (2010) Network organization of the human autophagy system. *Nature*, **466**, 68-76.
294. Popovic, D., Akutsu, M., Novak, I., Harper, J.W., Behrends, C. and Dikic, I. (2012) Rab GTPase-activating proteins in autophagy: regulation of endocytic and autophagy pathways by direct binding to human ATG8 modifiers. *Mol Cell Biol*, **32**, 1733-1744.
295. Kuma, A., Matsui, M. and Mizushima, N. (2007) LC3, an autophagosome marker, can be incorporated into protein aggregates independent of autophagy: caution in the interpretation of LC3 localization. *Autophagy*, **3**, 323-328.
296. Buckingham, E.M., Carpenter, J.E., Jackson, W. and Grose, C. (2014) Nuclear LC3-positive puncta in stressed cells do not represent autophagosomes. *Biotechniques*, **57**, 241-244.
297. Lee, Y.K., Jun, Y.W., Choi, H.E., Huh, Y.H., Kaang, B.K., Jang, D.J. and Lee, J.A. (2017) Development of LC3/GABARAP sensors containing a LIR and a hydrophobic domain to monitor autophagy. *EMBO J*, **36**, 1100-1116.

298. Stolz, A., Putyrski, M., Kutle, I., Huber, J., Wang, C., Major, V., Sidhu, S.S., Youle, R.J., Rogov, V.V., Dotsch, V. *et al.* (2017) Fluorescence-based ATG8 sensors monitor localization and function of LC3/GABARAP proteins. *EMBO J*, **36**, 549-564.
299. Culley, S., Tosheva, K.L., Matos Pereira, P. and Henriques, R. (2018) SRRF: Universal live-cell super-resolution microscopy. *Int J Biochem Cell Biol*, **101**, 74-79.
300. Symington, L.S. and Gautier, J. (2011) Double-strand break end resection and repair pathway choice. *Annu Rev Genet*, **45**, 247-271.
301. Bai, H., Inoue, J., Kawano, T. and Inazawa, J. (2012) A transcriptional variant of the LC3A gene is involved in autophagy and frequently inactivated in human cancers. *Oncogene*, **31**, 4397-4408.
302. Martens, S. and Fracchiolla, D. (2020) Activation and targeting of ATG8 protein lipidation. *Cell Discov*, **6**, 23.
303. Castellanos-Serra, L., Ramos, Y. and Huerta, V. (2005) An in-gel digestion procedure that facilitates the identification of highly hydrophobic proteins by electrospray ionization-mass spectrometry analysis. *Proteomics*, **5**, 2729-2738.
304. Shevchenko, A., Tomas, H., Havlis, J., Olsen, J.V. and Mann, M. (2006) In-gel digestion for mass spectrometric characterization of proteins and proteomes. *Nat Protoc*, **1**, 2856-2860.
305. Ewing, R.M., Chu, P., Elisma, F., Li, H., Taylor, P., Climie, S., McBroom-Cerajewski, L., Robinson, M.D., O'Connor, L., Li, M. *et al.* (2007) Large-scale mapping of human protein-protein interactions by mass spectrometry. *Mol Syst Biol*, **3**, 89.
306. Rolland, T., Tasan, M., Charloteaux, B., Pevzner, S.J., Zhong, Q., Sahni, N., Yi, S., Lemmens, I., Fontanillo, C., Mosca, R. *et al.* (2014) A proteome-scale map of the human interactome network. *Cell*, **159**, 1212-1226.
307. Vinayagam, A., Stelzl, U., Foulle, R., Plassmann, S., Zenkner, M., Timm, J., Assmus, H.E., Andrade-Navarro, M.A. and Wanker, E.E. (2011) A directed protein interaction network for investigating intracellular signal transduction. *Sci Signal*, **4**, rs8.
308. Zellner, S., Schifferer, M. and Behrends, C. (2021) Systematically defining selective autophagy receptor-specific cargo using autophagosome content profiling. *Mol Cell*, **81**, 1337-1354 e1338.
309. Liang, J.R., Lingeman, E., Ahmed, S. and Corn, J.E. (2018) Atlastins remodel the endoplasmic reticulum for selective autophagy. *J Cell Biol*, **217**, 3354-3367.
310. Cabrera, S., Fernandez, A.F., Marino, G., Aguirre, A., Suarez, M.F., Espanol, Y., Vega, J.A., Laura, R., Fueyo, A., Fernandez-Garcia, M.S. *et al.* (2013) ATG4B/autophagin-1 regulates intestinal homeostasis and protects mice from experimental colitis. *Autophagy*, **9**, 1188-1200.
311. Lassen, K.G., Kuballa, P., Conway, K.L., Patel, K.K., Becker, C.E., Peloquin, J.M., Villablanca, E.J., Norman, J.M., Liu, T.C., Heath, R.J. *et al.* (2014) Atg16L1 T300A variant decreases selective autophagy resulting in altered cytokine signaling and decreased antibacterial defense. *Proc Natl Acad Sci U S A*, **111**, 7741-7746.
312. Mareninova, O.A., Hermann, K., French, S.W., O'Konski, M.S., Pandol, S.J., Webster, P., Erickson, A.H., Katunuma, N., Gorelick, F.S., Gukovsky, I. *et al.* (2009) Impaired autophagic flux mediates acinar cell vacuole formation and trypsinogen activation in rodent models of acute pancreatitis. *J Clin Invest*, **119**, 3340-3355.
313. Herhaus, L., Bhaskara, R.M., Lystad, A.H., Gestal-Mato, U., Covarrubias-Pinto, A., Bonn, F., Simonsen, A., Hummer, G. and Dikic, I. (2020) TBK1-mediated phosphorylation of LC3C and GABARAP-L2 controls autophagosome shedding by ATG4 protease. *EMBO Rep*, **21**, e48317.
314. Lystad, A.H., Carlsson, S.R., de la Ballina, L.R., Kauffman, K.J., Nag, S., Yoshimori, T., Melia, T.J. and Simonsen, A. (2019) Distinct functions of ATG16L1 isoforms in membrane binding and LC3B lipidation in autophagy-related processes. *Nat Cell Biol*, **21**, 372-383.
315. Wirth, M., Zhang, W., Razi, M., Nyoni, L., Joshi, D., O'Reilly, N., Johansen, T., Tooze, S.A. and Mouilleron, S. (2019) Molecular determinants regulating selective binding of autophagy adapters and receptors to ATG8 proteins. *Nat Commun*, **10**, 2055.

316. Hsu, S.H., Schacter, B.Z., Delaney, N.L., Miller, T.B., McKusick, V.A., Kennett, R.H., Bodmer, J.G., Young, D. and Bodmer, W.F. (1976) Genetic characteristics of the HeLa cell. *Science*, **191**, 392-394.
317. Landry, J.J., Pyl, P.T., Rausch, T., Zichner, T., Tekkedil, M.M., Stutz, A.M., Jauch, A., Aiyar, R.S., Pau, G., Delhomme, N. *et al.* (2013) The genomic and transcriptomic landscape of a HeLa cell line. *G3 (Bethesda)*, **3**, 1213-1224.
318. Macville, M., Schrock, E., Padilla-Nash, H., Keck, C., Ghadimi, B.M., Zimonjic, D., Popescu, N. and Ried, T. (1999) Comprehensive and definitive molecular cytogenetic characterization of HeLa cells by spectral karyotyping. *Cancer Res*, **59**, 141-150.
319. Hara, T., Nakamura, K., Matsui, M., Yamamoto, A., Nakahara, Y., Suzuki-Migishima, R., Yokoyama, M., Mishima, K., Saito, I., Okano, H. *et al.* (2006) Suppression of basal autophagy in neural cells causes neurodegenerative disease in mice. *Nature*, **441**, 885-889.
320. Qu, X., Yu, J., Bhagat, G., Furuya, N., Hibshoosh, H., Troxel, A., Rosen, J., Eskelinen, E.L., Mizushima, N., Ohsumi, Y. *et al.* (2003) Promotion of tumorigenesis by heterozygous disruption of the beclin 1 autophagy gene. *J Clin Invest*, **112**, 1809-1820.
321. Qu, X., Zou, Z., Sun, Q., Luby-Phelps, K., Cheng, P., Hogan, R.N., Gilpin, C. and Levine, B. (2007) Autophagy gene-dependent clearance of apoptotic cells during embryonic development. *Cell*, **128**, 931-946.
322. Singh, R., Xiang, Y., Wang, Y., Baikati, K., Cuervo, A.M., Luu, Y.K., Tang, Y., Pessin, J.E., Schwartz, G.J. and Czaja, M.J. (2009) Autophagy regulates adipose mass and differentiation in mice. *J Clin Invest*, **119**, 3329-3339.
323. Taneike, M., Yamaguchi, O., Nakai, A., Hikoso, S., Takeda, T., Mizote, I., Oka, T., Tamai, T., Oyabu, J., Murakawa, T. *et al.* (2010) Inhibition of autophagy in the heart induces age-related cardiomyopathy. *Autophagy*, **6**, 600-606.
324. Cadwell, K. and Debnath, J. (2018) Beyond self-eating: The control of nonautophagic functions and signaling pathways by autophagy-related proteins. *J Cell Biol*, **217**, 813-822.
325. Clevers, H.C. and Bevins, C.L. (2013) Paneth cells: maestros of the small intestinal crypts. *Annu Rev Physiol*, **75**, 289-311.
326. Bel, S., Pendse, M., Wang, Y., Li, Y., Ruhn, K.A., Hassell, B., Leal, T., Winter, S.E., Xavier, R.J. and Hooper, L.V. (2017) Paneth cells secrete lysozyme via secretory autophagy during bacterial infection of the intestine. *Science*, **357**, 1047-1052.
327. DeSelm, C.J., Miller, B.C., Zou, W., Beatty, W.L., van Meel, E., Takahata, Y., Klumperman, J., Tooze, S.A., Teitelbaum, S.L. and Virgin, H.W. (2011) Autophagy proteins regulate the secretory component of osteoclastic bone resorption. *Dev Cell*, **21**, 966-974.
328. Roy, S., Leidal, A.M., Ye, J., Ronen, S.M. and Debnath, J. (2017) Autophagy-Dependent Shuttling of TBC1D5 Controls Plasma Membrane Translocation of GLUT1 and Glucose Uptake. *Mol Cell*, **67**, 84-95 e85.
329. Kimura, T., Jia, J., Kumar, S., Choi, S.W., Gu, Y., Mudd, M., Dupont, N., Jiang, S., Peters, R., Farzam, F. *et al.* (2017) Dedicated SNAREs and specialized TRIM cargo receptors mediate secretory autophagy. *EMBO J*, **36**, 42-60.
330. Biering, S.B., Choi, J., Halstrom, R.A., Brown, H.M., Beatty, W.L., Lee, S., McCune, B.T., Dominici, E., Williams, L.E., Orchard, R.C. *et al.* (2017) Viral Replication Complexes Are Targeted by LC3-Guided Interferon-Inducible GTPases. *Cell Host Microbe*, **22**, 74-85 e77.
331. Selleck, E.M., Orchard, R.C., Lassen, K.G., Beatty, W.L., Xavier, R.J., Levine, B., Virgin, H.W. and Sibley, L.D. (2015) A Noncanonical Autophagy Pathway Restricts Toxoplasma gondii Growth in a Strain-Specific Manner in IFN-gamma-Activated Human Cells. *mBio*, **6**, e01157-01115.
332. Hou, P., Yang, K., Jia, P., Liu, L., Lin, Y., Li, Z., Li, J., Chen, S., Guo, S., Pan, J. *et al.* (2021) A novel selective autophagy receptor, CCDC50, delivers K63 polyubiquitination-activated RIG-I/MDA5 for degradation during viral infection. *Cell Res*, **31**, 62-79.

333. Nthiga, T.M., Kumar Shrestha, B., Sjottem, E., Bruun, J.A., Bowitz Larsen, K., Bhujabal, Z., Lamark, T. and Johansen, T. (2020) CALCOCO1 acts with VAMP-associated proteins to mediate ER-phagy. *EMBO J*, **39**, e103649.
334. Soudah, N., Padala, P., Hassouna, F., Kumar, M., Mashahreh, B., Lebedev, A.A., Isupov, M.N., Cohen-Kfir, E. and Wiener, R. (2019) An N-Terminal Extension to UBA5 Adenylation Domain Boosts UFM1 Activation: Isoform-Specific Differences in Ubiquitin-like Protein Activation. *J Mol Biol*, **431**, 463-478.
335. Banerjee, S., Kumar, M. and Wiener, R. (2020) Decrypting UFMylation: How Proteins Are Modified with UFM1. *Biomolecules*, **10**.
336. Hochstrasser, M. (2009) Origin and function of ubiquitin-like proteins. *Nature*, **458**, 422-429.

8. Abbreviations

ABC	Ammonium bicarbonate
ACN	Acetonitrile
ACS	Acyl-CoA synthetase
ACSL3	Long-chain-fatty-acid CoA ligase 3
AD	Adenylation domain
AIM	ATG8 family-interacting motif
APS	Ammonium peroxydisulphate
ATF6	Activating transcription factor 6
ATG	Autophagy-related
ATGL	Adipose triglyceride lipase
BafA1	Bafilomycin A1
bp	Base pairs
BSA	Bovine Serum Albumin
Btz	Bortezomib
C20orf116	Alternative name of DDRGK1
C53	Alternative name of CDK5RAP3
Cas	CRISPR associated protein
CDK5RAP3	CDK5 regulatory subunit-associated protein 3
CIDE	Cell death-inducing DNA fragmentation factor alpha (DFFA)-like effector
CMF	Crude microsomal fraction
CMV	Cytomegalovirus
CoA	Coenzyme A
CP	Core particle
(pre-)crRNA	(precursor) CRISPR RNA
CRISPR	Clustered regularly interspaced short palindromic repeats
DDRGK1	DDRGK domain-containing protein 1
DMEM	Dulbecco`s modified Eagle`s Medium
DMSO	Dimethyl sulfoxide
DSB	Double-strand break
DTT	Dithiothreitol

DUBs	Deubiquitinating enzymes
EBSS	Earle’s balanced salt solution
EDTA	Ethylenedinitrilotetraacetic acid
ER	Endoplasmic reticulum
ERAD	ER associated degradation
EtOH	Ethanol
FBS	Fetal Bovine Serum
FA	Formic acid
FIT	Fat inducing transcript
FSP27	Cell death activator CIDE-3; alternative name is CIDEC
g	Gravity
GABARAP	γ-aminobutyric acid receptor-associated protein
GABARAPL1/2	γ-aminobutyric acid receptor-associated protein-like 1/2
GAP	GTPase activating proteins
GATE16	Alternative name of GABARAPL2
GEF	Guanine nucleotide exchange factors
GO	Gene ontology
GST	Glutathione S-transferase
HA	Hemagglutinin
hATG8	Human ATG8 proteins
HDR	Homology directed repair
HEK cells	Human embryonic kidney cells
HeLa cells	Epithelial cells derived from cervical cancer
HOPS	Homotypic fusion and protein sorting
HSL	Hormone sensitive lipase
IAA	Iodoacetamide
IP	Immunoprecipitation
IRE1	Inositol-requiring enzyme 1
LAP	LC3-associated phagocytosis
LB	Lysogeny broth
LD	Lipid droplet
LDS	LIR-docking site

LIR	LC3-interacting region
LSM	Laser scanning microscopy
LZAP	Alternative name of CDK5RAP3
(MAP1)LC3A/B/C	Microtubule-associated protein 1A/1B light chain 3 A/B/C
MGL	Monoglyceride lipase
MRN	MRE11-RAD50-NBS1
MS	Mass spectrometry
NHEJ	Non-homologous end joining
NP-40	Igepal
OD	Optical density
o/n	Overnight
Opti-MEM	Optimal modified Eagle`s Medium
ORF	Open reading frame
p62	Sequestosome-1 (alternative name: SQSTM1)
PAM	Proto-spacer adjacent motifs
PAS	Phagophore assembly site
PBS	Phosphate buffered saline
PCR	Polymerase chain reaction
PDB	Protein data bank
PE	Phosphatidylethanolamine
PERK	PKR-like ER protein kinase
PFA	Paraformaldehyde
PLEKHM1	Pleckstrin homology domain containing family M member 1
PLIN	Perilipin
PMF	post mitochondrial fraction
PMSF	Phenylmethylsulfonyl fluoride
PNS	Post nuclear fraction
PVM	Parasitophorous vacuole membrane
RP	Regulatory particle
RPL26	60S ribosomal protein L26
rpm	Rotations per minute
RT	Room temperature

SDS	Sodium dodecyl sulfate
SDS-PAGE	Sodium dodecyl sulfate polyacrylamide gel electrophoresis
sgRNA	Single guide RNA
SILAC	Stable-isotope labelling by amino acids in cell culture
siRNA	Small interfering RNA
SRRF	Super-resolution radial fluctuations imaging
TAG	Triacylglycerols
TCA	Trichloroacetic acid solution
TECPR2	Tectonin beta-propeller repeat-containing protein 2
TFA	Trifluoroacetic acid
tracrRNA	Transactivating crRNA
Ub	Ubiquitin
UBD	Ubiquitin binding domain
UBS	UFC1 binding sequence
Ubl	Ubiquitin-like modifier
UBA5	Ubiquitin-like modifier-activating enzyme 5
UDS	UIM-docking site
UFBP1	Alternative name of DDRGK1
UFC1	Ubiquitin-fold modifier-conjugating enzyme 1
UFL1	E3 UFM1-protein ligase 1
UFM1	Ubiquitin-like protein ubiquitin fold modifier 1
UFSP2	UFM1-specific protease 2
UIM	Ubiquitin-interacting motif
UIS	UFM1 interaction sequence
ULK1	Unc-51-like kinase 1
UPR	Unfolded protein response
UPS	Ubiquitin-proteasome system
WT	Wild type

9. Acknowledgments

Zum Abschluss ist es mir ein Anliegen, mich bei allen zu bedanken, die mich in dieser Zeit begleitet und unterstützt haben.

Mein besonderer Dank gilt Christian Behrends, der mir die Möglichkeit gegeben hat, meine Doktorarbeit in seiner Arbeitsgruppe durchzuführen. Er hat sich stets Zeit genommen, um mit mir über Ergebnisse, Methoden und Hypothesen zu diskutieren und neue Ideen zu entwickeln. Auch hat er eine eigenständige Arbeitsweise und die Umsetzung eigener Ideen gefördert. Außerdem bin ich sehr dankbar, dass Christian es mir ermöglich, hat an mehreren Konferenzen teilzunehmen, um meine Arbeit vorzustellen und meine Fähigkeiten durch die Teilnahme an Fortbildungen zu verbessern. Ein besonderer Abschnitt während meiner Promotion war der Umzug des Labors von Frankfurt nach München. Auch in dieser sehr stressigen Zeit habe ich immer Unterstützung von Christian bekommen. Ausdrücklich möchte ich mich für das mir entgegengebrachte Vertrauen bedanken, die Organisation des Labors mitgestalten zu dürfen.

Während meiner Promotion habe ich gemerkt, dass mich besonders der Rückhalt, die Hilfsbereitschaft und die kollegiale Atmosphäre innerhalb der Arbeitsgruppe angespornt und motiviert haben. Deshalb danke ich sehr herzlich den Mitgliedern meiner damaligen Arbeitsgruppe in Frankfurt: Jenny, Heide, Francois, Tihana, Mira, Daniela, Steffi und Sabine und meinen Arbeitskollegen in München: Alex, Julia, Susa, Vanessa, Karsten, Laura, Lukas, Hanna, Sophie und Debjani. Meine Kollegen hatten für mich immer ein offenes Ohr und neue Ideen: Der große Zusammenhalt und die Hilfsbereitschaft haben mir stets weitergeholfen, experimentelle Schwierigkeiten zu überwinden und Lösungen für Probleme zu finden.

Sehr herzlich gedankt sei allen Mitgliedern des „thirdfloor“ am BMC für den angenehmen Start am Institut, die Hilfsbereitschaft, die anregenden und hilfreichen Diskussionen über Methoden, die tollen Social-Events und die Freundschaften. Das gleiche gilt auch für die Mitgliedern des Instituts für Biochemie II in Frankfurt.

Ich bin sehr froh darüber, dass ich Teil des SFB1177 Autophagy Netzwerks sein durfte und möchte meinen Dank an die Sprecher, Koordinatoren und Mitglieder aussprechen. Besonders der persönliche Austausch auf den Retreats und Konferenzen mit den Mitgliedern des SFB1177 hat mir neuen Input und Motivation für meine Doktorarbeit gegeben.

Zudem gilt mein Dank allen Mitgliedern der Prüfungskommission für das Lesen und Bewerten meiner Arbeit.

Ich bin sehr dankbar für all die Freundschaften, die ich auch außerhalb meiner Arbeitsgruppe in Frankfurt und München knüpfen durfte. Dies gilt insbesondere für Mareike, Paula und Katrin, die meine Doktorarbeit gelesen und korrigiert haben.

Last but not least bin ich meiner Familie und meinen Freunden, die mich über die Jahre uneingeschränkt unterstützt, motiviert und an mich geglaubt haben, zu großem Dank verpflichtet.

10. Eidesstattliche Erklärung

Ich erkläre hiermit an Eides statt, dass ich die vorliegende Dissertation mit dem Titel:

„GABARAPL2-ACSL3 interaction links ufmylation and lipid droplet formation“

selbständig verfasst, mich außer der angegebenen keiner weiteren Hilfsmittel bedient und alle Erkenntnisse, die aus dem Schrifttum ganz oder annähernd übernommen sind, als solche kenntlich gemacht und nach ihrer Herkunft unter Bezeichnung der Fundstelle einzeln nachgewiesen habe.

Ich erkläre des Weiteren, dass die hier vorgelegte Dissertation nicht in gleicher oder in ähnlicher Form bei einer anderen Stelle zur Erlangung eines akademischen Grades eingereicht wurde.

München, 10.04.2022	Franziska Eck
Ort, Datum	Franziska Eck